

Physics and Chemistry of Lakes

Edited by

Abraham Lerman, Dieter M. Imboden
and Joel R. Gat

With Contributions by

L. Chou, W. Davison, S.J. Eisenreich, J.R. Gat
J. Hamilton-Taylor, K.C. Hornbuckle, S.W. Hostetler
D.M. Imboden, R. Ishiwatari, D. Mackay
F.T. Mackenzie, M. Meybeck, P.A. Meyers, J. Schnoor
W. Stumm, S. Vink, P. Vlahos, T.C. Winter
R. Wollast, **A. Wüest**

With 176 Figures and 48 Tables

Springer-Verlag
Berlin Heidelberg New York London Paris
Tokyo Hong Kong Barcelona Budapest

100-336c

4 Mixing Mechanisms in Lakes

D.M. IMBODEN and A. WÜEST

1 Transport and Mixing

Transport phenomena are among the most important processes in natural systems. Chemical compounds, the constituents of biogeochemical systems, are in continual motion in all parts of the earth. The thermal motion of atoms and molecules is perceived on the macroscopic level as *molecular diffusion*, i.e., as the slow but persistent movement "down along the concentration gradient."

Although the average speed of the atoms is on the order of tens to hundreds of meters per second, the net transport is small, because the molecules do not maintain the same direction long enough. Thus, typical molecular diffusion coefficients of solutes in water are approximately $10^{-9} \text{ m}^2 \text{s}^{-1}$, corresponding to characteristic annual transport distances of approximately 20 cm. In solids the diffusion coefficients even drop to values as low as $10^{-14} \text{ m}^2 \text{s}^{-1}$ or less.

Obviously, motion at the molecular level can only be a significant source of macroscopic transport, either over very short distances or over very long time scales. Indeed, transport through interfaces is controlled by molecular diffusion, and the kinetics of certain chemical transformations is influenced by the molecular motion of the reagents. Furthermore, geochemical processes in the lithosphere mostly occur at time scales on which molecular processes begin to become important.

However, a major part of the environment (the atmosphere and the hydrosphere) is fluid in nature. Because internal friction in air and water is small, even minor external forces can cause macroscale motion. It is true that the energy of such motion is small compared with that stored in thermal motion, but the flow patterns are structured and long lasting, thus giving rise to a kind of

transport called *advection*, which in many cases is much more efficient than molecular diffusion.

Diffusive and advective transport is expressed in terms of the flux vector \mathbf{F} describing the net flow of mass along a certain axis per unit area perpendicular to this axis per unit time. In the case of diffusive transport, \mathbf{F} is given by the well-known first Fickian Law. Thus, transport is clearly defined; but what is mixing? In his classical study, Eckart (1948) distinguishes between *stirring* and *mixing* by defining the former as a process resulting in an increase in spatial gradients, whereas the latter results in decreasing spatial gradients. Following Eckart, stirring is due to advection: It occurs even during nonturbulent fluid motion when different advection velocities acting on different portions of the volume cause distortion of the fluid. In contrast, the sharp gradients between fluid parcels that are generated by stirring are smoothed out by mixing, a process that can only occur as a result of molecular diffusion as the final step. This distinction, although conceptually correct, is not satisfactory from an intuitive viewpoint. Because molecular diffusion acts on small structures more efficiently than on large ones, some kind of "fine" stirring in combination with molecular diffusion results in the complete "disintegration" of the structure. Thus, advective transport leading to spatial-concentration structures of "subcritical" size can be defined as mixing as well. This kind of advection is, of course, linked to the turbulent nature of the flow. We use the term turbulent mixing in order to distinguish it from purely molecular mixing. The distance over which molecular diffusion becomes effective is proportional to the square root of elapsed time. Thus, the typical spatial scale separating stirring from mixing is not fixed, but increases with observation time.

Transport, stirring, and mixing are of tremendous importance for the pace at which chemical and biological processes develop. The aim of this chapter is to derive the time and space scales

resulting from the physics of fluid motion, and to combine them with the scales of the transformation processes. Depending on the nature of these transformations each compound will "feel" its own physical scenery and its individual "view" of movement, either as transport, stirring, or mixing. It is the combination of physical characteristics with the chemical and biological processes that makes the various aquatic systems so varied in appearance.

2 Lakes as Physical Systems

Lakes are complicated and diverse physical systems. One reason for this is the complexity of fluid motion – a property lakes share with other environmental systems such as the ocean and the atmosphere – and another is the large variety in lake size and shape, which results in different boundary effects. We discuss the hydrodynamic aspects first.

The motion of mass is determined by Newton's momentum equation, which states that the acceleration of a body is proportional to the force applied. It is valid for solid as well as fluid systems, but the resulting equations are much more complicated for the latter than for the former. Whereas a solid element of mass keeps its identity while moving across space, a fluid element continually changes its shape and interacts strongly with other fluid elements such that no "empty" space is left behind. Thus, the momentum equation combined with the so-called continuity equation (the equation expressing the conservation of mass of the fluid) results in a complex system of nonlinear differential equations containing the three components of flow velocity as well as the pressure and density of water. Water density, in turn, depends on temperature, pressure, and the chemical composition of the water as described by the so-called *equation of state*.

Two peculiarities arise from the special form of the basic equations of fluid dynamics. First, empirical concepts such as the physicochemical properties of water are essential for describing the macroscopic properties of fluid motion. In fact, the set of equations describing fluid motion includes the equation of state, but also equations describing the friction between fluid elements of different velocity in terms of the fluid viscosity, another material-specific physicochemical property of the fluid.

As a second peculiarity of fluid dynamics we note the much stronger influence of nonlinear effects, which are responsible for turbulence phenomena. In principle there is no way of separating large-from small-scale motion: Large-scale energy of motion is eventually lost to turbulence, and turbulence, in turn, influences large-scale motion. In order to derive a set of equations that solely describe the large-scale motion of the fluid, it is necessary to introduce new empirical macroscopic variables such as Reynolds' stress and turbulent diffusivity.

The large variability in topography and external forcing (Table 1) is responsible for the wide variety in physical appearance exhibited by lakes. Imagine, on one end of the spectrum, a small shallow pond exposed to the wind. We expect to find a well-mixed water body with little or no density stratification and a simple mixing pattern. If we now turn to deeper and larger lakes new phenomena become important. The vertical density structure separates the wind-mixed surface layer from the deep water in which mixing is driven by indirect forcing. Size introduces the effect of the earth's rotation through the Coriolis acceleration, leading to the so-called inertial motions, and, in combination with gravity, to Rossby waves (see Sect. 6.1). Furthermore, size also brings about an increasing sensitivity to meteorological or even climatic gradients: For instance, a small lake tends to react to a passing low-pressure zone instantaneously and as a whole, whereas an air-pressure gradient moving across a large lake may give rise to specific waves and frontal motions.

In most cases mixing is highly variable in both time and space. This variability results mainly from the temporal and spatial structure of the principal driving forces, weather and climate. The topography of the lake and its surroundings may also be responsible for heterogeneous mixing. For instance, the so-called thermal bar, a peculiar mixing phenomenon (Fig. 19), which is frequently observed in large lakes during the initial phase of thermal stratification, is caused by the fact that close to the shore the water column heats up faster than in the middle of the lake. Yet even in smaller lakes differences in the exposure of different parts of the lake to the wind may cause very special mixing patterns (Fig. 22).

As a consequence it is more difficult to account for the size effect when dealing with heterogeneous mixing. It is true that large-scale mixing

Table 1. The variability of lacustrine systems

Shape ^a			
Volume	max. ≈	23 000 km ³	(Baikal)
Area	max. ≈	374 000 km ²	(Caspian Sea)
Maximum depth	max.	1637 m	(Baikal)
Mean depth	max.	730 m	(Baikal)
Topography			
Aspect ratio (maximum depth divided by square root of surface area) ^b			
Large		0.084 ^c	(Tazawa, Japan)
Typical		0.082 ^c	(Crater Lake, USA)
Typical		10 ⁻³	
Hydrology			
Hydraulic loading (water input per unit surface area)			
Large		200 m yr ⁻¹	(Lake Biel, Switzerland)
Typical		1–20 m yr ⁻¹	
Chemistry			
Concentration of total dissolved solids (salinity S)	max. ≈	280 g kg ⁻¹	(Dead Sea)
		35 g kg ⁻¹	(average seawater)
		0.1–0.3 g kg ⁻¹	(typical freshwater)
Climate			
Maximum water temperature		>30 °C	
Stratification ($T_{\text{max}}/T_{\text{min}}$ within water column)		≈25 °C/4 °C	
Annual variation of heat content per unit area ^c			
Typical (temperate lakes)		1.0 × 10 ⁹ J m ⁻²	
Extreme values		2.7 × 10 ⁹ J m ⁻²	(Baikal)
		2.2 × 10 ⁹ J m ⁻²	(Michigan)
Average absolute heat flux ^d			
Typical		65 W m ⁻²	
Extreme value		170 W m ⁻²	(Baikal)

^aFrom Herdendorf (1990).^bFrom Imboden et al. (1988). Hutchinson (1957), based on an expression of Delebecque's, uses the so-called relative depth, which is 89 times the aspect ratio.^cFrom Hutchinson (1957).^dCalculated from the annual variation of heat content, assuming two equal periods of half a year each, during which the lake is either gaining or losing heat at a constant rate.

in the world ocean is driven mainly by persistent wind patterns and the gradient in the heat flux from low-to-high latitudes. Therefore, in the ocean we find typical current systems like the Gulf Stream and Kuroshio Current, or the thermohaline circulation for which no permanent analog exists in lakes. Based on new and better data on water temperature and currents in lakes, however, a picture is evolving according to which horizontal mixing may often be caused by horizontal density currents, which, in turn, are the result of heterogeneous vertical mixing. Thus, the main difference between lacustrine and oceanic systems is the temporal persistence of currents,

rather than their existence. Whereas the oceanic circulation pattern is quasi-permanent, its lacustrine counterpart, depending on the weather conditions, may be switched on and off within minutes or hours.

Because of its influence on density, the chemical composition of lake water represents another key variable, which, independently of lake size, determines the lacustrine environment. In lakes the concentration of total dissolved solids, which, even for pure (or fresh) water is often called *salinity*, ranges from virtually zero to saturation. The upper limit is roughly ten times greater than the average salinity of sea water (Table 1). Most

lakes are horizontally stratified, at least temporarily. Chemically induced vertical gradients may strongly influence the vertical mixing regime. This applies also to lakes with extremely low salinity, provided that the water temperature is close to 4°C, where the thermal expansion coefficient of water approaches zero.

The density stratification is of great importance for the pattern of mixing in lakes. Although the horizontal extension of a lake is usually much larger than its vertical extension, mixing is commonly faster horizontally than vertically. In fact, stratification not only slows down vertical mixing, it also enhances horizontal mixing by channeling the mechanical energy along horizontal surfaces. Furthermore, for increasing stratification the influence of the earth's rotation on currents becomes more pronounced even at small horizontal scales.

In connection with mixing, terms such as horizontal and vertical need some clarification: Because the surfaces of constant density, the so-called *isopycnals*, are hardly ever quiescent, but are rather dynamically distorted by internal waves and external forces, mixing cannot simply be characterized by horizontal and vertical currents. If we need to be more precise, the terms *isopycnal* and *diapycnal* mixing are employed to distinguish the fast transport along the isopycnals from the slower transport across them.

In summary, we find lake size, external forcing, and stratification to be the major factors that select the physical processes relevant in any given lake. The temporal evolution of thermally induced stratification has been used by early limnologists to classify lakes in terms of their mixing regime (e.g., see Hutchinson 1957). With better physical instrumentation it has been found that lakes are too complex to be typified in such a way. In this chapter the reader will thus not find terms such as holomictic or dimictic.

3 Fluid Dynamics: Mathematical Description of Advection and Diffusion

3.1 Equations of Fluid Motion

There are two ways to describe the motion of a fluid. In the first method, the *Lagrangian* representation, the temporal variation of the relevant variables (velocity, pressure, density, etc.) is described for a "moving fluid element." In

the second method, the *Eulerian* representation, the dynamic equations for the variables are formulated at "fixed points" (e.g., in a Cartesian coordinate system). For any scalar property f , the two descriptions are related by

$$\left(\frac{df}{dt} \right)_{\text{Lagrange}} = \frac{\partial f}{\partial t} + U_1 \frac{\partial f}{\partial x_1} + U_2 \frac{\partial f}{\partial x_2} + U_3 \frac{\partial f}{\partial x_3}, \quad (1)$$

where $\partial f / \partial t$ is the Eulerian derivative, x_i ($i = 1-3$) are the three Cartesian coordinates with the x_3 coordinate chosen as positive upward, and U_i are the corresponding components of the velocity vector \mathbf{U} .

The dynamics of the Lagrangian element is determined by the following processes: (a) gravity (acting only along vertical axis x_3), (b) pressure gradients, and (c) internal friction (viscosity). Because of the rotation of the earth, the chosen Cartesian reference system is not inertial. Therefore, an additional (pseudo) acceleration, the Coriolis acceleration (d), appears in the equations of motion. From Eq. (1) with f as one of the velocity components U_i ($i = 1-3$), we obtain:

$$\left(\frac{dU_i}{dt} \right)_{\text{Lagrange}} = -\delta_{i3}g - \frac{1}{\rho} \frac{\partial p}{\partial x_i} + \Psi_i - \Gamma_i \quad (a) \quad (b) \quad (c) \quad (d) \quad (2)$$

(acceleration of gravity $g = 9.81 \text{ m s}^{-2}$; $\delta_{i3} = 1$ for $i = 3$, and 0 otherwise; ρ = density of water; p = pressure, Ψ_i = effect of internal friction; Γ_i = Coriolis acceleration). At the boundaries additional terms appear in Eq. (2) that describe the external forces such as wind stress (see Sect. 5.3). For a detailed discussion of the last two terms of the momentum equation, Eq. (2), the reader is referred to the numerous textbooks that exist on fluid mechanics and physical oceanography (e.g., Gill 1982). For small-scale motions relevant to mixing processes, the Coriolis term can be neglected. In addition, incompressible flow can be assumed. Under these conditions the *continuity equation* can be written

$$\sum_i \frac{\partial U_i}{\partial x_i} = 0. \quad (3)$$

(Note: If not otherwise stated in this and the following equations, the summation is always over all three Cartesian coordinates, i.e., $i = 1-3$.)

Neglecting the spatial variability of the viscosity of water, the frictional term for incompressible flow can be written as

$$\Psi_i = \nu \sum_j \frac{\partial^2 U_i}{\partial x_j^2}, \quad (4)$$

where ν is kinematic viscosity. Finally, expressed in Eulerian form, we arrive at the three equations:

$$\begin{aligned} \frac{\partial U_i}{\partial t} + \sum_j U_j \frac{\partial U_i}{\partial x_j} &= -\delta_{i3} g - \frac{1}{\rho} \frac{\partial p}{\partial x_i} + \nu \sum_j \frac{\partial^2 U_i}{\partial x_j^2}, \\ (e) \quad (a) \quad (b) \quad (c) \\ i = 1-3, \end{aligned} \quad (5)$$

where term (e) describes the acceleration due to velocity gradients relative to the spatially fixed Eulerian system. Equation (5) is called the *Navier-Stokes Equation* for viscous, incompressible flow on a nonrotating earth.

For a scalar quantity, such as concentration C or water temperature T , a similar approach can be adopted by substituting the appropriate expressions on the right side of Eq. (5). The sum of the terms (a) and (b) is replaced by an *in situ* production/consumption rate, which for concentration is S_C and for temperature is $\frac{S_T}{c_p \rho}$, where S_T is the *in situ* production/consumption of heat, and c_p is specific heat of water at constant pressure. Term (c) is substituted by the molecular diffusivity of concentration, D^C , and of temperature, D^T , respectively, and combined with the corresponding second spatial derivatives. Thus, for concentration we get

$$\begin{aligned} \frac{\partial C}{\partial t} + \sum_j U_j \frac{\partial C}{\partial x_j} &= S_C + D^C \sum_j \frac{\partial^2 C}{\partial x_j^2}, \\ (e) \quad (b) \quad (c) \end{aligned} \quad (6)$$

and for temperature

$$\begin{aligned} \frac{\partial T}{\partial t} + \sum_j U_j \frac{\partial T}{\partial x_j} &= \frac{S_T}{c_p \rho} + D^T \sum_j \frac{\partial^2 T}{\partial x_j^2}. \\ (e) \quad (b) \quad (c) \end{aligned} \quad (7)$$

3.2 Turbulence, Reynolds' Stress, and Eddy Diffusion

We are still one important step away from our general goal of describing transport and mixing. Two kinds of motion appear in Eqs. (5–7), viz. advection (term e) and molecular diffusion (term c). As mentioned in Section 1 turbulent mixing is

usually faster than molecular diffusion. This fast mixing is linked to the fine structure of the flow (turbulence) still hidden in the advective term (e).

The usual way to separate (large-scale) advective from (small-scale) turbulent flow is by splitting variables f , such as velocity u_i , temperature T , and concentration C , into two parts, a temporal mean \bar{f} and a fluctuation f' about the mean:

$$f = \bar{f} + f', \quad \text{where } \bar{f}(t) = \frac{1}{T} \int_{t-T/2}^{t+T/2} f(t') dt'. \quad (8)$$

Note that a certain degree of ambiguity is inherent in this procedure (often called Reynolds' decomposition), because the length of the time interval T over which the mean is calculated determines to a certain extent the size of \bar{f} and thus of f' . The dynamics of the atmosphere commonly exhibit a so-called spectral gap at time scales of approximately 1 h, within which little variation of wind speed occurs (Van der Hoven 1957). At time scales longer than those of the spectral gap we find synoptic processes, and at shorter time scales we find turbulent fluctuations. Thus, for the atmosphere a scale of approximately 1 h is a natural choice for Eq. (8). Aquatic systems usually do not have such a natural gap separating the time scales of important processes. Nevertheless, Reynolds' decomposition is used for aquatic systems as well, although its scale-dependence often requires special consideration, e.g., by using different intervals T for different purposes.

Let us apply Reynolds' decomposition to the product of two variables, f_1 and f_2 :

$$\begin{aligned} f_1 f_2 &= (\bar{f}_1 + f'_1)(\bar{f}_2 + f'_2) \\ &= \bar{f}_1 \bar{f}_2 + \bar{f}_1 f'_2 + f'_1 \bar{f}_2 + f'_1 f'_2. \end{aligned} \quad (9)$$

Taking a time average over both sides of Eq. (9) we obtain

$$\overline{f_1 f_2} = \bar{f}_1 \bar{f}_2 + \overline{f'_1 f'_2}. \quad (10)$$

In Eq. (10) we have used the rules $\bar{\bar{f}} = \bar{f}$ and $\bar{f}' = 0$. For details the reader is referred to standard textbooks (e.g., Stull 1988). The essential point of the decomposition procedure expressed in Eq. (10) is the following: Calculation of the time average of the product of two variables results in two terms, viz. the product of the means ($\bar{f}_1 \bar{f}_2$) and the mean of the product of the fluctuations ($\overline{f'_1 f'_2}$). The latter, the so-called covariance of the two variables f_1 and f_2 , vanishes if the two vari-

ables f_1 and f_2 are statistically mutually independent. This is obviously not the case if f_1 and f_2 refer to velocity, temperature, pressure, etc. In other words, whenever the equations contain nonlinear terms (e.g., products of variables), Reynolds' decomposition introduces new terms, the physical meaning of which will soon become clear.

We will not go through the algebra of the Reynolds' decomposition of Eqs. (5–7) step by step. An excellent treatment can be found, for example, in Stull (1988). Let us look at the results. Defining

$$U_i = \bar{U}_i + u'_i, \quad i = 1-3, \quad (11)$$

Eq. (5) becomes

$$\begin{aligned} \frac{\partial \bar{U}_i}{\partial t} + \sum_j \bar{U}_j \frac{\partial \bar{U}_i}{\partial x_j} &= -\delta_{i3}g - \frac{1}{\rho} \frac{\partial p}{\partial x_i} \\ \text{(e)} &\quad \text{(a)} \quad \text{(b)} \\ &+ \nu \sum_j \frac{\partial^2 \bar{U}_i}{\partial x_j^2} \\ \text{(c)} & \\ - \sum_j \frac{\partial (\bar{u}'_i \bar{u}'_j)}{\partial x_j} & \quad \text{(f)} \end{aligned} \quad (12)$$

As a consequence of Reynolds' decomposition, a new term (f) emerges from the nonlinear advection term (e). Using Eq. (3), this term has been transformed into a symmetrical form and moved to the right side of Eq. (12). Term (f) describes the influence of turbulence on the mean motion \bar{U}_i . The covariances are usually expressed in terms of the so-called Reynolds' stress:

$$\tau_{ij} = -\bar{\rho}(\bar{u}'_i \bar{u}'_j). \quad [\text{N m}^{-2}] \quad (13)$$

In the same way, Reynolds' decomposition transforms Eqs. (6) and (7) into the equations for mean scalar properties (e.g., $\bar{C} = C - C'$; $\bar{T} = T - T'$):

$$\begin{aligned} \frac{\partial \bar{C}}{\partial t} + \sum_j \bar{U}_j \frac{\partial \bar{C}}{\partial x_j} &= S_C + D^C \sum_j \frac{\partial^2 \bar{C}}{\partial x_j^2} \\ \text{(c)} & \\ - \sum_j \frac{\partial (\bar{u}'_j \bar{c}')}{\partial x_j} & \quad \text{(f)} \end{aligned} \quad (14)$$

and

$$\begin{aligned} \frac{\partial \bar{T}}{\partial t} + \sum_j \bar{U}_j \frac{\partial \bar{T}}{\partial x_j} &= S_T + D^T \sum_j \frac{\partial^2 \bar{T}}{\partial x_j^2} \\ \text{(c)} & \\ - \sum_j \frac{\partial (\bar{u}'_j \bar{T}')}{\partial x_j} & \quad \text{(f)} \end{aligned} \quad (15)$$

The last terms (f) in each equation, the divergence of the turbulent fluxes,

$$F_j^C = \bar{u}'_j \bar{c}' \quad \text{and} \quad F_j^T = \bar{u}'_j \bar{T}', \quad (16)$$

express the additional transport due to turbulent fluctuations of u_i , C , and T . These terms are much larger than the molecular terms (c), so that the latter are usually omitted.

This new set of equations has introduced several new unknowns, i.e., the covariances (such as the Reynolds' stress terms and the turbulent fluxes). It is possible to derive new dynamic equations for the description of the double correlations, but unfortunately these equations contain triple correlations, e.g., expressions such as $\bar{T}' \bar{u}'_i \bar{u}'_j$. Thus, any attempt to derive enough equations to solve for all the unknowns leads to an even larger number of unknowns. There is no way out, unless we find some approximation that expresses the higher-order correlations using lower-order terms (and not the other way around). This procedure is called *closure approximation* (e.g., see Stull 1988).

There are closure schemes of various order. In the simplest of these, the first-order closure scheme, terms including means (such as \bar{f}) are retained while all covariances of the form $\bar{f}_1 \bar{f}_2$ are parameterized. Analogously, a second-order procedure retains the expressions up to the second order, while the covariances of the third order appearing in the dynamic equation of the second order, such as $\partial(\bar{f}_1 \bar{f}_2)/\partial t$, are parameterized. Two methods of parameterization can be distinguished, known as *local* and *nonlocal* approximations. In the former an unknown at any given point in space is expressed in terms of certain variables solely at this point; in the latter, the unknown quantity is approximated by values of known quantities within some spatial environment of the point. We first deal with the more common local closure models and restrict our discussion to the first order. Nonlocal schemes are explored in Section 3.4.

In the first-order local closure approximation, the second-order covariance is expressed by

derivatives of the mean quantities. If f is a scalar, then the turbulent flux of the scalar property along the j axis, F_j^f , is approximated by

$$F_j^f = \bar{u}'_j f' = -K_j^f \frac{\partial \bar{f}}{\partial x_j}, \quad (17)$$

where K_j^f is a positive coefficient with dimensions $[L^2 T^{-1}]$. [Note that in Eq. (17) it is assumed that the coordinates x_i are principal axes; otherwise, additional terms would appear containing the derivatives with regard to the other axes.] Thus, the scalar f flows in the direction of its negative gradient, i.e., "it flows down the local gradient". Equation (17) is called the *gradient-transport* (or eddy) formulation (Fig. 1a). For f we can insert temperature, concentration, or one of the three velocity components U_i , and apply Eq. (17) to Eqs. (12), (14), and (15). If f stands for concentration C , the theory is identical to *Fick's First Law*. If f stands for the velocity component U_i , we can relate the eddy formulation to the Reynolds' stress introduced in Eq. (13):

$$\bar{u}'_i \bar{u}'_j = -K_{ij}^m \frac{\partial \bar{U}_i}{\partial x_j}, \quad (18)$$

where K_{ij}^m is the turbulent or eddy diffusion coefficient for momentum (also called eddy viscosity) and K_j^T and K_j^C are the eddy diffusion coefficients of temperature and of mass for substance of concentration C , respectively.

By neglecting molecular viscosity and diffusion relative to the turbulent flux terms one obtains:

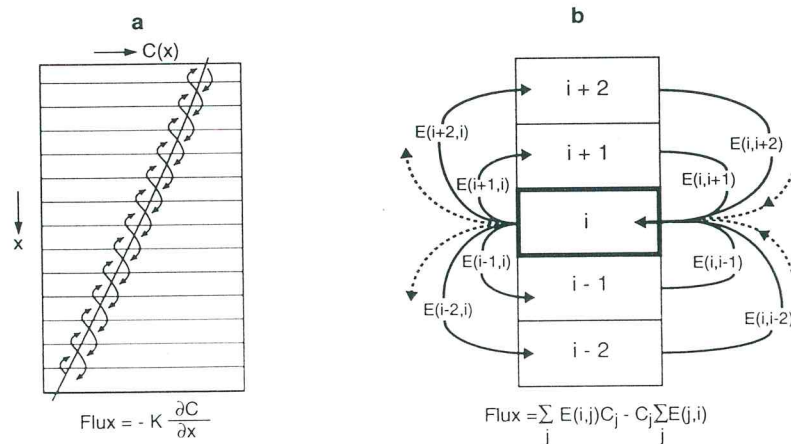


Fig. 1. a The local exchange model leads to the gradientflux model (Eq. 20) as exemplified, for the case of mass fluxes, by Fick's First Law: $F_i = -K \cdot \partial C / \partial x_i$. b In contrast, the nonlocal exchange model (Imboden 1981), also named Transient Turbulence Theory (Stull 1984,

$$\begin{aligned} \frac{\partial \bar{U}_i}{\partial t} + \sum_j \bar{U}_j \frac{\partial \bar{U}_i}{\partial x_j} &= -\delta_{i3} g - \frac{1}{\rho} \frac{\partial p}{\partial x_i} \\ &+ \sum_j \frac{\partial}{\partial x_j} \left(K_{ij}^m \frac{\partial \bar{U}_i}{\partial x_j} \right), \quad i = 1-3; \end{aligned} \quad (19)$$

$$\frac{\partial \bar{C}}{\partial t} + \sum_j \bar{U}_j \frac{\partial \bar{C}}{\partial x_j} = S_C + \sum_j \frac{\partial}{\partial x_j} \left(K_j^C \frac{\partial \bar{C}}{\partial x_j} \right); \quad (20)$$

$$\frac{\partial \bar{T}}{\partial t} + \sum_j \bar{U}_j \frac{\partial \bar{T}}{\partial x_j} = S_T + \sum_j \frac{\partial}{\partial x_j} \left(K_j^T \frac{\partial \bar{T}}{\partial x_j} \right). \quad (21)$$

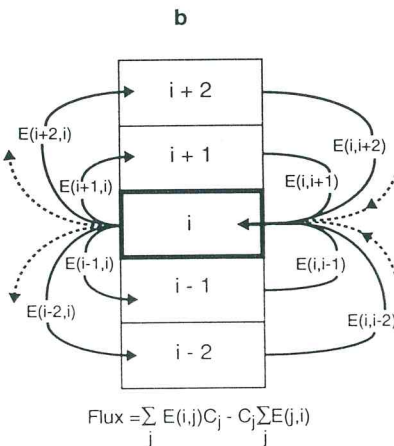
The subscript j refers to the direction of the eddy flux. For stratified fluids the eddy diffusivity along the horizontal axis is usually much larger than along the vertical axis (e.g., $K_z^C \ll K_x^C, K_y^C$).

3.3 Vertical Momentum Equation

The vertical component ($i = 3$) of the momentum equation (Eq. 19), at steady state and in the absence of spatial velocity gradients, yields the simple *hydrostatic equation*

$$\frac{\partial p}{\partial x_3} = -g\rho. \quad (22)$$

In turn, if Eq. (22) is inserted into the general vertical momentum equation, the first and second term on the right side of Eq. (19) cancel out. The resulting equation is called the *hydrostatic approximation*.



1986), describes the mass flux from box i into box j by the matrix $E(j,i)$. The two boxes do not have to be neighbors. See Eq. (28) for the continuous formulation of the model

A special kind of motion evolves from Eq. (5) if we concentrate our discussion on the vertical direction by assuming horizontal current velocities to be zero, and by neglecting (molecular and turbulent) friction. After performing the Reynolds' decomposition, and in the absence of a mean vertical flow ($\bar{U}_3 = 0$), the only remaining term on the left side of Eq. (12) is the Lagrangian acceleration of the velocity fluctuation u_3' . It is equal to the sum of the two remaining terms on the right side, i.e., the acceleration due to gravity (term a) and the vertical pressure gradient (term b). Multiplying both sides by ρ yields

$$\rho \left(\frac{du_3'}{dt} \right)_{\text{Lagrange}} = -g\rho - \frac{\partial p}{\partial x_3}. \quad (23)$$

This is the equation of motion of a water parcel moving vertically within the water column. At an equilibrium depth z_o , its density is equal to the mean (depth-dependent) density of the surrounding water. If the vertical displacement from the equilibrium depth is small and of short duration, the effect of pressure and of the exchange of heat or salt between the water parcel and its surroundings can be neglected. This means that the density ρ of the water parcel is constant. However, by changing its depth the water parcel is exposed to a different pressure gradient than that prevailing at its equilibrium depth:

$$\frac{\partial p}{\partial x_3} \Big|_{z_o + \zeta} = \frac{\partial p}{\partial x_3} \Big|_{z_o} + g \frac{d\bar{\rho}}{dz} \zeta = -g\bar{\rho} + g \frac{d\bar{\rho}}{dz} \zeta \quad (24)$$

where ζ is the vertical displacement of the parcel from its equilibrium depth. Replacing this expression for the pressure gradient in Eq. (23), and using $\bar{\rho} = \rho$, yields

$$\left(\frac{du_3'}{dt} \right)_{\text{Lagrange}} = \frac{\partial^2 \zeta}{\partial t^2} = \frac{g}{\bar{\rho}} \frac{d\bar{\rho}}{dz} \zeta = -N^2 \zeta. \quad (25)$$

This is the equation of motion of a linear oscillator with eigenfrequency

$$N = \left(-\frac{g}{\bar{\rho}} \frac{d\bar{\rho}}{dz} \right)^{1/2}. \quad [\text{s}^{-1}] \quad (26)$$

N is called the *stability frequency* or *Brunt-Väisälä frequency*, and is defined for $\frac{d\bar{\rho}}{dz} < 0$ (Table 5). N is often used to quantify the strength of the density stratification. A more exact definition of N is given by Eq. (41).

3.4 Nonlocal Diffusion and Transient Mixing

The eddy formulation of Eq. (16) is based on the assumption that turbulent motion (expressed by u'_j) occurs over small distances, so that the resulting flux F_j^f can be parameterized by the gradient of the mean value of property f "at this very location." Mathematicians call such a relationship *local*, in contrast to an expression in which F_j^f depends on values of \bar{f} at other locations as well, which can be named a *nonlocal* theory (Imboden 1981; Stull 1984; Boudreau and Imboden 1987). The existence of large eddies that can transport fluid across finite distances before they lose their identity due to the action of small-scale eddy mixing may invalidate concepts of local diffusion such as those embodied in Fick's First Law. The natural nonlocal extension of this law is to replace Eq. (24) by the following expression (Imboden 1981):

$$F_j^f(x_j) = - \int_a^b k_j^f(x_j, \tilde{x}_j) \frac{\partial \bar{f}}{\partial x_j} \Big|_{\tilde{x}_j} d\tilde{x}_j, \quad (27)$$

where $k_j^f(x_j, \tilde{x}_j)$ is a generalized eddy diffusivity (dimensions LT^{-1}) for property f along the x_j direction, measuring the influence of the \bar{f} gradient at \tilde{x}_j on the turbulent flux at x_j . Parameters a and b are either the boundaries of the system along the x_j axis or the limits beyond which \bar{f} no longer has an effect on the flux at x_j . Equation (27) includes the Fickian expression as the special case $k_j^f(x_j, \tilde{x}_j) = K_j^f \delta(x_j - \tilde{x}_j)$, where $\delta(x) = \infty$ for $x = 0$, and $\delta(x) = 0$ otherwise.

An alternative nonlocal concept is the *exchange model* (Imboden 1981), called *Transient Turbulence Theory* by Stull (1984, 1986). In its discrete form the model is formulated in terms of a matrix (the transilient matrix), which expresses the probability of fluid exchange between any two finite spatial boxes (Fig. 1b). In its continuous form the last term on the right side of Eqs. (20) or (21) is replaced by the integral

$$\int_a^b E_j^f(x_j, \tilde{x}_j) \bar{f}(\tilde{x}_j) d\tilde{x}_j - \bar{f}(x_j) \int_a^b E_j^f(\tilde{x}_j, x_j) d\tilde{x}_j, \quad (28)$$

where \bar{f} stands for \bar{C} or \bar{T} . $E_j^f(x_j, \tilde{x}_j)$ is the exchange probability along the j axis from location \tilde{x}_j to x_j .

A more detailed exposition of nonlocal theories would go beyond the scope of this chapter. Nonlocal theories are more complex than local

theories and require a considerable quantity of field data for their application. This may explain why there have been few applications such as mixing within sediments (Boudreau and Imboden 1987) or mixing in the atmospheric boundary layer (Stull 1988). Still, nonlocal transport models offer a way to overcome some of the problems of the eddy formulation, which are apparent in many situations where transport does not occur in the direction of the local negative gradient.

4 Density and Stability of Water Column

4.1 Equation of State of Water

The density of water, defined as the ratio of mass to volume, depends on temperature, pressure, and the physicochemical properties of the water. In order to calculate the density of distilled water exactly, even the exact isotopic composition [e.g., the abundance of the heavy isotopes ^2H (deuterium) and ^{18}O] and the concentration of dissolved gases (e.g., air) has to be known. Rather detailed expressions for the thermodynamic properties of natural waters covering the limnological range are given by Chen and Millero (1986). They approximate $\rho_o(T)$ for pure water in equilibrium with air at $p = 1013 \text{ mbar}$ (mean pressure at sea level) by a sixth-order polynomial. A simpler expression is given by Bührer and Ambühl (1975; T in $^\circ\text{C}$):

$$\begin{aligned} \rho_o(T) = & 999.84298 + 10^{-3}(65.4891 \cdot T \\ & - 8.56272 \cdot T^2 \\ & + 0.059385 \cdot T^3). \quad [\text{kg} \cdot \text{m}^{-3}] \end{aligned} \quad (29)$$

This equation is valid for temperatures between 1 and 20°C with a relative deviation from measured values, $\delta\rho/\rho$, of less than 2×10^{-6} .

The thermal expansivity of water, α , is defined by

$$\alpha = -\frac{1}{\rho} \left(\frac{\partial \rho}{\partial T} \right)_{C_n, p}, \quad [\text{K}^{-1}] \quad (30)$$

where the subscripts indicate that the derivative is calculated by keeping pressure p and concentration C_n of every solute n constant. Because the process of thermal expansion is accompanied by a volume change, the C_n values have to be expressed in terms of the mass of dissolved substance n per total mass of solution.

For pure water at $p = 1013 \text{ mbar}$, α changes

sign at the temperature of maximum density $T_{\rho_{\max}} = 3.9839^\circ\text{C}$, where ρ_o reaches its maximum value of $\rho_{\max} = 999.972 \text{ kg m}^{-3}$ (Chen and Millero 1986). (Note that the approximation Eq. (29), gives slightly different values.) For temperatures $T > T_{\rho_{\max}}$, density decreases with increasing temperature and $\alpha > 0$; at $T = T_{\rho_{\max}}$, $\alpha = 0$; and for $T < T_{\rho_{\max}}$, $\alpha < 0$.

Although the "direct" effect of pressure p on density ρ (the compressibility of water) is not relevant for the stability of the water column (see Sect. 4.2), pressure plays an important "indirect" role through its influence on α and $T_{\rho_{\max}}$. In fact, $T_{\rho_{\max}}$ decreases with increasing pressure and thus with increasing depth (Chen and Millero 1986):

$$\begin{aligned} T_{\rho_{\max}} = & 3.9839 - 1.9911 \times 10^{-2} p \\ & - 5.822 \times 10^{-6} p^2, \quad [\text{°C}] \end{aligned} \quad (31)$$

where p is in bar. Note that in fresh water the hydrostatic pressure increases by approximately 0.0981 bar per meter. Thus, $T_{\rho_{\max}}$ decreases roughly by 0.2°C for every 100 m of depth. The influence of pressure on α (*thermobaric effect*) and temperature (*cabbeling*), can affect the sinking and rising of water masses in the ocean and in deep lakes (McDougall 1987a; see also Sect. 6.6). Selected values of $\rho_o(T)$ and $\alpha(T, p)$ are given in Table 2.

A further influence on ρ , α , $T_{\rho_{\max}}$, and other physical properties originates from the chemical composition of the water. At sufficiently large dilution the effect of solute $n = 1, 2, \dots$ (with concentration C_n) on ρ can be expressed by the linear superposition

$$\rho(T, C_1, C_2, \dots) = \rho_o(T)[1 + \beta_1 C_1 + \beta_2 C_2 + \dots], \quad (32)$$

where

$$\begin{aligned} \beta_n = & \frac{1}{\rho} \left(\frac{\partial \rho}{\partial C_n} \right)_{T, p, C_m}, \\ m = 1, 2, \dots \text{ but } m \neq n \end{aligned} \quad (33)$$

is the specific expansion coefficient of water due to solute n . The coefficient β_n is temperature-dependent; values for various solutes at $T = 25^\circ\text{C}$ are given in Table 3. For dissolved gases β_n can be negative, which means that the density of the water decreases with increasing gas concentration. Equation (33) can also be applied to describe the influence of suspended solids on the density of water.

Table 2. Physical properties of pure water as a function of temperature and pressure^a

T [°C]	Density $\rho(T)^b$ [kg m ⁻³]		Thermal expansivity $\alpha(T,p)$ [10 ⁻⁶ K ⁻¹]			
	p = 0	p = 0	p = 20	p = 50	p = 100	p = 180
0	999.839	-68.00	-60.64	-49.59	-31.18	-1.72
1	999.898	-50.09	-43.03	-32.43	-14.78	13.48
2	999.940	-32.77	-26.00	-15.85	1.08	28.17
3	999.964	-16.01	-9.53	0.20	16.42	42.37
4	999.972	0.22	6.43	15.75	31.27	56.11
5	999.964	15.96	21.90	30.81	45.66	69.42
10	999.700	87.99	92.70	99.76	111.52	130.35
15	999.100	150.89	154.55	160.05	169.21	183.86
20	998.204	206.76	209.58	213.79	220.82	232.07
25	997.045	257.17	259.33	262.55	267.93	276.54

^aThe hydrostatic pressure p [bar] is 0 at the water surface.^bDensity at atmospheric pressure of 1013 mbar.**Table 3.** Influence of dissolved or suspended substances on the density of water

Substance	β_n [(g/kg) ⁻¹] ^a
Ca(HCO ₃) ₂	0.807 × 10 ⁻³
Mg(HCO ₃) ₂	0.861 × 10 ⁻³
Na(HCO ₃)	0.727 × 10 ⁻³
K(HCO ₃)	0.669 × 10 ⁻³
Fe(HCO ₃) ₂	0.838 × 10 ⁻³
NH ₄ (HCO ₃)	0.462 × 10 ⁻³
CO ₂	0.273 × 10 ⁻³
CH ₄	-1.250 × 10 ⁻³
Air	-0.090 × 10 ⁻³
Suspended solids ^b with $\rho_s = 2.65 \text{ g cm}^{-3}$	0.623 × 10 ⁻³
with $\rho_s = 1.1 \text{ g cm}^{-3}$	0.091 × 10 ⁻³
Electrical conductivity (β_k) due to Ca(HCO ₃) ₂	0.705 × 10 ⁻⁶ ($\mu\text{S}/\text{cm}$) ⁻¹

^a β_n values for T = 25 °C as defined in Eqs. (33–35).^b ρ_s is dry density of suspended solids.

If the relative chemical composition of the water is constant (as is nearly the case for seawater), the influence of the different components can be represented by a single parameter such as the concentration of total dissolved solids S (salinity), which is expressed as the total mass of dissolved solids (in g) per unit total mass of (salt) water (in kg). The influence of S on ρ is described by β_S , often called the *coefficient of haline contraction*, as follows:

$$\rho(T,S) = \rho_0(T)[1 + \beta_S S], \quad (34)$$

with $\beta_S = \frac{1}{\rho} \left(\frac{\partial \rho}{\partial S} \right)_{T,p}$

Unlike seawater, the relative chemical composition of lake water is not constant. Not only does the concentration of total dissolved solids vary considerably from lake to lake, from the nearly pure water of alpine lakes to the nearly saturated salt water of the Dead Sea (Table 1), but the chemical composition of the total dissolved solids also varies. In some cases the chemistry of lake water is dominated by a single anion/cation pair, e.g., by calcium and bicarbonate. The electrical conductivity κ_{20} (the subscript refers to the reference temperature of 20 °C) can then serve as a direct measure of the total concentration of these ions. Given their specific electrical conductivity and ionic volumes, we can obtain an

expression for the dependence of ρ on κ_{20} . For the case of calcium carbonate the following relationship is obtained:

$$\rho(T, \kappa_{20}) = \rho_0(T)[1 + \beta_\kappa \kappa_{20}],$$

$$\beta_\kappa = \frac{1}{\rho} \frac{\partial \rho}{\partial \kappa_{20}} = 0.705 \times 10^{-6} (\mu\text{S}/\text{cm})^{-1}, \quad (35)$$

with κ_{20} as the electrical conductivity of water at 20°C (in $\mu\text{S}/\text{cm}$). Similar relationships can be obtained for other ionic water compositions as long as the concentrations of nonionic species (which have no effect on κ_{20}) are negligible.

Both the temperature of maximum density $T_{\rho_{\max}}$ and the thermal expansivity α change with salinity. In fact, at a salinity of 24.8 g/kg, $T_{\rho_{\max}}$ sinks below the freezing temperature, which, at this salinity, is $T = -1.34^\circ\text{C}$. Seawater (with a typical salinity of 35 g/kg) does not exhibit such a density anomaly; α is always positive, i.e., density always increases with decreasing temperature.

4.2 Potential Temperature and Local Vertical Stability

To discuss the concept of local vertical stability two water parcels that are separated by a very small vertical distance are considered. Imagine that the upper parcel is displaced isentropically (i.e., without exchange of heat and salt with the surrounding water) to the depth of the lower one where the densities of the two parcels are then compared. If the density of the water parcel originating from the upper position is smaller than the density of the water parcel from the lower position, the water is said to be locally stable. Because of the buoyancy force, the displaced water parcel is pushed back to the depth from where it originated, i.e., the displacement is reversible. If the density difference is zero, the water column is referred to as neutrally stable. The two water parcels could exchange their positions without altering the potential energy of the water column. Finally, if the water parcel displaced from above has a greater *in situ* density than the water parcel at the deeper position, the water is referred to as locally unstable. In the latter case exchanging the positions of the two water parcels results in a decrease of the potential energy of the water column. Spontaneous convection is initiated, which continues until the density instability has vanished.

Because the displacement of the water parcels are infinitesimally small, the stability depends on the “local” density gradient; hence, the expression *local stability*. The vertical movement of a displaced water parcel close to its equilibrium depth is described by Eq. (25), i.e., by the stability frequency N . In contrast, the concept of *global stability* of a water mass addresses the question of how the total potential energy of the water masses changes if the water is completely mixed adiabatically. Given the very special properties of the density of water as a function of temperature, salt, and pressure it is possible that a water mass is globally unstable despite being locally stable everywhere. The problem of global stability is beyond the scope of this chapter.

Note that local stability does not depend directly on the compressibility of the water, because the densities are compared at the same depth. In other words, an increase in *in situ* density with depth is not sufficient to guarantee local stability. The indirect effect of pressure on stability still has to be taken into account, however. The decompression of a water parcel that is being moved upwards isentropically leads to a small temperature decrease, which is accompanied by a slight density increase if $T > T_{\rho_{\max}}$ (and a small density decrease if $T < T_{\rho_{\max}}$).

The so-called *adiabatic temperature gradient*,

$$\left(\frac{dT}{dz} \right)_{ad} = - \frac{ga(T + 273.15)}{c_p}, \quad (36)$$

given by (Kelvin 1875) (the vertical coordinate z is chosen as positive upward), corresponds to the change in *in situ* temperature in a neutrally stable water column. Thus, for $\alpha > 0$ (i.e., $T > T_{\rho_{\max}}$) the *in situ* temperature increases with depth at neutral stability. In the deep parts of cold freshwater lakes, $\left(\frac{dT}{dz} \right)_{ad}$ is usually very small, because water temperatures are close to the temperature $T_{\rho_{\max}}$ at which α approaches zero. For instance, at a temperature $T = 4^\circ\text{C}$ and a hydrostatic pressure $p = 20$ bar (corresponding to a depth of approximately 200 m), $\left(\frac{dT}{dz} \right)_{ad}$ is approximately $-4.2 \times 10^{-6} \text{ K m}^{-1}$.

The condition for local stability can be expressed as follows:

$$\alpha \left[\frac{dT}{dz} - \left(\frac{dT}{dz} \right)_{ad} \right] > 0. \quad (37)$$

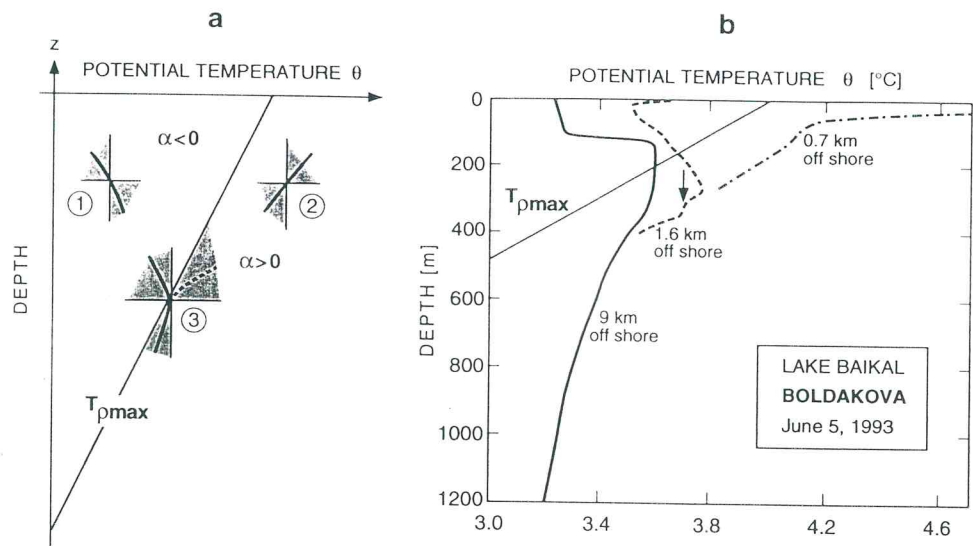


Fig. 2. **a** Conditions for local stability derived from Eqs. (37) and (38). Stable temperature profiles characterized by $\alpha \cdot \frac{d\theta}{dz} > 0$ lie in the shaded segments. ① For $T < T_{\rho\max}$, $\alpha < 0$; hence, local stability implies $\frac{d\theta}{dz} < 0$. ② For $T > T_{\rho\max}$, $\alpha > 0$; hence, local stability implies $\frac{d\theta}{dz} > 0$. ③ The temperature profile cannot cross the

$T_{\rho\max}$ line from right to left while depth is increasing. Note that the effect of salinity gradients on stability is not considered here. **b** Vertical temperature profiles from Lake Baikal demonstrate the effect of the pressure dependence of the temperature of maximum density, $T_{\rho\max}$. Except for the top 200 m, the temperature decreases with depth, but always remains above the *in situ* $T_{\rho\max}$

The consequences of this inequality are illustrated schematically in Fig. 2a. Temperature profiles from Lake Baikal (Siberia) shown in Fig. 2b demonstrate the effect of the pressure dependence of $T_{\rho\max}$ on the vertical stability of the water column.

It is often convenient to replace the *in situ* temperature by the so-called potential temperature θ , defined by the differential equation

$$\frac{d\theta}{dz} = \frac{dT}{dz} - \left(\frac{dT}{dz} \right)_{ad}. \quad (38)$$

For an absolute definition of θ a reference depth z_0 has to be selected at which T and θ are taken to be equal. In the ocean, z_0 is often chosen to lie at 4 km depth, but for lakes it is more appropriate to choose z_0 at the surface. Thus,

$$\theta(z) = T(z) - \int_z^{z_0} \left(\frac{dT}{dz} \right)_{ad} dz'. \quad (39)$$

Because $\left(\frac{dT}{dz} \right)_{ad}$ depends on depth, temperature, and salinity, and may even change sign over the integration interval, the evaluation of Eq. (39) is not always trivial.

To include the effect of salt on the stability condition Eq. (37) has to be completed by a term that contains the *in situ* salt gradient and the corresponding expansion coefficient for salt:

$$\left(\alpha \frac{d\theta}{dz} - \beta_s \frac{dS}{dz} \right) = \left(\alpha \left[\frac{dT}{dz} - \left(\frac{dT}{dz} \right)_{ad} \right] - \beta_s \frac{dS}{dz} \right) > 0. \quad (40)$$

We can now define the stability frequency introduced in Eq. (17) more exactly (for the sake of simplicity $\bar{\rho}$ is replaced by ρ):

$$N = \left[\frac{g}{\rho} \left(\alpha \frac{d\theta}{dz} - \beta_s \frac{dS}{dz} \right) \right]^{1/2}. \quad (41)$$

5 Energy Fluxes: Driving Forces Behind Transport and Mixing

All mixing and transport phenomena in the aquatic environment, with the exception of molecular diffusion, are driven by external forces. The mixing patterns that evolve are the result of both external forces and internal properties of the

system such as the morphometry of the water body or the stability of the water column. In fact, the external forces are built into the boundary conditions of the equations of motion derived in Sect. 3. Rather than deal with the mathematical solutions of these equations, however, in this section the various energy fluxes and the way they become apparent in lakes are discussed. Following physical tradition a distinction is made between *thermal* and *mechanical* energy; the latter is further subdivided into *potential* and *kinetic* energy. Thermal energy is stored in the random-velocity distribution of atoms and molecules. Its direct influence on mixing, as manifested in molecular diffusion, is small. Indirectly, however, thermal energy affects mixing very strongly through its influence on water density (Sects. 4 and 6). Compared with thermal energy mechanical energy is highly ordered, and, although its flux is relatively small, it plays a crucial role for mixing in lakes.

Figure 3 illustrates typical orders of magnitude for energy fluxes (energy per unit area per unit time, in W m^{-2}) and energy content (energy per unit area, in J m^{-2}) for lakes. The reason that these values are normalized by dividing by the surface area is that most exchange of momentum and energy is at the water surface (e.g., heat exchange and wind energy). We first briefly explain how energy is stored in a lake. The largest storage term, ΔE_{heat} , is related to thermal energy. Because there is no meaningful way to define absolute thermal energy content, we use the energy amplitude that is the difference between the

maximum and minimum thermal energy content of the water column. ΔE_{heat} is usually approximately 10^9 J m^{-2} , but may exceed $2.7 \times 10^9 \text{ J m}^{-2}$ (e.g., Lake Baikal; Table 1). It is by far the largest term in the total energy balance. Next in size is the potential energy term ΔE_{pot} (typically $\approx 10^3 \text{ J m}^{-2}$), which depends on the vertical-density stratification of the water column. In saline lakes, where the density of water depends not only on temperature but also on salinity, ΔE_{pot} may be much larger. In the Dead Sea, for instance, the potential energy associated with the stratification of the highly saline water reached a value of $4 \times 10^5 \text{ J m}^{-2}$ in early 1980 (Anati et al. 1987). The smallest storage term (although the most spectacular one if we consider the often devastating power of surface waves!) is given by the kinetic energy of the water, E_{kin} , contained in currents, waves, and turbulent motion. The kinetic energy brought into the lake by inlets (shown on the left side of Fig. 3) varies by several orders of magnitude depending on water-renewal rate. A value of 10^{-4} W m^{-2} for E_{kin} is typical for lakes with mean water residence times between 0.5 and 5 years.

The second law of thermodynamics gives a clear meaning to the classification of the different energy terms: Although mechanical energy can be fully transformed into thermal energy, the reverse is not possible. The kinetic energy of water currents is eventually transformed into heat by internal friction. It is possible to drive currents simply by cooling, but only a small fraction of the thermal-energy flux is actually retrieved by the

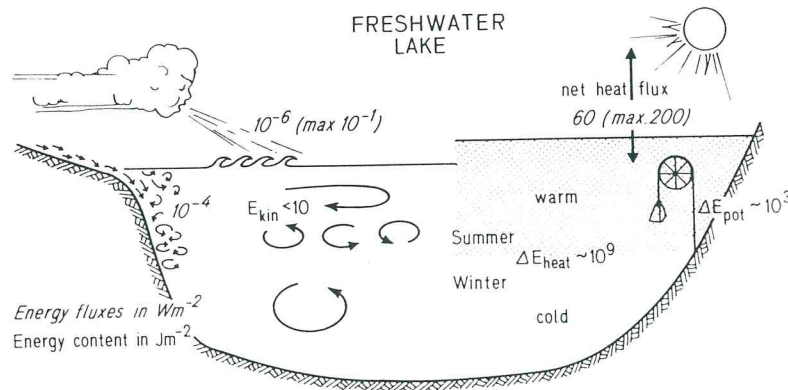


Fig. 3. Typical magnitudes of the energy contents and energy fluxes in a freshwater lake. The thermal energy amplitude, ΔE_{heat} , corresponds to the annual variation between winter and summer. Potential energy, ΔE_{pot} ,

describes the effect of density stratification. In saline lakes ΔE_{pot} can attain values 2 to 3 orders of magnitude greater than in freshwater lakes

kinetic energy of the flow. Energy transformations are directional and to a large extent irreversible, and therefore a simple comparison of the numbers alone does not reveal the roles played by different energy terms. We now discuss various energy fluxes in greater detail.

5.1 Thermal Energy

The net heat exchange H_{net} between atmosphere and water consists of seven main components (Fig. 4):

$$H_{\text{net}} = H_S + H_A + H_W + H_E + H_C \\ + H_P + H_I. \quad [\text{W m}^{-2}] \quad (42)$$

These terms are defined as positive when directed into the water. They describe the radiative heat fluxes due to solar radiation (H_S) and to the infrared radiation emitted from the sky (H_A) and from the surface of the water (H_W), the nonradiative heat fluxes due to evaporation/condensation (H_E) and convection (H_C), precipitation onto the water surface (H_P), and the effect of the throughflow of water by inlets and outlets (H_I).

The three radiative heat-flux terms are the largest. Two well-separated wavelength domains can be distinguished here: the visible range (wavelength $\approx 0.4\text{--}0.7\mu\text{m}$), to which the solar radiation H_S belongs, and the infrared range (a wavelength of approximately $10\mu\text{m}$) of the radiation from sky and water surface (H_A and H_W).

The radiative fluxes can be understood on the basis of the physical principles that describe the energy and wavelength distribution of radiation from a surface of (absolute) temperature T . The law discovered by Josef Stefan and Ludwig Boltzmann relates the total amount of energy H_{rad} radiated by a so-called black body per unit surface per unit time to its absolute surface temperature T as follows:

$$H_{\text{rad}} = E\sigma T^4, \quad [\text{W m}^{-2}] \quad (43)$$

where $\sigma = 5.67 \times 10^{-8} \text{ W m}^{-2} \text{ K}^{-4}$ is known as the Stefan-Boltzmann constant. The emissivity E of a body is unity in the case of a black body and less than unity for natural surfaces.

Empirical expressions for flux terms are summarized in Table 4. The infrared terms H_A and H_W are formulated according to the Stefan-Boltzmann law (Eq. 43). Water is nearly a black body (emissivity $E_W \approx 0.97$), but E_A is more variable, because the atmosphere is not a homogeneous body. E_A increases with air temperature, moisture content, and cloud cover. Empirical relationships are given by Swinbank (1963) and Brutsaert (1975).

In order to demonstrate the relative importance of the different terms, the mean seasonal variation of the various fluxes is plotted in Fig. 5 for the average meteorological conditions calculated for Lake Zurich (Switzerland) by Kuhn (1979). If real meteorological data from a specific year are used instead, the terms H_S , H_E , H_C , and H_P fluctuate greatly about their means, whereas H_A

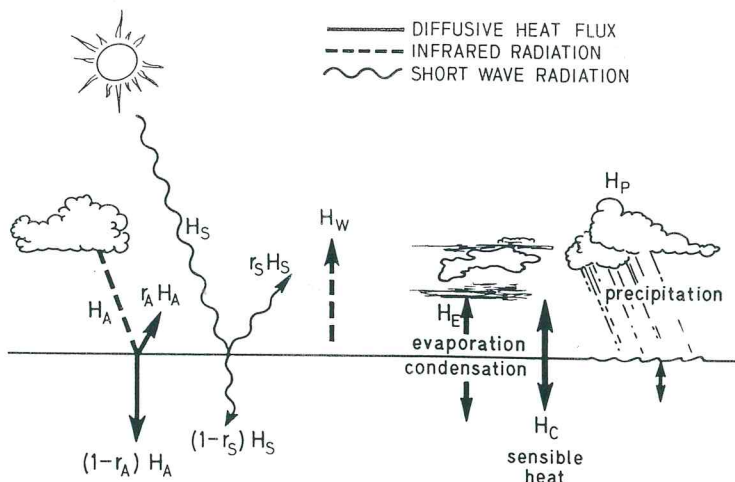


Fig. 4. Heat exchange processes between water and atmosphere (see Eq. 42 and Table 4 for definitions). Not shown here is the term H_I , which describes the influence of inflows and outflows on the heat balance

Table 4. Thermal energy fluxes at water surface

Shortwave radiation from sky (direct and diffuse)	
$H_S = (1 - r_S) H_S^O f_S (C)$	
$H_S^O [W m^{-2}]$	Clear-sky solar radiation
$r_S (C) [-]$	Reflection of shortwave radiation from water surface. Typical values lie between 0.04 (June) and 0.20 (December)
$f_S (C) = 1 - 0.65 C^2$	Shading by clouds; empirical relationship of Barry and Chorley (1976)
C	Relative cloud cover of sky
Infrared radiation from sky	
$H_A = (1 - r_A) E_A \sigma T_A^4$	
$r_A [-]$	Reflection of infrared radiation from water surface; typical value 0.03
$E_A [-]$	Emissivity of atmosphere; empirical relations by Swinbank (1963) and Brutsaert (1975); typical values between 0.6 and 0.9
$\sigma = 5.67 \times 10^{-8} W m^{-2} K^{-4}$	Stefan-Boltzmann constant
$T_A [K]$	Absolute temperature of the atmosphere
Infrared radiation from the water surface	
$H_W = -E_W \sigma T_W^4$	
$E_W [-]$	Emissivity of water, approximately 0.97
$T_W [-]$	Absolute temperature of water surface
Flux of sensible heat (convection)	
$H_C = -f(u, \dots) (T_W - T_A)$	
$f(u, \dots) [W m^{-2} K^{-1}]$	Transfer function depending on wind velocity u and other meteorological parameters; typical values lie between $3 W m^{-2} K^{-1}$ ($u \approx 0$) and $15 W m^{-2} K^{-1}$ ($u \approx 10 m s^{-1}$)
Flux of latent heat (evaporation, condensation)	
$H_E = -f^*(u, \dots) (e_W - e_A)$	
$e_W [mbar]$	Water vapor saturation pressure at temperature of water T_W ; value reduced in saline waters
$e_A [mbar]$	Atmospheric water-vapor pressure
$f^*(u, \dots) [W m^{-2} mbar^{-1}]$	Transfer function Note: f/f^* (Bowen coefficient) is roughly constant ($\approx 0.61 mbar K^{-1}$)

Heat fluxes directed from air to water are defined as positive.

and H_W are more stable (Marti and Imboden 1986). In addition, superimposed on the meteorologically induced variations are the diurnal cycles, which, obviously, are especially pronounced in the case of the solar shortwave radiation H_S .

It should also be mentioned that the influence on H_{net} of precipitation onto the lake surface (H_P) is only rarely significant. Changes in surface temperature T_W during rainy weather are usually the result of changes in the flux terms H_W , H_C , and H_E . Also, the heat imported into the water body by inflows and exported via the outlet (H_I) are only of importance in lakes with very high flushing rates.

The geothermal heat flux represents another source of thermally driven mixing. Although usually very small (typically $\approx 0.1 W m^{-2}$), it influences water temperature in those deep zones

that are often only slightly, or not at all, affected by the surface heat flux H_{net} . As shown in Sections 6.4 and 6.5, the stratification and mixing of hypolimnetic water can be dominated by exceptionally strong geothermal heat fluxes.

5.2 Potential Energy

As in the case of thermal energy there is no absolute definition of potential energy; we deal rather with changes in energy. The potential energy contained in a stratified water column can be defined as the potential energy difference relative to the situation in which the same water is homogeneously mixed. To characterize changes in potential energy two kinds of quantities are defined, viz., the buoyancy flux J_b (a local quan-

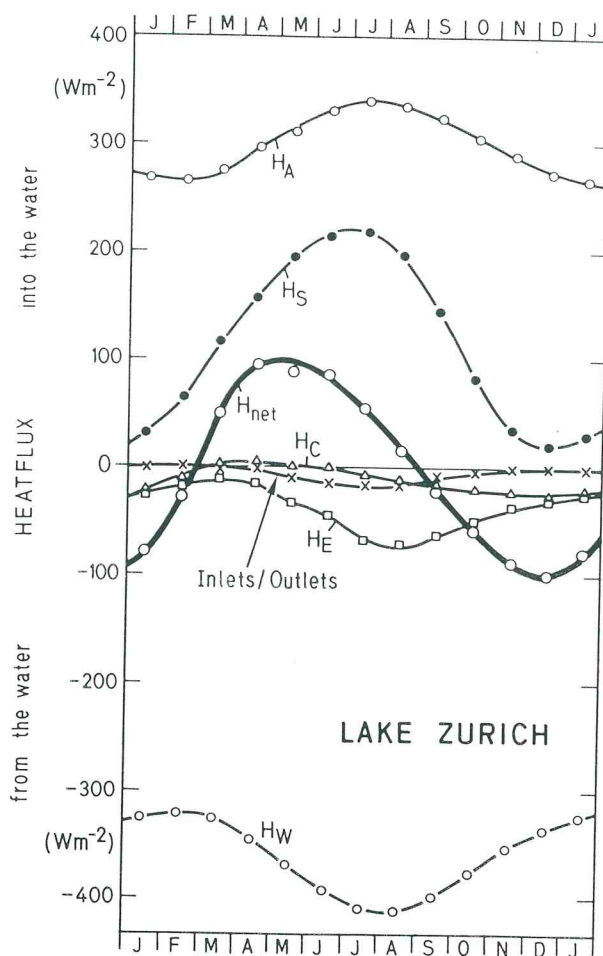


Fig. 5. Monthly mean heat fluxes [W m^{-2}] between water and atmosphere calculated for Lake Zurich (Switzerland) from average meteorological conditions. See Table 4 for definitions of the terms. H_i is given by the curve marked *Inlets/Outlets*. (Redrawn from Kuhn 1979)

ity) and the mixed-layer buoyancy fluxes J_b^o and J_b^b (bulk quantities). J_b^o is defined for the surface layer and J_b^b for the benthic boundary layer.

The *buoyancy flux* J_b quantifies the production of potential energy, due to density changes within the water column. It is related to the local vertical exchange of water masses of different density, which, in turn, can be expressed in terms of the local vertical turbulent diffusivity K_z^o and the local stability frequency N (Table 5). A negative J_b increases the potential energy of the water column by extracting energy from turbulent currents. Therefore, turbulent mixing in a stably stratified water column always produces a negative buoyancy flux. In contrast, if heavier water is trans-

ported downward (convective mixing), J_b is positive, and turbulent kinetic energy is produced.

The *surface buoyancy flux* J_b^o is due to the rate of change of density, $d\rho/dt$, of a well-mixed surface layer of depth h_{mix} (Table 5). It is defined as positive if the surface water is contracting, i.e., if ρ is increasing. Again, a positive J_b^o feeds energy into the water currents and increases mixing. A density change $d\rho$ causes a corresponding change in the mixed layer depth of $dh = -(h_{\text{mix}}/\rho)d\rho$. As a result the center of gravity of the mixed-water column is displaced vertically by an amount $dh/2$. Thus, the change in potential energy per unit area per unit time, P_{pot} , is related to J_b^o by

$$P_{\text{pot}} = \frac{dE_{\text{pot}}}{dt} = -\frac{1}{2} g h_{\text{mix}}^2 \frac{d\rho}{dt}$$

$$= -\frac{1}{2} \rho h_{\text{mix}} J_b^o \quad [\text{W m}^{-2}] \quad (44)$$

The following processes result in a positive buoyancy flux: cooling of the surface water if $T > T_{\rho_{\text{max}}}$, warming of the surface water if $T < T_{\rho_{\text{max}}}$, evaporation from a salt lake, freezing at the surface of a salt lake, and the inflow of river water (note that the density of the river water can be high because of low temperature, high salinity, high concentration of suspended particles, or a combination of these factors).

The “inverse” processes will obviously result in negative buoyancy fluxes. Specifically, the addition of fresh water to the surface of a salt lake, e.g., by precipitation, river input, or melting of ice at the surface of salty water, will give rise to a negative buoyancy flux.

The *bottom buoyancy flux* J_b^b , referring to the well-mixed layer that is frequently observed at the bottom of a lake (the benthic boundary layer; see Sect. 6.4), can be defined analogously (Table 5). Note that now J_b^b is positive if less dense water is added to the lake bottom, because such water can rise spontaneously, producing turbulence. An example of the production of positive-bottom buoyancy flux is the input of geothermal heat (if $T > T_{\rho_{\text{max}}}$), whereas the addition of cold, salty (i.e., denser) spring water at the bottom of a lake results in a negative bottom buoyancy flux.

5.3 Kinetic Energy

Water in a lake is never at rest. Currents are induced by the wind acting at the water surface,

Table 5. Buoyancy flux, Richardson Numbers, and Monin-Obukhov Length

Buoyancy flux J_b	$J_b = -\overline{uw' \rho'} \frac{g}{\rho} = K_z'' \frac{g}{\rho} \frac{d\rho}{dz} = -K_z'' N^2$	$[W kg^{-1}]$
$K_z'' [m^2 s^{-1}]$	Vertical turbulent diffusion coefficient for density	
$N = \left(-\frac{g}{\rho} \frac{d\rho}{dz} \right)^{1/2} [s^{-1}]$	Stability (Brunt-Väisälä) frequency ^a	
Surface buoyancy flux J_b^o		
$J_b^o = \frac{gh_{mix}}{\rho} \frac{d\rho}{dt}$		$[W kg^{-1}]$
$g = 9.81 m s^{-2}$	Acceleration due to gravity	
$h_{mix} [m]$	Depth of (homogeneous) layer at surface with density ρ	
If $d\rho$ is due to temperature change dT caused by heat flux at water surface H_{net} ,		
$J_b^o = -\alpha g h_{mix} \frac{dT}{dt} = -\frac{\alpha g}{c_p \rho} H_{net}$		$[W kg^{-1}]$
$\alpha [K^{-1}]$	Thermal expansion coefficient of water	
$c_p [J kg^{-1} K^{-1}]$	Specific heat of water at constant pressure ($4180 J kg^{-1} K^{-1}$)	
$H_{net} [W m^{-2}]$	Net heat flux at water surface (positive, if directed into the water)	
If $d\rho$ is due to change of salinity S caused by evaporation or precipitation,		
$J_b^o = gh_{mix} \beta_S \frac{dS}{dt} = \frac{g \beta_S S}{\rho} m_E = -\frac{g \beta_S S}{\rho \lambda_e} H_E$	^b	$[W kg^{-1}]$
$\beta_S [-]$	Coefficient of haline contraction	
$m_E [kg m^{-2} s^{-1}]$	Evaporation rate (or precipitation onto lake surface if $m_E < 0$)	
$H_E [W m^{-2}]$	Heat flux due to evaporation (H_E negative for positive m_E)	
$\lambda_e [J kg^{-1}]$	Latent heat of evaporation of water	
Flux Richardson Number R_f (used for $J_b < 0$)		
$R_f = -J_b/J_R$	$[-]$	
$J_R = -\overline{u'w'} \frac{\partial u}{\partial z}$ $[W kg^{-1}]$	Rate of production of turbulent kinetic energy due to Reynolds' stress (see Eqs. 50 and 51)	
Monin-Obukhov Length L_M^c		
$L_M = -\frac{u_*^3}{k J_b^o}$	$[m]$	
$u_* [m s^{-1}]$	Friction velocity (see Eq. 62)	
$k = 0.41$	von Kármán constant	
Gradient Richardson Number R_i		
$R_i = \frac{N^2}{(\partial u / \partial z)^2}$	$[-]$	
$u [m s^{-1}]$	Horizontal current velocity	

All definitions are made for a Cartesian coordinate system with its vertical axis z defined as positive upward.

^a N is defined for stable stratification only, i.e., for $\frac{d\rho}{dz} < 0$.

^b Replace S/β_S by $\kappa_{20}\beta_k$ if salinity is expressed by electrical conductivity κ_{20} (Eq. 35).

^c Note that for *positive* J_b^o (condition of convection), L_M is negative and defines a depth at which the buoyancy flux and wind shear are of equal importance for the production of turbulent kinetic energy (TKE). Below this depth buoyancy is the dominant source of TKE. For *negative* J_b^o (stabilizing conditions), L_M is positive and defines the depth to which the wind shear can mix the water column against the stabilizing effect of the density stratification, which is produced either by warming or by input of less saline water.

by inflows, by density gradients caused by differential heating and cooling, or by varying concentrations of dissolved substances (see Sect. 4.1). Strong winds during storm events are often the largest source of kinetic energy (Fig. 3).

The wind force creates a stress τ_0 at the lake surface that is assumed to be constant within a certain layer extending from the air into the water (constant stress layer). It is difficult to measure τ_0 directly; therefore, it is commonly parameterized by the square of the wind speed, W_{10} , measured at a standard height of 10 m above the water surface:

$$\tau_0 = \rho_{\text{air}} C_{10} W_{10}^2, \quad [\text{N m}^{-2}] \quad (45)$$

where ρ_{air} is the density of air ($\approx 1.2 \text{ kg m}^{-3}$ at 20°C) and C_{10} is the so-called drag (or wind stress) coefficient, which has been the subject of a great number of experimental investigations. Not very surprisingly, it appears that C_{10} is not really a constant, because the coupling between air and water depends on the roughness of the interface, i.e., on the wave field. In the ocean or in large lakes, C_{10} is expected to be larger than in a small lake. Also, because wave heights increase with increasing wind speed, C_{10} should be larger for large W_{10} . Based on data from numerous investigators Amorocho and DeVries (1980) identified three wind-speed regimes for C_{10} . For $W_{10} \leq 7 \text{ m s}^{-1}$, where the wind waves do not break, C_{10} is approximately 0.001; in an intermediate regime, characterized by the onset of breaking waves, C_{10} increases steadily up to a value of 0.0025 at $W_{10} = 17$ to 20 m s^{-1} ; and at higher wind speeds breaker saturation is attained and C_{10} becomes constant.

Connected with the stress τ_0 acting on the lake surface is an energy flux from the atmosphere down to the air-water interface. At a height of 10 m above the water surface the energy flux, P_{10} , is given by

$$P_{10} = \tau_0 W_{10} = \rho_{\text{air}} C_{10} W_{10}^3, \quad [\text{W m}^{-2}] \quad (46)$$

It is generally found that a small fraction χ of approximately 1–2% of P_{10} is transferred to the water and is available for mixing in the surface layer (Denman and Miyake 1973). Thus, the kinetic energy flux from the wind field into the lake is

$$P_{\text{kin},W} = \chi \rho_{\text{air}} C_{10} W_{10}^3 = \eta W_{10}^3, \quad [\text{W m}^{-2}] \quad (47)$$

where $\eta = \chi \rho_{\text{air}} C_{10}$ typically lies between 1 and $5 \times 10^{-5} \text{ kg m}^{-3}$. (Note that when η is expressed in

kg m^{-3} and W_{10} in m s^{-1} , $P_{\text{kin},W}$ will be expressed in W m^{-2} .)

The vertical structure of mixing, characterized by the production of turbulent kinetic energy, is related to the vertical-shear profile, which is the result of the wind-induced energy flux. The dependence of mixing in the surface layer on the wind stress is discussed in Section 6.2.

Rivers entering a lake are another external source of kinetic energy, which, if normalized by the lake surface area, can be expressed as

$$P_{\text{kin},R} = \frac{1}{2} \rho q \bar{u}_R^2, \quad [\text{W m}^{-2}] \quad (48)$$

where $q [\text{m s}^{-1}]$ is the inflow of water per unit lake area (hydraulic loading) and \bar{u}_R^2 is the mean square water velocity at the river mouth. In order for $P_{\text{kin},R}$ to reach a size comparable to the effect of a continuous wind speed of, say, $W_{10} = 1 \text{ m s}^{-1}$ (say, 1% of $P_{10} = 1.2 \times 10^{-5} \text{ W m}^{-2}$), assuming a typical $\bar{u}_R^2 = 0.25 \text{ m}^2 \text{s}^{-2}$, the hydraulic loading q has to be on the order of 12 m yr^{-1} , a value attained by an appreciable number of freshwater lakes (Table 1). Thus, from a purely energetic point of view inflows are important; however, their kinetic energy undergoes a great degree of local dissipation, and so inflows affect lake dynamics differently than does the wind, which acts on the whole lake surface.

5.4 Turbulent Kinetic Energy Balance in Stratified Water

As stated in the introduction, mixing results from the turbulent part of the advective motion. In contrast to the mean flow, turbulence is nondirectional, although it may be anisotropic. Thus, the turbulent kinetic energy (TKE), defined by

$$\text{TKE} = \frac{1}{2} \sum_i \bar{u}_i'^2, \quad (49)$$

is the relevant property to describe turbulent mixing. As discussed in Section 3.2 the separation of mean flow from turbulent velocity fluctuations (Eq. 11) is arbitrary to a certain extent, and inherently selects some time and space scale, which, in turn, depends on the system and process under consideration. Such scales are discussed in Section 7.1.

Let us assume that the appropriate scale can be chosen. The momentum equation can then be

used to derive a dynamic equation for TKE similarly to the way the expression for the mean flow (Eq. 12) was derived by Reynolds' decomposition (e.g., see Stull 1988 for details). For homogeneous conditions (no spatial gradients of TKE), one obtains the following expression ($i, j = \text{Cartesian coordinates } x, y, z; z \text{ positive upward}, v \text{ viscosity}$):

$$\frac{\partial}{\partial t} (\text{TKE}) = - \sum_{ij} \overline{u'_i u'_j} \frac{\partial \bar{U}_i}{\partial x_j} - \overline{\rho' u'_3} \frac{g}{\rho} \quad (1) \quad (2)$$

$$-v \sum_{ij} \left(\frac{\partial u'_i}{\partial x_j} + \frac{\partial u'_j}{\partial x_i} \right) \frac{\partial u'_i}{\partial x_j}. \quad [W \text{ kg}^{-1}] \quad (3) \quad (50)$$

The terms on the right side describe the sources and sinks of the turbulent kinetic energy (see also Table 5). For horizontal mean flow along the x axis ($\bar{U}_1 \equiv U, \bar{U}_2 = \bar{U}_3 = 0$, and $u'_3 \equiv w'$), and for homogeneous and isotropic turbulence, the three terms take on the following simple forms:

1. Rate of production of TKE (J_R) due to the Reynolds' stress:

$$J_R = -\overline{u' w'} \frac{\partial U}{\partial z} \quad (51)$$

2. Buoyancy flux (J_b ; change of potential energy of the water column):

$$J_b = -\overline{\rho' w'} \frac{g}{\rho} = K_z \frac{\partial \rho}{\partial z} \frac{g}{\rho} = -K_z N^2 \quad (52)$$

3. Rate of dissipation of TKE (ε) by viscous (internal) friction:

$$\varepsilon = 7.5v \left(\frac{\partial u'}{\partial z} \right)^2 \quad (53)$$

(The factor 7.5 applies to the special situation, which is assumed here.) Thus, for homogeneous turbulence the temporal change in TKE is due to the balance of TKE production from the mean flow J_R (through the Reynolds' stress), the buoyancy flux J_b , and the TKE dissipation ε by viscous forces:

$$\frac{\partial}{\partial t} (\text{TKE}) = J_R + J_b - \varepsilon. \quad (54)$$

Note that J_R and ε are always positive, whereas J_b can take on either sign. For $J_b < 0$, mixing is "against the density gradient," and the potential energy of the water column is increased, whereas

for $J_b > 0$, TKE is produced by the sinking of heavier or rising of lighter water parcels (convective turbulence). For turbulence produced by Reynolds' stress it is common to define a ratio expressing the consumption of TKE by the storage of potential energy, J_b , relative to the production of TKE. Two quantities are defined to describe the efficiency of the transfer to buoyancy flux, the Flux Richardson Number (Table 5)

$$R_f = -J_b/J_R, \quad (55)$$

and the *mixing efficiency*

$$\gamma_{\text{mix}} = -J_b/\varepsilon = K_d N^2/\varepsilon. \quad (56)$$

For stationary conditions Eq. (54) can be written as $\varepsilon = J_R + J_b$. Thus, the mixing efficiency can be expressed as $\gamma_{\text{mix}} = R_f/(1 - R_f)$.

Only a small fraction of the available kinetic energy is used for mixing against the density gradient and is transferred into potential energy, because turbulent motion cannot efficiently generate low-entropy potential energy. Furthermore, viscous dissipation occurs in each velocity component, whereas the production of negative buoyancy occurs only via the diapycnal component. Experimentally, γ_{mix} has been found to lie within the range 0.05–0.25 depending on the mixing regime (Sect. 6.3).

This concept has also occasionally been used for negative buoyancy flux produced by the increase in stability resulting from heating of the water column (Sect. 6.2). In this case R_f is the ratio of the TKE suppressed by the negative buoyancy flux, due to heating to the TKE production J_R . In the well-mixed surface layer this approach serves to calculate the dynamics of the depth of the mixed layer (Sect. 6.2).

5.5 Internal Turbulent Energy Fluxes: Turbulence Cascade

Equation (50) expresses the TKE balance regardless of the spatial and temporal scales among which it is distributed. In order to understand the consequences of the Reynolds' decomposition (Eq. 11), we should also address the question of how the TKE is typically distributed in space and time. Energy is brought into lakes at different length scales. Major turbulent production by Reynolds' stress occurs at large scales, termed the *energy-containing range*, where a significant part of the energy input also occurs. Energy is generally

transferred from low to high frequencies and from large to small scales. This flow, called the *turbulence cascade*, is generated by nonlinear interactions originating in the nonlinear term of the momentum Eq. (5). At the smallest scales, given by the Kolmogorov Scale $L_K = (v^3/\epsilon)^{1/4}$, the turbulent kinetic energy is converted into heat by molecular viscosity v . According to L_K the size of the smallest existing eddies depends only on the level of turbulence (and the viscosity): A higher level of turbulence is able to produce smaller scales before the energy dissipates. In summary, isopycnal eddy sizes cover a range extending from the size of the lake itself down to a few millimeters. A summary of the various relevant scales describing turbulence is given in Table 6.

Under isotropic, homogeneous, and stationary conditions a range of eddy size develops in which

the spectrum of turbulent kinetic energy is independent of both the production of TKE and the energy dissipation due to viscosity. If energy is neither added by the mean flow nor removed by viscous dissipation, the energy flux across the so-called *inertial subrange* is constant and equal to the energy dissipation rate at the small-scale end of the spectrum. The spectrum of turbulent kinetic energy $E(k)$ depends only on the dissipation rate ϵ . $E(k)dk$ is the energy of eddies with wave numbers between k and $k + dk$ ($k = 2\pi/\text{length of eddy}$). Dimensional analysis yields

$$E(k) = \alpha \epsilon^{2/3} k^{-5/3}. \quad [\text{W kg}^{-1} \text{ m s} = \text{m}^3 \text{ s}^{-2}] \quad (57)$$

Experimental determination put the value of the nondimensional constant α at approximately 1.56 (Wyngaard and Cote 1971). Because of the re-

Table 6. Turbulence length scales

Length scale	Definition	Typical range	Significance
Energy-containing	L_i	1 to 10^3 m	Scale at which energy is brought into system, e.g., length scale of lake for seiches, mixed-layer depth for surface mixing
Kolmogorov	$L_K = (v^3/\epsilon)^{1/4}$	10^{-3} to 10^{-2} m	Viscous force equals inertial force: lower end of TKE and dissipation spectra, i.e., velocity fluctuations (gradients) disappear for smaller scales
Batchelor	$L_B = (vD^2/\epsilon)^{1/4}$	$\approx 10^{-4}$ (salt) to $\approx 10^{-3}$ m (temperature)	Lower end of dissipation spectrum of a passive scalar (temperature, salt, etc.): fluctuations (gradients) of the scalar disappear for smaller scales
Ozmidov	$L_O = (\epsilon/N^3)^{1/2}$	10^{-2} to 1 m	Buoyancy force equals inertial force: maximum vertical scale of eddies; larger eddies are suppressed by buoyancy
Thorpe-displacement	Δ_T		Absolute vertical displacement of a water parcel from its "equilibrium position" in the corresponding smooth and stable (reordered) profile
Thorpe	$L_T = (\overline{\Delta_T^2})^{1/2}$		Root mean square of Thorpe displacements Δ_T within a water column: L_T is a statistical measure for the vertical size of the overturning eddies
Monin-Obukhov length	$L_M = -\frac{u_*^3}{k J_b^0} =$	1 to 10^2 m	Depth (height) where production of TKE by shear is equal to production of TKE by buoyancy flux

Definitions and typical sizes of relevant parameters:

v , kinematic viscosity, 1 to $2 \cdot 10^{-6} \text{ m}^2 \text{ s}^{-1}$; ϵ , rate of dissipation of TKE, 10^{-10} to $10^{-7} \text{ m}^2 \text{ s}^{-3}$ (W kg^{-1}); N , stability frequency, 10^{-3} to 10^{-2} s^{-1} (deep hypolimnion down to 10^{-4} s^{-1}); D , molecular-diffusion coefficient of scalar property (temperature, salt, etc.), 10^{-10} to $10^{-9} \text{ m}^2 \text{ s}^{-1}$ for salt and $\approx 1.4 \cdot 10^{-7} \text{ m}^2 \text{ s}^{-1}$ for temperature.

quired isotropy, the inertial subranges are restricted to nonstratified water layers such as the well-mixed boundary layers (the epilimnion and the bottom boundary layer), and consequently extend only over a range of several meters to decimeters. In Fig. 6 an example is given for Lake Tahoe (Dillon and Powell 1979).

A conservative scalar property (salt, temperature, etc.) mixed by a turbulent flow produces a fluctuation spectrum that again covers the range from the energy-containing eddies to the smallest scales limited by molecular properties. The smallest scales not only depend on ε and v (as does L_K), but also on the molecular diffusivity D of the scalar. The corresponding scale, often called the *Batchelor Scale*, $L_B = (vD^2/\varepsilon)^{1/4}$, is smaller than L_K , because the molecular diffusivities, D^T and D^C , are always smaller than v . For wave numbers k well below L_B^{-1} , the molecular diffusivity of heat or salt does not influence the spectrum very much; therefore, the spectra are similar to the velocity spectrum $E(k)$, which falls off proportional to $k^{-5/3}$ (inertial-convective subrange). For smaller scales, velocity fluctuations

are reduced progressively by viscosity, but the diffusivity of heat or salt is not yet effective (viscous-convective subrange). This part of the spectrum, also called the *Batchelor Spectrum* (Batchelor 1959), is depicted in Fig. 6 as the range in which $E(k)$ falls off proportional to k^{-1} . Its upper limit is determined by $k = L_B^{-1}$.

Large eddies tend to be anisotropic, because their structure is related to the energy input. Successive interaction between the three space components redistributes the turbulent kinetic energy equally among the components, leading to progressive isotropy at smaller scales. Because of stratification, however, complete isotropy is seldom attained, not even at the smallest scales. For the dissipation range ($k \sim L_K^{-1}$) to be isotropic, Gargett et al. (1984) found that the turbulence level ε has to obey the condition $\varepsilon > 200 vN^2$. This means that the stronger the stratification (expressed by N) and the higher the viscosity (expressed by v) of the water, the larger the critical size of ε .

6 Mixing Processes in Lakes

In density-stratified lakes small-scale turbulence is essential for energy and mass transfer. Although the energy is brought into the system at much larger scales, it is the small-scale turbulent motion that brings different water masses in close enough contact for mixing by viscosity and diffusivity to occur (Eckart 1948). In addition, in density-stratified water only small-scale eddies can exist. Because of space limitations, this section concentrates on these small-scale processes. Descriptions of additional phenomena may be found in other textbooks (e.g., Imberger and Patterson 1990).

In lakes two principal sources of turbulent kinetic energy (TKE) in Eq. (54) have to be considered, viz., Reynolds' stress J_R and buoyancy flux J_b . Because dissipation ε is the main TKE sink, ε is a quantitative measure of the rate of production of TKE, and is therefore characteristic of the level of turbulence. In the absence of stratification ($N = 0$) and for homogeneous and steady conditions, the TKE equation (Eq. 54) states that the rate of production of turbulence is equal to its dissipation rate. Explicitly, this implies that $J_R = \varepsilon$ in the surface and bottom boundary layers, and $J_b = \varepsilon$ for convectively driven surface mixing and double diffusion. Usually, however,

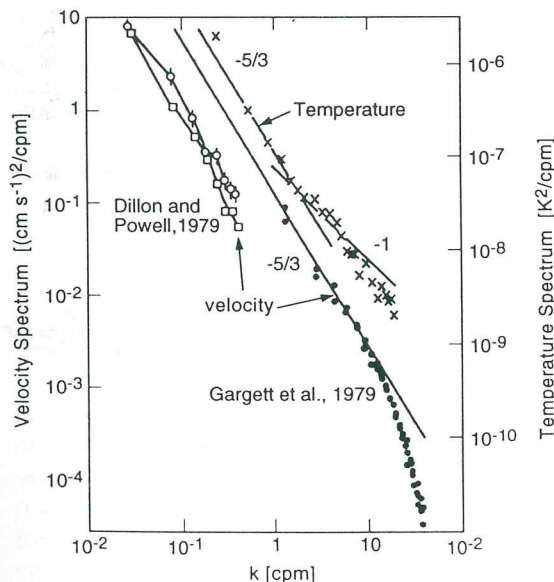


Fig. 6. Velocity and temperature spectra measured in the surface mixed layer of the ocean by Gargett et al. (1979). Because of viscosity, at $k > 10 \text{ cpm}$ (cycles per meter) the velocity spectrum drops below the $k^{-5/3}$ line. The cutoff in the temperature spectrum (Batchelor wave number), located just above the upper end of the plotted points, is not resolved. The two lowest curves represent the velocity spectra observed by Dillon and Powell (1979) in the mixed layer of Lake Tahoe

most of the water column is stratified to some extent. Because the mixing of stratified water always results in an increase in potential energy, the buoyancy flux also has to be included as a (minor) sink of TKE in Eq. (54).

Because of the large diversity in the characteristic properties of lakes, the basic sources of mixing can lead to very different mixing phenomena in real situations. Some of these are outlined schematically in Fig. 7. In any given lake the relevant mixing processes depend on external forcing (river inflow and outflow, turbidity currents, underwater springs, wind, surface heat flux, geothermal heat flux, etc.) as well as lake morphometry (boundary mixing, differential heating/cooling/mixing, etc.). The goal of this chapter is to describe the most important mixing mechanisms. Specific examples are added for illustration. We start with an overview of the various types of waves occurring in lakes, because waves play a crucial role in energy storage and also act as the link between the input of energy and the production of turbulence.

6.1 Waves and Mixing

6.1.1 "Wave Zoo" in Lakes

Immediately apparent to any observer are lake-surface gravity waves. These are, however, only one of many types of wave existing in lakes, some of which have practically no effect on the water surface. For wave motion to exist two forces are required: one tending to initiate motion and one tending to restore equilibrium. Different equilibria and restoring forces give rise to numerous types of waves (Lighthill 1978). Waves in lakes are excited mostly by wind stress. In larger lakes, however, atmospheric pressure changes and tidal forces can be important as well. Although rare, waves of exceptionally large amplitude can be induced by seismic activity and landslides (Bünti 1914; Siegenthaler and Sturm 1991).

Waves are usually categorized with regard to equilibrium state and restoring force (Table 7). A lake water body can oscillate at its surface and internally about surfaces of equal density. Because in the latter case the surfaces of constant density do not coincide with the surfaces of constant pressure, these internal waves are referred to as *baroclinic*. In contrast, surface waves are referred

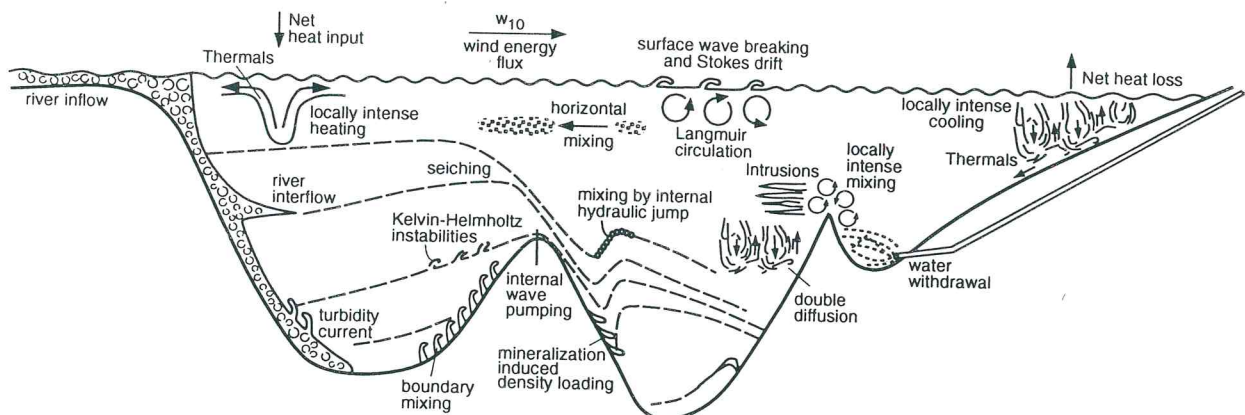


Fig. 7. Schematic overview of mixing processes in lakes. Wind introduces kinetic energy and produces turbulence by means of surface waves and drift-shear (Stokes' drift) in a relatively thin surface layer of typically a few meters of thickness (Fig. 9a). This layer is also subject to vertical Langmuir circulation if the wind speed exceeds approximately 3 m s^{-1} . Convective mixing, driven by density production (usually cooling), efficiently mixes the surface layer by causing the sinking and rising of water parcels (thermals). A decrease in density (usually brought about by heating) stabilizes the water column and consequently suppresses vertical

exchange. Waves (internal seiches; Fig. 8) are activated by the wind and lead to horizontal currents (Fig. 14a), and, therefore, to internal mixing (Fig. 12), and especially to boundary mixing (Fig. 14b). The subsequent small-scale (eddy-type) turbulent diffusion (Fig. 11) recycles nutrients and affects the exchange through the sediment-water interface. Density currents, e.g., turbidity flow from tributaries or currents stimulated by differential mixing (or heating/cooling), transport water masses vertically and horizontally on a basinwide scale (Fig. 22).

Table 7. "Wave zoo" in lakes

Wave	Restoring force	Characteristics of governing wave equation	Dispersion relation
Capillary	Surface tension		$k^3 = \frac{\rho}{\delta} \omega^2$
Surface gravity	Gravity	First class, barotropic	$\tanh(kH) = \omega^2/gk$ long: $k^2 = \omega^2/gH$ short: $k = \omega^2/g$
Internal gravity	Gravity in density-stratified fluid	$\rho = \text{variable}$	$k^2 = \frac{\omega^2 - f^2}{N^2 - \omega^2} m^2$
Inertial	Coriolis force		
Poincaré (or Sverdrup)	Gravity and Coriolis force	First class, long gravity waves affected by Coriolis force $f \neq 0, \rho = \text{const}$	$k^2 = \frac{\omega^2 - f^2}{gh}$
Kelvin	Like Poincaré, but with boundary conditions	$f = \text{const}, \text{depth } H = \text{const}, u_{\text{boundary}} = 0$	$k = \frac{\omega}{\sqrt{gH}}$
Planetary or Rossby	Gravity, Coriolis force; potential vorticity	Large scale, long period, 2nd class, f linear approximation of $\phi, \rho = \text{const}, H = \text{const}$	$k^2 = -\frac{\beta k}{\omega}$
Topographical Rossby waves	Gravity, Coriolis force; potential vorticity	Similar to Rossby waves, but water depth $H \neq \text{const}$	

Definitions: First class: gravity waves modified by rotation; Second class: variation of potential vorticity; ω , wave frequency; ρ , density of water; k , horizontal wave numbers; m , vertical wave number; N , buoyancy frequency; H , water depth; δ , surface tension; $f = 2\Omega \sin \phi$, inertial frequency ($\Omega = 7.27 \cdot 10^{-5} \text{ s}^{-1}$); ϕ , geographical latitude; $\beta = (2\Omega/R) \cos \phi$, change of f with latitudinal distance (R = earth radius).

Variables for two-layer Merian Formula (Eq. 58):

$$g' = \frac{\Delta\rho}{\rho} g \quad \text{Reduced gravity } (\Delta\rho: \text{density difference between layers}).$$

$$h' = h_1 \cdot h_2 / (h_1 + h_2) = [(1/h_1) + (1/h_2)]^{-1} \quad \text{Reduced depth } (h_1, h_2: \text{depth of layers}).$$

to as *barotropic*. They do not require the existence of density gradients in the water for their excitation. The restoring forces are: surface tension (capillary waves), gravity (gravity waves), Coriolis force (inertial waves), and change of potential vorticity (Rossby waves). Change of potential vorticity can be due either to a change in inertial frequency (planetary waves) or to a change in basin depth (topographical Rossby waves). It is obvious that combinations of restoring forces are often present such as, for example, gravity and Coriolis force (Poincaré or Sverdrup waves). For a detailed discussion of waves in lakes the reader is referred to Mortimer (1974), Hutter (1983),

Stocker and Hutter (1987), and LeBlond and Mysak (1978).

Capillary waves, with wavelengths on the order of 1 cm, are the shortest waves present at the lake surface. Surface gravity waves are omnipresent in lakes: both short gravity waves (with wavelengths less than water depth) and long gravity waves (with wavelengths greater than water depth) are excited simultaneously. The longest surface waves are the long basin standing waves (*seiches*) first observed by Forel (1876) in Lake Geneva. This barotropic seiching motion can easily be observed with a limnigraph (water-level recorder) especially at the end of a lake, but its observation

is possible even in deep water using high-sensitivity current meters.

A water parcel moving with velocity u , assumed to be subject only to the Coriolis force, follows a circle with radius $R = u/f$, the so-called inertial circle ($f = 1.46 \times 10^{-4} \sin \phi [s^{-1}]$ is the inertial frequency and $\phi [^{\circ}]$ is the geographical latitude). Gravity waves in lakes with dimensions greater than R are affected by Coriolis forces. Poincaré waves can be observed especially in the central part of such lakes. A good example of this is given by Mortimer (1974) for Lake Michigan. Near the shore of the water basin the Coriolis force leads to another kind of wave called Kelvin waves. The amplitudes of Kelvin waves are largest at the lake shore, decaying exponentially with distance from the shore. In the northern hemisphere their direction of propagation is such that with the shore on the right, they move anticlockwise around the basin. An impressive illustration of Kelvin waves is given by Mortimer (1975).

Potential vorticity depends on both inertial frequency and total water depth. Because of the limited north-south extent of lakes, the latitude ϕ , and thus the inertial frequency f , does not change much within any one lake. However, lake topography does change much more than f ; therefore, Rossby waves, also known as topographical (Rossby) waves, can exist in lakes. In the simplest case the whole basin oscillation consists of parallel currents on opposite sides of the basin with a jet across the lake center. These low-frequency oscillations have been observed in lakes by Saylor et al. (1980) and Mysak et al. (1983; see also Fig. 8).

6.1.2 Surface-Wave Mixing

With regard to mixing (both internal and surficial), gravity waves are the most important type of wave. A glance at the surface of a lake demonstrates how surface waves cause mixing. During strong winds, breaking surface waves lead to an efficient mixing of surface water. During most of the time, however, surface waves have small amplitudes and their motions are almost reversible. In this case only little energy is lost by turbulence at the open lake surface, but some surface mixing still occurs along the shoreline. Stokes' drift is then the dominant irreversible component of wave motion, causing a horizontal net transport. Stokes' drift results from the fact that the

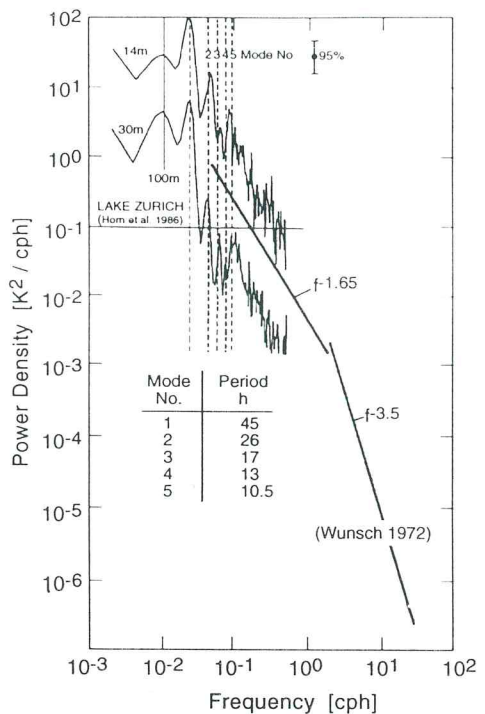


Fig. 8. Spectra of temperature fluctuations $(T')^2$ in Lake Zurich (Switzerland) by Horn et al. (1986) reveal the "red" nature of internal waves (energy drops at high frequencies). Long-term fluctuations are due principally to internal seiches. Note that the basin modes of the first vertical seiche mode (indicated by the numbers 1-5) are not harmonics in the strict sense, i.e., their periods are not whole fractions of 45 h. The maximum at 100 h may be due to topographical Rossby waves. The straight lines summarize the spectrum from temperature fluctuations measured in the thermocline of the Atlantic Ocean near Bermuda (Wunsch 1972). The internal-wave spectra from both the lake and the ocean fall off proportionally to $f^{-5/3}$. cph: Cycles per hour

orbits of the water parcels are not properly closed, because the horizontal velocity component of the orbits decreases with depth. During calm and sunny days strong temperature gradients at the very top of the water column demonstrate the absence of surface-wave mixing.

Another minor contribution to mixing comes from the internal currents associated with surface waves. Those currents, which can be observed even at the deep sediment boundary, are, however, of less importance for boundary mixing than the currents originating from internal waves. Boundary mixing generated by internal waves is discussed in Section 6.4.

6.1.3 Internal-Wave Mixing

Internal waves are crucial for mixing in the stratified water column below the energetic surface layer. They induce shear in the interior of the water column (especially in the zone between hypolimnion and epilimnion) as well as at the sediment boundary.

Internal gravity waves are mostly generated by wind. The wind stress piles up surface water at the leeward end of the lake. At the same time water from greater depth rises closer to the surface at the windward end. When the wind relaxes the tilted interface starts to oscillate. Because the solid barrier of the lake boundary reflects internal waves, the superposition of the original and reflected waves gives rise to standing internal waves called *internal seiches*. These are a prominent feature of closed basins and can be found in nearly all internal-wave spectra (Figs. 8 and 14). In addition, the internal-wave field contains a large variety of other modes with frequencies ranging from the inertial frequency f to the stability frequency N .

In a stratified fluid an infinite number of eigenvalues exists with periods $T_{n,m}$, which can be labeled with two "quantum numbers" associated with the horizontal mode (n) and the vertical mode (m). In the simplest case of the first vertical mode ($m = 1$), corresponding to a two-layer system, longitudinal oscillation periods $T_{n,1}$ and wavelength $\lambda_{n,1}$ for a basin of length L can be approximated by the generalized Merian Formula

$$T_{n,1} = \frac{2L}{n} (g'h')^{-1/2}; \quad \lambda_{n,1} = \frac{2L}{n}, \quad (58)$$

where n is the number of nodal lines and g' and h' are reduced gravity and depth, respectively, as defined in Table 7. An example of an internal-temperature spectrum that clearly shows higher horizontal modes up to $n = 5$ of the first vertical mode ($m = 1$) is given in Fig. 8. A better approximation is given by the extended Defant procedure (Mortimer 1979). Examples are given by Lemmin and Mortimer (1986). These examples (Fig. 8) show that frequencies of higher horizontal modes are not harmonics in the strict sense, as is the case in acoustics.

In order to describe higher vertical modes, a finer vertical grid is needed. An impressive example of a second vertical seiche mode ($m = 2$) (Fig. 14) has been described by Münnich et al.

(1992) using both three-layer and continuous-stratification models. An even more detailed description is given by a two-dimensional model that includes lake topography as well as a continuous stratification. Münnich (1993) has shown that several modes with similar periods and spatial scales, but differing spatial structures, become possible if both these factors are taken into account.

Internal waves produce horizontal currents in the hypolimnion that may lead to turbulent mixing provided they are strong enough to overcome the density stratification. As long as the Gradient Richardson Number R_i , which expresses the ratio of the vertical shear $\partial u / \partial z$ to the vertical density stability N (Table 5), remains much greater than approximately 0.25, turbulence, and thus mixing, is suppressed (Fig. 12). The thermocline then acts as a slippery surface permitting relative motions of the surface layer with regard to the hypolimnion. Under such conditions internal waves have relatively small amplitudes and are well within the linear range. When turbulence is nearly absent energy dissipation is low and internal waves can persist for weeks (Lemmin 1987). Internal seiches of higher vertical mode ($m > 1$) correspond to the oscillation of an $(m + 1)$ -layer system. Their amplitudes are generally smaller, but the induced horizontal currents change sign over smaller vertical scales giving rise to larger shear (Münnich et al. 1992).

For $R_i < 0.25$, streamlines become increasingly disturbed until they turn over and irreversibly mix adjacent layers (Fig. 11). In this case the energy dissipation is large and the internal-wave field decays quickly (Fig. 21). The wave-induced growth of the so-called Kelvin-Helmholtz billows, and their subsequent breakdown has been beautifully documented in natural waters with dye experiments in the Mediterranean thermocline by Woods (1968). The corresponding irreversible mixing across density interfaces is discussed in Section 6.3.

6.2 Mixing in the Surface Layer

Wind stress, surface buoyancy flux, and river inflows supply the energy required for turbulent mixing in the surface layer of a lake. Although wind stress is usually responsible for mixing in the uppermost part, the sharp density interface com-

monly found at the end of the stratification period results from the positive buoyancy flux produced by surface cooling and subsequent convection in the mixed layer. Whereas wind and convective turbulence are discussed in this section, mixing due to river inflows is not considered further, because this complicated process is beyond the scope of this chapter.

6.2.1 Wind-Driven Turbulence

As shown in Section 5.3 wind introduces turbulent kinetic energy to the lake by creating a stress τ_o acting on the lake surface (Eq. 45). This wind stress, which is usually assumed to be constant within a layer extending from the air into the water (constant-stress layer), can be expressed as

$$\tau_o = \rho_{\text{air}} \overline{u'_\text{air} w'_\text{air}} = \rho \overline{u' w'}, \quad [\text{N m}^{-2}] \quad (59)$$

where u' and w' are the horizontal- and vertical-velocity fluctuations, respectively, and the variables without indices refer to the water column. In contrast to the definition introduced in Eq. (13), the sign of τ_o is chosen in order to indicate a stress acting from the atmosphere to the water.

Based on dimensional arguments it can be shown that in the constant-stress layer at steady state, the functional dependence of the horizontal velocity u on depth h (positive downward, $h = -z$) is given by the "law of the wall":

$$\frac{\partial u}{\partial h} = -\frac{(\tau_o/\rho)^{1/2}}{kh}, \quad [\text{s}^{-1}] \quad (60)$$

where $k = 0.41$ is the von Kármán constant. Integration yields the well-known logarithmic profile

$$u(h) = -\frac{u_*}{k} \ln\left(\frac{h}{h_o}\right), \quad (61)$$

with the following definition for the friction velocity:

$$u_* = (\tau_o/\rho)^{1/2}. \quad (62)$$

According to *Fick's Second Law*, the rate of production of turbulent kinetic energy per unit mass J_R is proportional to the vertical gradient of the energy flux, $\partial(\tau_o \cdot u)/\partial z$. Within the constant-stress layer ($\partial\tau_o/\partial z = 0$), J_R is then given simply by

$$J_R = -\tau_o/\rho \frac{\partial u}{\partial h} = -\overline{u' w'} \frac{\partial u}{\partial h}. \quad [\text{W kg}^{-1}] \quad (63)$$

Inserting Eqs. (60) and (62) into Eq. (63) yields the following expression for the rate of production of TKE:

$$J_R = \frac{(\tau_o/\rho)^{3/2}}{kh} = \frac{u_*^3}{kh}, \quad [\text{W kg}^{-1}] \quad (64)$$

which is specific to the logarithmic boundary layer. For homogeneous and stationary conditions TKE production J_R and dissipation ε are in balance. In the nonstratified surface water (where buoyancy flux $J_b = 0$), production must be equal to dissipation, i.e.,

$$\varepsilon = J_R = \frac{u_*^3}{kh} = \left(\frac{\rho_{\text{air}} C_{10}}{\rho}\right)^{3/2} \frac{W_{10}^3}{kh}, \quad [\text{W kg}^{-1}] \quad (65)$$

and consequently we can estimate the level of wind-induced turbulence within the mixed layer from the wind velocity W_{10} alone.

Experimental verification of Eq. (65) is sparse. Temperature microstructure measurements in lakes carried out by Dillon et al. (1981), Imberger (1985), and Piepke et al. (unpubl.) support a relationship of the form $\varepsilon = \text{const}/h$ (Fig. 9a). Turbulence measurements made by Oakey and Elliott (1982) using the *dissipation method* (Table 8) in an ocean mixed layer are consistent with $\varepsilon = \text{const } W_{10}^3$. Measurements carried out by Lombardo and Gregg (1989) in an ocean-surface boundary layer show that dissipation rates match both the vertical decay of ε proportional to h^{-1} and the magnitude of the scaling for wind-driven turbulence. They found that the relationship

$$\varepsilon_{\text{exp}} = 1.8 \cdot \left(\frac{\rho_{\text{air}} C_{10}}{\rho}\right)^{3/2} \frac{W_{10}^3}{kh} \quad [\text{W kg}^{-1}] \quad (66)$$

gave the best fit to data measured during periods of wind-dominated turbulence. Measurements in lakes yield a coefficient somewhat smaller than 1.8 (Piepke et al. unpubl.). Although this factor (for several reasons) is not well established experimentally, the overall level of turbulence in a well-mixed and stationary surface layer can be predicted relatively well.

An epilimnion subjected to wind-stress forcing is, however, not always well mixed with regard to density. If some stability (N^2) remains the buoyancy term cannot be omitted from Eq. (50). In such cases mixing can be described by a process analogous to diffusion. The corresponding vertical eddy diffusion coefficient K_z can be estimated by assuming that at every depth a constant fraction

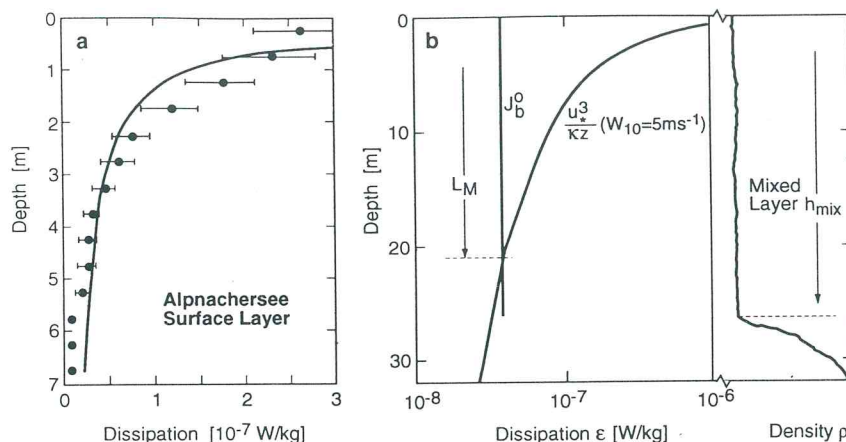


Fig. 9. a Rate of dissipation of turbulent kinetic energy ε as a function of depth as measured in Alpnachersee (Switzerland). Within the well-mixed surface boundary layer (the uppermost 5 m), dissipation follows similarity scaling within the 63% confidence level and decreases as h^{-1} (Eq. 65). In the stratified water column (below 5 m) the production of turbulent kinetic energy collapses rapidly due to decreasing shear stress τ and suppression by the stratification N^2 . (Data by Piepke et al., unpubl.) b Definition of the Monin-Obukhov Length L_M for

positive surface buoyancy flux J_b^0 (due to net heat loss at the water surface) and wind-induced turbulence ε . L_M is the depth at which the contribution to mixing from J_b^0 (constant with depth) and from the wind friction ($u^3/k \cdot h$; decreasing with depth) are equal. As a typical example, values for J_b^0 and ε were calculated from $T = 15^\circ\text{C}$, $H_{\text{net}} = -100 \text{ W m}^{-2}$, and a wind speed of 5 ms^{-1} . In this case L_M is smaller than h_{mix} , and thus entrainment at the base of the mixed layer occurs due to convection. (See text for symbols)

Table 8. Methods for estimating diapycnal eddy diffusivity

Method	Assumptions	Equation ^a	References
Budget-gradient	Rate of change of property C below z solely by local diapycnal flux (C can be replaced by T)	$K_d(z) = \frac{\int_z^{\infty} A(z') \frac{\partial C}{\partial t}(z') dz'}{A(z) \frac{\partial C}{\partial z}(z)}$	Powell and Jassby (1974)
Tracer ^b	Broadening of a tracer distribution; the vertical variance (σ^2) depends on K_d only	$K_d = \sigma^2/2t$	Numerous
Cox Number	Rate of production of temperature variance (fluctuations) by turbulence equals rate of diffusive smoothing	$K_d = 3 \cdot D_T \frac{(\partial T'/\partial z)^2}{(\partial T/\partial z)^2}$	Osborn and Cox (1972)
Dissipation	A fraction γ_{mix} of the dissipated turbulent kinetic energy ε is transformed to potential energy (buoyancy flux)	$K_d = \gamma_{\text{mix}} \varepsilon / N^2$	Osborn (1980) Oakey (1982) Gregg (1987)
Ozmidov or fine scale	Thorpe scale equals Ozmidov scale and same assumptions as dissipation method ^c	$K_d = \gamma_{\text{mix}} L_T^2 N$	Thorpe (1977) Dillon (1982) Peters et al. (1988)

^a Note that the vertical coordinate z is positive upward.

^b This method is not applicable when a nonconservative tracer (e.g., radon-222) is used in nonstationary turbulence.

^c For definition of L_T see Table 6.

γ_{mix} (Eq. 56) of the wind-produced TKE, J_R (Eq. 64), is fed into the buoyancy flux $J_b = -K_z N^2$. Thus, the dependence of K_z on wind forcing is given by

$$K_z = \gamma_{\text{mix}} \left(\frac{\rho_{\text{air}} C_{10}}{\rho} \right)^{3/2} \frac{W_{10}^3}{N^2 kh}. \quad (67)$$

Kullenberg et al. (1973) have demonstrated that the vertical dispersion of dye did indeed follow this relationship over several orders of magnitude. If no specific data are available, we can consider Eq. (67) as a realistic estimate (or perhaps a good guess) for diapycnal diffusivity in the epilimnion.

6.2.2 Convective Mixing

Another source of TKE for mixing in the surface boundary layer is the positive surface buoyancy flux J_b^o . As described in Section 5.2, J_b^o can result from cooling (or heating for $\alpha < 0$), from an increase in salinity due to evaporation of saline water, or from a combination of both processes. As summarized in Table 5, J_b^o for these two processes is quantified by

$$J_b^o = -\frac{\alpha g}{cp\rho} H_{\text{net}} + \frac{g\beta_s S}{\rho} m_E. \quad (68)$$

The two terms on the right side describe the effects of heat loss ($H_{\text{net}} < 0$) and evaporation ($m_E > 0$), respectively. In fresh water ($S = 0$), evaporation produces no buoyancy flux. Because the thermal expansion coefficient α is negative below $T = 4^\circ\text{C}$, J_b^o also becomes negative if the water is undergoing warming ($H_{\text{net}} > 0$). The temperature range over which α is negative exists only for salinities S smaller than approximately 24.7‰ (see Sect. 4.1).

It is usually assumed that the convection process is initiated by the sinking of heavier water parcels from the lake surface after a certain degree of instability is exceeded. Because of the continuity of mass, these sinking plumes (Fig. 7) imply the existence of simultaneous rising plumes, and thus the surface layer is subject to intense stirring. For this reason it is intuitively plausible that the relevant physical parameter describing the TKE balance is the surface buoyancy flux J_b^o . Energy dissipation ε is therefore usually scaled by the surface buoyancy flux J_b^o once stationary conditions have been reached:

$$\varepsilon = a J_b^o. \quad (69)$$

The relatively rare experimental studies of convection in the mixed layer show a gradual decrease of $a = \varepsilon(z)/J_b^o$ with depth (Lombardo and Gregg 1989), indicating a slightly nonuniform loss of energy of the sinking plumes. It is fascinating to note that the factor a , if plotted as a function of the nondimensional depth z/D (D : depth of the mixed layer), i.e., $a = a(z/D)$, follows a universal curve for atmospheric and for different oceanic regimes (Shay and Gregg 1986). However, turbulence measurements reveal that $\varepsilon(z)/J_b^o$ also depends on the state of convection, i.e., on whether J_b^o and the depth of the mixed layer are in steady state or changing (see Sect. 7.1).

The detailed structure of convection in the surface layer is poorly resolved, especially in the horizontal. Recent measurements (Soloviev 1990) indicate that sinking and rising plumes show similar spatially coherent, organized structures (on scales of tens of meters) as observed in the atmosphere, but not much more insight is available. Despite this insufficiency, for this regime a parametrization also exists that is a good enough approximation for practical purposes, i.e., $\varepsilon = 0.5 J_b^o$.

6.2.3 Mixed-Layer Dynamics and the Monin-Obukhov Length

As demonstrated in laboratory experiments by Deardorff et al. (1969), sinking thermals still have part of their kinetic energy when they reach the bottom of the mixed layer. Consequently, the sinking water parcels can overshoot the density surface at the base of the mixed layer and partly penetrate through the pycnocline into the hypolimnion below (penetrative convection). A fraction of that energy is available for the entrainment of heavier water from below into the mixed layer, leading to *mixed-layer deepening*. Finally, a minor part of the energy from the sinking plumes may be transferred to the hypolimnion by internal waves. The example given in Fig. 10 (*inset*) agrees with the assumption that 30% of the production of potential energy by surface cooling (P_{pot} in Eq. 44) goes into increasing the potential energy of the mixed layer. This fraction is related to the mixing efficiency, defined as the ratio of potential energy production to dissipation, $\gamma_{\text{mix}} = J_b/c$ (Eq. 56). Because the energy of sinking plumes is more directed than that of shear turbulence, plumes generally have a greater mixing efficiency ($\gamma_{\text{mix}} \approx$

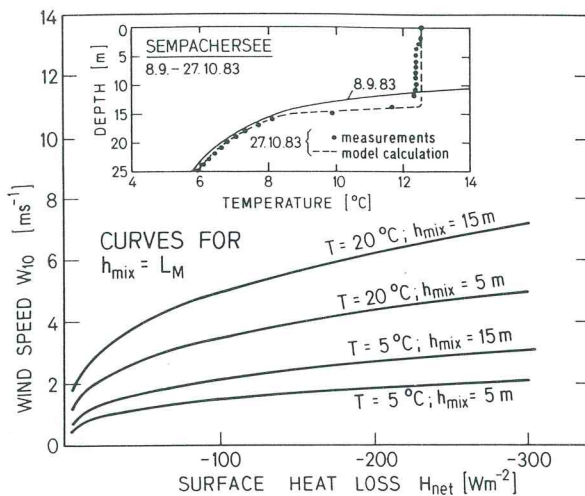


Fig. 10. Relationship between surface heat loss H_{net} and wind speed W_{10} for which the Monin-Obukhov Length L_M and the mixing depth h_{mix} (chosen as 5 and 15 m) are equal. The curves show that the influence of the wind on entrainment increases with decreasing mixed layer depth h_{mix} and decreasing water temperature T . Calculated from Eqs. (68) and (70) with $m_E = 0$ and $C_{10} = 1.5 \times 10^{-3}$. Inset Comparison between measured temperature profiles and model calculations during convective mixing due to surface heat loss (in Sempachersee). The measurements agree with the assumption that 70% of the energy is dissipated within the mixed layer and 30% is used for entrainment at the base of the mixed layer. (Redrawn from Wüest 1987)

0.20–0.25) than turbulence produced by Reynolds' stress (see Sect. 6.3).

Convective turbulence is not the only agent for the entrainment of thermocline water into the surface mixed layer; another source is provided by wind stirring (Eq. 47). The relative importance of these two agents changes with depth h : the effect of the wind is inversely proportional to h , whereas the effect of convection (a in Eq. 69) decrease more gradually with depth. For the sake of simplicity it is assumed that the turbulence level for convective mixing is constant with depth and that $a = 1$ (in Eq. 69). The Monin-Obukhov Length L_M (Table 5) is defined as the depth $h = L_M$ at which the two quantities $\varepsilon = J_R$ (Eq. 65) and $\varepsilon = J_b^o$ (Eq. 68) are equal:

$$L_M = -\frac{u_*^3}{kJ_b^o} = -\left(\frac{\rho_{\text{air}} C_{10}}{\rho}\right)^{3/2} \frac{W_{10}^3}{kJ_b^o}. \quad (70)$$

The negative sign is chosen by convention in order to distinguish this situation from the case with negative buoyancy flux J_b^o (e.g., warming of

the water column). Note that the major contribution to entrainment is convection if $L_M < h_{\text{mix}}$ and wind if $L_M > h_{\text{mix}}$. A schematic diagram of all the quantities discussed is provided in Fig. 9.

In Fig. 10 the effect of the two mixing processes is compared quantitatively. The relationship between surface heat loss H_{net} and wind speed W_{10} is plotted for two different mixing depths with $h_{\text{mix}} = L_M$ (equal contributions to entrainment, i.e., equal levels of turbulence at the base of the mixed layer). Because L_M decreases with increasing α (Eq. 70 and Table 5), and thus with water temperature T , entrainment in temperate lakes is usually controlled by cooling. However, when the surface temperature approaches 4°C , L_M becomes large and wind remains as the only stirring agent.

6.2.4 Langmuir Circulation

In addition to wind-induced small-scale turbulence, an organized vertical motion of the scale of the epilimnion depth also evolves under the action of surface wind stress. The hydrodynamics of these vortices, termed Langmuir cells, is not simple; the reader is referred to Leibovich (1983) for an overview of the relevant theories.

When the wind speed exceeds a certain threshold speed of roughly 3 ms^{-1} , within a few minutes streaks, aligned approximately parallel to the wind direction and composed of floating objects such as bubbles and leaves, can appear on the lake surface. As Langmuir (1938) showed, these streaks, which are obvious even to the non-limnologist, result from the convergence of two counter-rotating vortices at the top of the epilimnion with axes nearly parallel to the wind. Hence, surface water is transported downward at the streaks and upwelling occurs in between.

This circulation pattern establishes itself independently of surface heating or cooling. A destabilizing surface heat flux may lower the threshold for the onset of these convective rolls. At wind speeds exceeding 3 ms^{-1} , however, the strength and form of the circulation are apparently not much altered even under conditions of negative surface buoyancy flux (i.e., stabilizing conditions due to heating).

The form of the rolls is asymmetrical, but the lateral width (approximately half of the streak spacing L) and the vertical penetration depth of the rolls are observed to be approximately equal.

The spacing L of the streaks generally increases with wind speed W_{10} and can be approximated by

$$L \approx (2 \text{ to } 5 \text{ s}) W_{10} \quad [\text{m}] \quad (71)$$

(Leibovich 1983). However, the vertical size of the circulation is obviously limited by the base of the mixed layer, where strong density gradients inhibit vertical motion. Thus, Eq. (71) can only hold as long as $L/2$ is smaller than the epilimnion depth. Hence, the wind threshold and the epilimnion depth put lower and upper limits on the size of the Langmuir vortices. In fact, the size of the cells in lakes is mostly on the order of 10 m.

Downwelling at the convergence streaks can be very vigorous. Observed maximum vertical velocities attain 1% of the wind speed. The structure of the rolls is asymmetrical, with the downwelling currents being of higher velocity than the upwelling currents. Downwelling velocities generally increase with wind speed and are comparable to wind-induced surface drift.

High downwelling velocities suggest that Langmuir circulation may represent an important epilimnion mixing mechanism. Although observations led Langmuir (1938) to believe that the vortices are largely responsible for the formation and maintenance of the mixed layer, presently it is not certain whether Langmuir circulation is responsible for a significant part of the stirring. Turbulence measurements by Lombardo and Gregg (1989) indicate that Langmuir circulation does not invalidate the similarity scaling of the rate of dissipation of TKE (Eq. 65). Langmuir cells can possibly be considered as just a component of the largest-scale motion related to the dynamics of the surface boundary layer, implying that it is not necessary to add an additional term to the TKE budget (Eq. 54) to account for it.

Langmuir cells are nevertheless important for the ecology of lakes, because the environment to which an algal cell is exposed – especially light intensity – may depend critically on whether it is undergoing vertical transport by such vortices.

6.3 Diapycnal Mixing

6.3.1 Kelvin-Helmholtz Instabilities

Diapycnal mixing (mixing across surfaces of equal density) is a complex process, and much less is known about the properties of turbulence in stratified fluids than in fluids of uniform density. This

complexity is due to intermittence in the production of turbulence, to its spatial heterogeneity, and to the fact that it is generally anisotropic as a result of density stratification. In large water bodies, such as ocean basins, an additional complication arises, due to the fact that the vertical direction is not necessarily identical to the diapycnal coordinate axis (Gregg 1987).

If no energy is applied to a stratified water body, the streamlines will remain laminar and heat and mass transfer will be molecular. Diapycnal shear, however, can generate turbulence when the stratification (quantified by N) is small relative to the vertical gradient of the horizontal current ($\partial u / \partial z$). This comparison is usually expressed by the *Gradient Richardson Number* $R_i = N^2 / (\partial u / \partial z)^2$. If R_i is small, e.g., below 1/4, so-called Kelvin-Helmholtz instabilities can occur. Fluid from adjacent layers is then wrapped around like a cinnamon roll, with a highly organized substructure. The billows thicken, become statically unstable, and collapse, leaving a small turbulent patch. The development of a Kelvin-Helmholtz billow is illustrated in Fig. 11a. The mixing of two fluids of different density increases the potential energy of the water column, as described by the buoyancy flux $J_b = -K_d N^2$. In the TKE equation (Eq. 54) the buoyancy flux is negative and thus represents a further sink for TKE (in addition to viscous dissipation).

6.3.2 Diapycnal Diffusivity

As explained in Section 5.4 only a small fraction of the kinetic energy is transformed to potential energy during the diapycnal mixing process, and therefore the mixing efficiency $\gamma_{\text{mix}} = -J_b / \varepsilon = K_d N^2 / \varepsilon$ (Eq. 56) is significantly smaller than 1. Peters and Gregg (1987) estimated the mixing efficiency in a strong shear zone of the Equatorial Countercurrent to be $\gamma_{\text{mix}} = 0.12$, a value that also seems to be typical for shear-induced mixing in lake hypolimnia (Ivey and Imberger 1991).

The practical importance of γ_{mix} is its applicability to turbulence measurements. Equation (56) can be used to relate dissipation to diapycnal diffusivity in a steady shear zone (Table 8):

$$K_d = \gamma_{\text{mix}} \varepsilon / N^2. \quad [\text{m}^2 \text{s}^{-1}] \quad (72)$$

Dissipation measurements are carried out with lift probes (Osborn 1974), which sense one com-

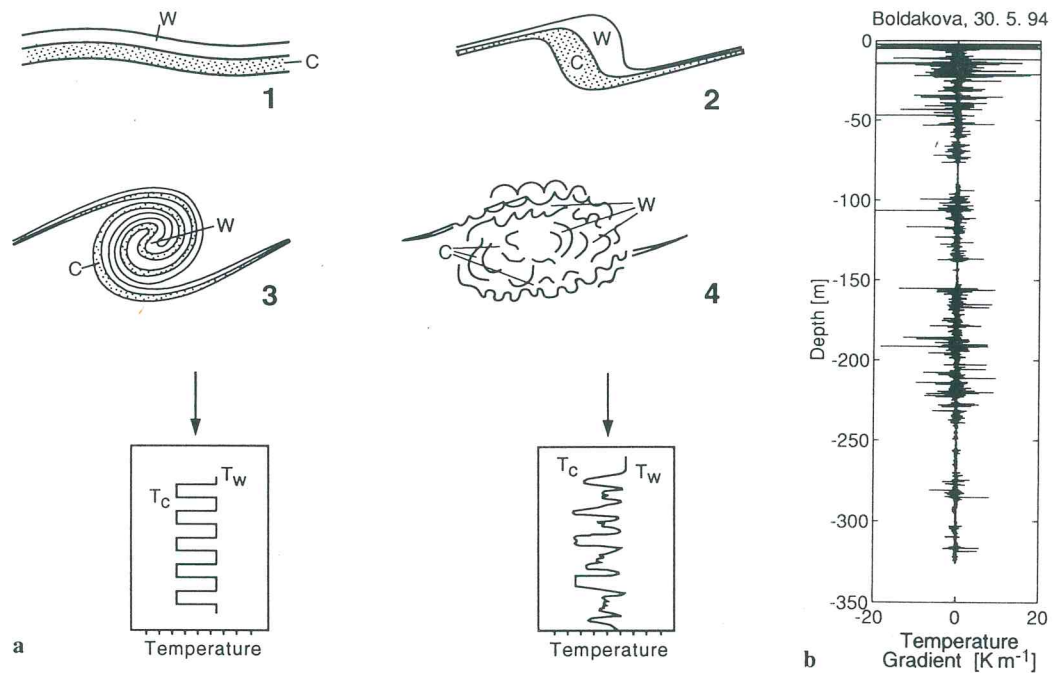


Fig. 11. a Schematic diagram of the mixing of two water masses C (cold) and W (warm) due to a Kelvin-Helmholtz instability in the stratified shear flow occurring for $R_i < 0.25$ (R_i = Gradient Richardson Number; see Table 5; modified from Thorpe 1969). b Vertical profile of temperature microstructure gradients

[K m^{-1}] measured in the top 325 m near Boldakova at the southern shore of Lake Baikal. The profile indicates large sections of vigorous mixing (large two-sided fluctuations) and sections of complete inactivity (e.g., from 80–90 m depth)

ponent of the shear with a spatial resolution of approximately 2 cm (Oakey 1982). Equation (53) is then employed to determine ε .

Another approach to diapycnal diffusivity is based on temperature fluctuations. Turbulent overturns in a well-defined mean temperature gradient $\partial T/\partial z$ produce fluctuations T' , because distorted water parcels retain their temperature during the turbulent event and for some time afterward (Fig. 11b). The steady-state balance equation for T'^2 in homogeneous turbulence states that the production due to overturns is equal to the rate of diffusive smoothing, i.e.,

$$-\overline{w'T'} (\partial T/\partial z) = 3 D^T \overline{(\partial T'/\partial z)^2}. \quad (73)$$

If the term $-\overline{w'T'}$ is replaced by a Fickian flux (Eq. 17), the diapycnal eddy diffusion coefficient for heat (Table 8) becomes

$$K_d^T = CD^T; \quad (74)$$

with the so-called Cox Number, C , given by $C = 3 (\partial T'/\partial z)^2 / (\partial T/\partial z)^2$ (Osborn and Cox 1972). Measurements of C are made with *fast-response thermistors* (Fozdar et al. 1985; Dillon and

Caldwell 1980), which can resolve spatial gradients down to a scale of less than 1 cm (Fig. 11b).

Depending on the available energy and on stratification, the maximum size of overturning eddies provides a further way of estimating diapycnal diffusivity (Table 8). The length scale at which buoyancy is suppressed by stratification is given by the *Ozmidov Scale*:

$$L_O = (\varepsilon/N^3)^{1/2}. \quad [\text{m}] \quad (75)$$

As mentioned previously, turbulence produces temperature fluctuations. The vertical displacement of an individual water parcel can be calculated by rearranging the discrete temperature values within a vertical profile such that the temperatures decrease monotonically with depth. The root mean square of all the displacements within a certain layer, termed the *Thorpe Scale* L_T (Thorpe 1977), provides a scale for the vertical extension of the overturning eddies. Measurements in lakes (Dillon 1982) and in the ocean (Peters et al. 1988) have shown that in well-defined temperature gradients, the Ozmidov and Thorpe Scales are nearly equal, i.e., $L_T \approx L_O$. By combin-

ing Eqs. (72) and (75) a link between the Thorpe Scale and the diapycnal eddy diffusivity can be derived:

$$K_d = \gamma_{\text{mix}} L_T^2 N. \quad (76)$$

A summary of the various mixing scales and the methods for estimating diapycnal diffusivity are given in Tables 6 and 8, respectively.

6.3.3 Experimental Observations

In order to describe aquatic systems quantitatively, it is often desirable to determine the rate of vertical exchange, which can be described by diapycnal diffusivity (Eq. 17). Attempts have therefore been made to find a parameterization for K_d in terms of easily measurable quantities. Peters et al. (1988) have systematically investigated the dependence of K_d on R_i as qualitatively postulated by the Kelvin-Helmholtz instability model illustrated in Fig. 11a. Among other parameters, they measured vertical shear $\partial u / \partial z$, temperature gradient $\partial T / \partial z$, stability frequency N , and dissipation rate ε , across the Equatorial Undercurrent in the Pacific Ocean. The coefficient of diapycnal diffusivity does indeed show a dramatic increase below $R_i = 0.3$ (Fig. 12). As their entire data set demonstrates, however, the parameterization is not at all simple.

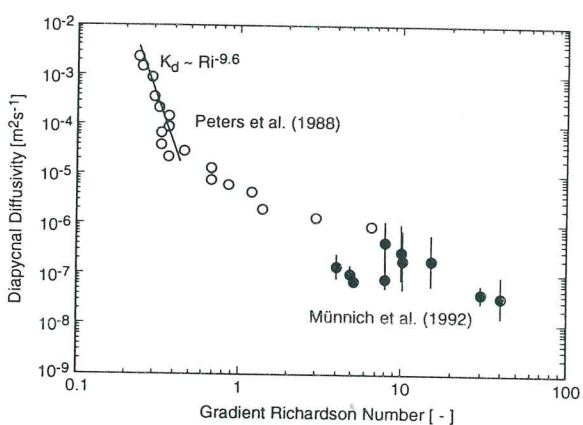


Fig. 12. Relationship between Gradient Richardson Number R_i and diapycnal eddy diffusivity of heat, K_d , measured in the Equatorial Undercurrent in the Pacific Ocean by Peters et al. (1988) (open circles) and in a small lake by Münnich et al. (1992) (filled circles). Whereas the diapycnal diffusivity increases only gradually with decreasing R_i for $R_i > 0.3$, it rises dramatically for $R_i < 0.3$.

As discussed in Sect. 6.1 internal seiches are often the main source of diapycnal shear in lake hypolimnia. The corresponding R_i values, however, are considerably in excess of 0.25. For example, for the intense seiching motion shown in (Fig. 14), the Gradient Richardson Numbers R_i at the center of the lake, calculated from the modal structure, lie between two and several hundred (Münnich et al. 1992), a range which seems to leave little chance for the development of turbulent overturn events. The diapycnal diffusivity measured by the temperature microstructure method (Table 8) in the interior of the hypolimnion of Alpnachersee is low, but still clearly above the molecular level (Fig. 12). Values of K_d are approximately the same as the molecular diffusivity of heat ($1.4 \cdot 10^{-7} m^2 s^{-1}$ at $4^\circ C$) which is still two orders of magnitude above the molecular diffusivity of dissolved matter ($\approx 10^{-9} m^2 s^{-1}$). The low but still present turbulence may be due to local regions of high shear produced by the superposition of different internal seiches and waves. The Gradient Richardson Number R_i calculated from one single internal mode (even if it is the dominant one) must be regarded as a baseline from which smaller-scale fluctuations produce locally intermittent low R_i values and turbulent patches. The monotonic decrease in mixing as a function of R_i , as shown in Fig. 12, also supports this assumption for $0.3 < R_i < 10$.

Figure 13 demonstrates another feature of diapycnal diffusivity in lakes. In contrast to the situation in the ocean, where internal wave energy has a residence time of months (Gregg and Sanford 1988), internal seiches in lakes, which are responsible for most of the diapycnal mixing, are often excited sporadically by storm events (Fig. 21; Sect. 7). As a result mixing in lakes has a much more intermittent character than it does in the ocean. Figure 13 shows an example of the enormous difference in K_d (nearly three orders of magnitude) between the typical long-term mean K_d (July to October) in Urnersee and the mean K_d in Zugersee during a storm event lasting a few days in November 1982. This is due to the enormous variation in TKE input from the wind, which varies with W_{10}^3 (Eq. 46). On November 7 and 8, 1982, Zugersee was hit by the strongest föhn storm this century (Fig. 21).

As clearly shown in Fig. 9a, turbulence in the hypolimnion is much weaker than in the mixed layer. Except after strong forcing, only a small fraction of the hypolimnion contains turbulent

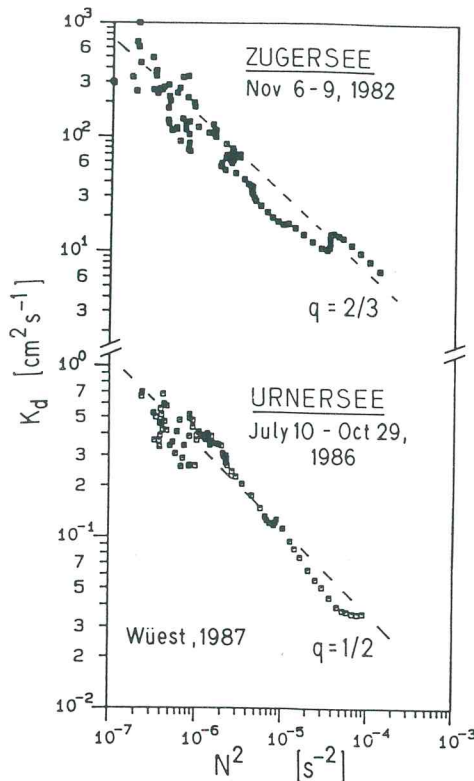


Fig. 13. Relation between diapycnal eddy diffusivity K_d and stability frequency N^2 from two neighboring lakes in central Switzerland. The data conform fairly well to the Welander (1968) parameterization $K_d = \text{const} (N^2)^{-q}$, which has a rational physical interpretation only in the upper thermocline. In deep-water layers (low N^2) diapycnal diffusivity is generally governed by other parameters (see Sect. 6.4). The large difference between long-term mean K_d values and those from November 1982 demonstrates the intermittent character of diapycnal mixing. On November 7/8, 1982, Zugersee was hit by an extremely strong storm (see also Fig. 21; redrawn from Wüest 1987)

patches: The pycnocline is an effective barrier against the transmission of epilimnetic turbulence. As a rule we can say that the rate of change of potential energy in the hypolimnion (buoyancy flux) is approximately 1% of the energy entering the epilimnion (Wüest 1987), which, in turn, is on the order of 1% of the energy flux P_{10} at a height of 10 m above the water surface (Eq. 46).

Typical long-term diapycnal eddy diffusion coefficients in medium-sized temperate lakes during strong stratification (determined indirectly from long-term tracer-diffusion studies) are on the order of $0.01\text{--}0.1 \text{ cm}^2 \text{ s}^{-1}$. These values are much larger than the diapycnal diffusivities induced by internal seiches at high Gradient

Richardson Numbers (Fig. 12) observed in the interior of the water column. This comparison allows us to conclude that boundary mixing has to be responsible for the discrepancy between interior and total diapycnal diffusivity. Internal seiches are accompanied by horizontal currents in the hypolimnion (Fig. 14), which do indeed generate boundary mixing above the lake sediment. It seems that the shearing induced by the vertical mode produces significantly more mixing at the sediment boundary than in the interior of the hypolimnion. This question is addressed in more detail in the following section.

6.4 Boundary Mixing

In lakes and oceans physical processes occurring at the sediment-water interface are of paramount importance, because they control the fluxes of chemical elements and compounds across the boundary. In addition, most diapycnal mixing occurs here. The energy for mixing at the boundary is provided by currents caused by internal and surface waves, by density currents (e.g., turbidity currents), and by inflowing rivers. In contrast to the boundary at the water surface, the sediment is rigid. Consequently, currents must fall to zero at the interface, where the fluid is in contact with the sediment. These currents at the sediment surface create a bottom stress τ_o . The boundary layer is defined as the region where the currents are affected by the presence of the boundary.

The theory of the bottom-boundary layer (BBL) is nevertheless closely related to the theory of wind shear as expressed in Section 6.2. A summary of the relevant equations and parameters is given in Table 9. For recent reviews on the dynamics of ocean boundary layers the reader is referred to Thorpe (1988), Garret (1991), and Woods (1991).

6.4.1 Velocity Structure of the Bottom-Boundary Layer

The main velocity gradient is localized in the viscous layer (Caldwell and Chriss 1979) and is strongly affected by viscosity. Its thickness δ_v (typically mm to cm) scales with v/u^* and is found experimentally to be approximately $\delta_v \approx 10 v/u^*$ (Hinze 1975), where u^* is the friction velocity

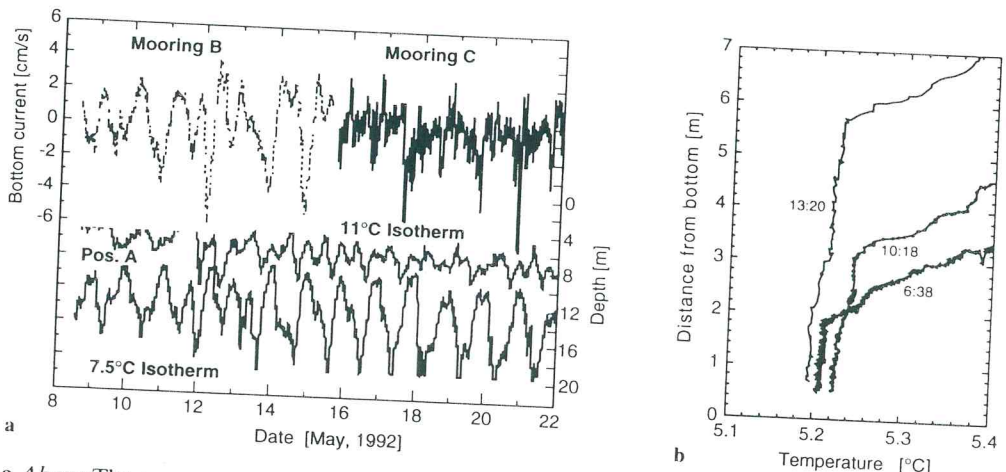


Fig. 14. **a** Above The component of the bottom current (driven by internal seiches) along the major axis of Alpnachersee lake at two sampling stations at the eastern end (*station C*) and in the middle (*station B*) of the lake. Note that velocities are approximately three times smaller than in the example given in Table 9. **Below** Time series of the depths of two selected isotherms recorded at the western end of the lake basin (*station A*). Coherence and phase spectra of bottom

current and isotherm depth reveal that seiching and currents were coherent with a phase lag of 90° , which is exactly the value expected for first horizontal seiche modes. (Redrawn from Gloor et al. 1994.) **b** Three examples of temperature profiles in the benthic boundary layer, generated by the bottom currents shown in **a**, indicating the layer to be well mixed. The numbers give the sampling time (h:m) on May 12, 1992. (Redrawn from Gloor et al. 1994)

(Table 9) defined as for the surface-boundary layer (Eq. 62). Within the viscous sublayer turbulent eddies are virtually absent. The *Reynolds Number* $Re = u\delta_v/v$ is on the order of 100 or smaller, and consequently the flow is likely to be laminar. Similar to Eq. (45), bottom stress τ_o , and thus friction velocity u^* , are related to the horizontal current velocity U_z measured at a height z above the sediment (Table 9).

Above the viscous layer turbulent eddies can exist with scales that increase with distance from the boundary. Within certain limits the stress τ_o can be assumed to be constant (constant-stress layer). As in Eq. (61) the "law of the wall" leads to a logarithmic velocity distribution with the roughness length z_o related to the topographical bottom structure of the sediment boundary. If the length scales z_s of the sediment structure is on the order of the viscous layer δ_v or less, the logarithmic velocity distribution does not depend on the bottom structure z_s . This case, called the *smooth flow regime*, applies when $z_s \lesssim v/u^*$; the roughness length is then $z_o \approx 0.1 v/u^*$ and much smaller than δ_v . For a coarser topography, i.e., $z_s \geq 3 v/u^*$, the roughness length is given by $z_o = z_s/30$ (*rough flow*; see Chriss and Caldwell 1982).

6.4.2 Energy Fluxes in Bottom-Boundary Layer

The agent for boundary-layer mixing is bottom friction. The total energy flux into the bottom layer of thickness z is given by

$$P_{\text{diss}} = \tau_o U_z = \rho C_z U_z^3 = \frac{\rho}{C_z^{1/2}} u^3, \quad [\text{W m}^{-2}] \quad (77)$$

where z (often chosen as 1 m) lies within the constant-stress layer ($\tau(z) = \tau_o$). An appreciable amount of the energy is dissipated within the viscous sublayer on a molecular level determined by the viscous stress (Table 9):

$$\varepsilon_v = \frac{\tau_o}{\rho} \frac{\partial u}{\partial z} = u^4/v \quad [\text{W kg}^{-1}] \quad (78)$$

Hence, the total dissipation in the viscous sublayer is given by

$$\begin{aligned} P_{\text{diss}}^v &= \rho \varepsilon_v \delta_v \\ &= \frac{\rho}{v} u^4 \delta_v \approx 10 \rho u^3. \quad [\text{W m}^{-2}] \end{aligned} \quad (79)$$

Comparing Eqs. (77) and (79) shows that $P_{\text{diss}}^v/P_{\text{diss}} = 10 C_{1m}^{1/2} \sim 0.4$. Thus, approximately 40% of the total energy entering the bottom layer is dissipated within the viscous sublayer, with the remainder being dissipated within the logarithmic layer. If no stratification is present, production due to Reynolds' stress is equal to dissipation:

Table 9. Characteristic equations and values for sediment-boundary-layer dynamics

Parameter	Equation	Value (for $U_{z=1m} = U_{1m} = 0.1 \text{ m s}^{-1}$) ^a	
Bottom stress	$\tau_o = \rho C_{1m} U_{1m}^2$	$\tau_o = 1.5 \cdot 10^{-2}$	[N m ⁻²]
Friction velocity	$u_* = (\tau_o/\rho)^{1/2} = C_{1m}^{1/2} U_{1m}$	$u_* = 4 \cdot 10^{-3}$	[m s ⁻¹]
Total energy dissipation by friction below 1 m	$P_{diss} = \tau_o U_{1m} = \rho C_{1m} U_{1m}^3$	$P_{diss} = 1.5 \cdot 10^{-3}$	[W m ⁻²]
<i>Viscous sublayer</i>			
Thickness of viscous sublayer	$\delta_v \approx 10 v/u_*$	$3 \cdot 10^{-3}$	[m]
Thickness of diffusive sublayer for heat	$\delta_T \approx \left(\frac{D^T}{v}\right)^{1/3} \delta_v$	$1.5 \cdot 10^{-3}$	[m]
Thickness of diffusive sublayer for salt	$\delta_s \approx \left(\frac{D^S}{v}\right)^{1/3} \delta_v$	$3 \cdot 10^{-4}$	[m]
Velocity gradient	$\partial u/\partial z = \frac{u^2}{v}$	12	[s ⁻¹]
Rate of viscous dissipation	$\varepsilon_v = \frac{\tau_o}{\rho} \partial u/\partial z = u_*^4/v$	$1.8 \cdot 10^{-4}$	[W kg ⁻¹]
<i>Logarithmic layer</i>			
Velocity distribution	$u(z) = \frac{u_*}{k} \ln(z/z_o)$		[m s ⁻¹]
Velocity gradient	$\partial u/\partial z(z) = u_*/kz$		[s ⁻¹]
Eddy coefficient for momentum	$K^m(z) = \frac{\tau_o}{\rho \partial u/\partial z} = k u_* z$		[m ² s ⁻¹]
Rate of dissipation of TKE	$\varepsilon(z) = \frac{\tau_o}{\rho} \frac{\partial u}{\partial z} = \frac{u_*^3}{kz}$		[W kg ⁻¹]

^aBottom friction coefficient $C_{1m} = 1.5 \times 10^{-3}$ (Elliott 1984).

$$\varepsilon = \frac{\tau_o \partial u}{\rho \partial z} = \frac{u_*^3}{k z} \quad [\text{W kg}^{-1}] \quad (80)$$

Thus, as in the surface layer turbulence decreases with increasing distance from the boundary (Fig. 9a).

Within the boundary layer the flux of heat and solutes also drops toward molecular levels. Because molecular diffusion is smaller than viscosity, the zone of pure molecular transport is confined to the so-called *diffusive sublayer*, which is thinner than the *viscous sublayer* (Table 9). The magnitude of the molecular diffusivity of heat results in the thickness of the *thermal diffusive sublayer* lying between those of the diffusive and viscous sublayers. The eddy diffusivities of both heat and salt increase rapidly with distance above their respective diffusive sublayers.

As long as the constant-stress-layer assumption

applies, the eddy coefficient for momentum K^m is given by

$$K^m = \frac{\tau_o}{\rho \partial u/\partial z} = k u_* z. \quad [\text{m}^2 \text{s}^{-1}] \quad (81)$$

The dependence of K^m on height z is related to the fact that eddy size increases with distance from the sediment surface. The dependence on u_* implies that the transfer rate increases with horizontal current velocity U_z . In Table 9 all properties discussed are listed for the example of a smooth flow regime with $U_{1m} = 0.1 \text{ m s}^{-1}$, an upper limit for typical current speeds in the hypolimnion.

The effects of boundary mixing induced by bottom currents are often observed in aquatic systems. The most prominent feature is a well-mixed layer (BBL) above the sediment–water interface. Whereas the existence of a well-mixed

BBL in the ocean is due to geostrophic or thermohaline circulation, seiching motions and the associated hypolimnetic bottom currents are responsible for intense mixing in the zone of high shear above the sediment in lakes. Because hypolimnetic currents are generally less energetic than deep-water currents in the ocean, the well-mixed BBLs in lakes are typically an order of magnitude thinner.

Figure 14a shows an example of internal seiching motion and the corresponding bottom currents, which are typically $\sim 3 \text{ cm s}^{-1}$ and peak around 7 cm s^{-1} . The bottom currents have established a distinct and relatively well-mixed BBL with a temporally varying thickness of 2–6 m (Fig. 14b). The temperature gradients within this layer are an order of magnitude smaller than those just above it. The time required to build up a mixed bottom layer of this thickness by continuous erosion of a background density stratification would be more than a month (see Sect. 7). It can therefore be concluded that the changing thickness is associated only with the seiching motion and not with erosion of the density gradient by intermittent boundary mixing (Gloer et al. 1994).

As mentioned in Sect. 6.3, diapycnal diffusivity in the hypolimnia of small to medium-sized lakes can be dominated by mixing within the BBL, where the main source of turbulent kinetic energy is located (Wüest et al. 1994). The vertical modal structure (see Sect. 6.1) and amplitudes of the internal seiches, as well as the lake topography (mainly the surface-to-volume ratio), are the main factors determining whether overall

diapycnal exchange is dominated by internal or boundary mixing.

We have not tested thus far whether the bottom buoyancy flux J_b^b has to be taken into account. In the same way as surface cooling generates a surface buoyancy flux J_b^o , the heat flux H from the sediments (of geothermal or other origin) releases potential energy and induces convection. Analogous to Table 4, the bottom buoyancy flux is given by

$$J_b^b = \frac{g\alpha}{\rho c} H. \quad [\text{W kg}^{-1}] \quad (82)$$

In mid-latitude lakes the geothermal heat flux leads to a typical value for J_b^b of $4 \times 10^{-12} \text{ W kg}^{-1}$ ($T_b = 5^\circ\text{C}$, $H = 0.1 \text{ W m}^{-2}$), which is much lower than friction-induced turbulence (Table 9). Consequently, free convection influences the boundary dynamics in rare cases only. For lakes with extensive geothermal springs, however, convectively induced mixing at the lake bottom can become the dominant mixing process. For example, in Lake Kivu (Fig. 16) a heat flux of approximately 1 W m^{-2} at $T \approx 26^\circ\text{C}$ gives rise to a bottom buoyancy flux of approximately $7 \times 10^{-10} \text{ W kg}^{-1}$, and to mixing by double diffusion (see Sect. 6.5).

Determination of boundary-layer characteristics in lakes or oceans is not simple. Methods that have been applied in natural waters (Table 10) all suffer from some drawback. For example, the inertial-dissipation-rate technique is applicable only to isotropic turbulence, a condition that is not always fulfilled in lakes, due to chemical stratification near the sediment boundary (Wehrli

Table 10. Methods to quantify macroscopic boundary layer characteristics

Method	Measured parameter	Derived parameters	Reference
Stress measurement	u^* (or τ)	K^m, ε, z_o (for smooth regime only)	Gust and Weatherly (1985) Soulsby (1983)
Velocity measurement	$u(z)$	U^* (or τ_o), z_o, K^m	Weatherly (1972) Chriss and Caldwell (1982, 1984)
Dissipation rate technique	$\varepsilon(z)$	u^*, K^m	Dewey et al. (1987) Dewey and Crawford (1988)
Inertial-dissipation rate technique	$E(k, z)$	$\varepsilon = \left(\frac{E(k)^3 k^5}{\alpha^3} \right)^{1/2}$ $u^* = \left(\frac{E(k) k^{5/3}}{\alpha} \right)^{1/2} (k z)^{1/3}$	Grant et al. (1984) Wimbush and Munk (1970) Dimai et al. (1994)

1993). This may lead to suppression of the diapycnal exchange. Direct estimation of skin friction (τ_0) measured with flush-mounted hot-film sensors (Gust 1982) requires great care to avoid additional drag from the sensors. Finally, if τ_0 is inferred from current measurements made well above the sediment surface, the unknown influence of the sediment structure is a further source of uncertainty, as discussed in Sect. 6.4.3.

6.4.3 Interaction of Currents with the Sediment

In addition to the force exerted on the particles at the sediment surface, known as *skin friction*, bottom irregularities experience a force analogous to the drag of a body in a stream. This force is known as *form drag*, because it depends on the shape and orientation of large-scale topographical features of the sediment surface. It is important to distinguish between the contribution of skin friction, which refers to the shear stress averaged over several grain diameters, and that of form drag, which is related to the length scale of the large-scale topographical features. The flow in the upper part of the boundary (the logarithmic layer) is influenced by the total stress, but erosion and near-bed sediment transport are related to skin friction alone. When form drag is significant the layer above the viscous sublayer may accordingly consist of more than one logarithmic layer. If the friction velocity u_* is determined from current measurements made a few tens of centimeters above the bottom, the values obtained are much larger than those due to skin friction alone (Chriss and Caldwell 1982, 1984; Dimai et al. 1994), resulting in an overestimate of the force exerted on the particles at the lake bottom.

In shear-generated turbulence close to the sediment boundary, the vertical-velocity fluctuations are asymmetrical, resulting in a vertical net momentum directed away from the sediment, which can hold sediment particles in the flow in equilibrium with gravity (Leeder 1983). Consequently, suspension or resuspension of sediment particles occurs when u_* (or U_{lm}) exceeds a threshold value that depends on the density, size, and degree of cohesion of the particles (Shields 1936; Miller et al. 1977). Note that algal and bacterial growth at the sediment–water interface can significantly alter particle cohesion, and thus the tendency for resuspension to occur.

The resuspension-settling cycles increase the

size of the zone of contact between particle surfaces and the water column, and thus enhance the fluxes from and to the particles. This exchange may be appreciable compared with molecular diffusion into the sediment. For example, the large specific surface area of small sediment particles emphasizes the importance of resuspension for the mineralization process.

6.4.4 Relevance of Bottom-Boundary Mixing for the Whole Lake

Recent experimental results indicate that mixing in the bottom-boundary layer may be important for the whole lake. In fact, for approximately the past 20 years the quantification of diapycnal diffusion near the bottom of the ocean and of lakes has been based on measurements of the diffusion of the naturally occurring radioisotope Rn-222 (with a half-life of 3.8 days) out of the sediments (Chung and Kim 1980). Imboden and Joller (1984) observed near-bottom diffusivities of $0.1\text{--}1 \text{ cm}^2 \text{s}^{-1}$ in the small Baldeggsee, and concluded that mixing is more intense near the boundary than in the interior of the water column. This observation is supported by recent microstructure measurements that show a strong increase in turbulence toward the sediment (Wüest et al. 1994). The contribution to the overall diapycnal fluxes in the hypolimnion of processes occurring at the bottom boundary may therefore be significant, especially in small to medium-sized lakes. This possibility, which was earlier evaluated for the ocean by Armi (1978, 1979), is supported by recent measurements conducted by Ledwell (1993) and Toole et al. (1994). Although not yet universally accepted, the importance of the contribution made by bottom-boundary mixing to overall mixing in all density-stratified natural water bodies must be taken into account (Garrett 1990).

Another important aspect is the mass flux between the sediment and the lake water through the diffusive sublayer. This flux is proportional to the vertical concentration gradient between sediment-pore water and the overlying water. However, it is not simple to relate the proportionality factor to the flow regime in the water column, because several factors complicate the picture. Firstly, as explained in this section the methods of characterizing the bottom-boundary layer (Table 10) are complex. Secondly, because of the episodic forcing, the parameters of the boundary layer are

extremely variable. In fact, the quantities developed for smooth flow using classical boundary-layer theory (Table 9) are only partially valid, and then only for mean values. Thirdly, there exists a feedback mechanism between physical and biogeochemical processes that can lead to so-called biogenic stratification, which is difficult to predict quantitatively. Mineralization and dissolution processes at the sediment surface fuel the fluxes of solutes into the deep water. If the energy input (and thus the mixing rate) is small, the solutes accumulate above the sediment (Wehrli 1993). Consequently, the density stratification becomes stronger, which slows down diapycnal mixing in the bottom-boundary layer even further. Vice versa, a larger energy input may prevent the build-up of a chemically induced density gradient, and may thus tend to maintain mixing. Both extremes, the well-mixed (Fig. 14b) and the highly stratified bottom-boundary layer, can be observed in nature, and the switch from one to the other may be triggered by small, difficult-to-predict changes in the production of TKE.

6.5 Double Diffusion

6.5.1 The Phenomenon

A temperature profile from Lake Kivu taken by Newman (1976; Fig. 16) shows fascinating step-like structures. Such phenomena are also observed in the ocean. They are related to double diffusion, a process based on the large difference between the molecular diffusivity of temperature and of salts. Because double diffusion can be the major process resulting in vertical mixing under certain conditions, this phenomenon deserves to be mentioned here.

Because the density of water depends on temperature and salinity, local stability (see Sect. 4) can be attained in different ways. In most temperate lakes temperature decreases and salinity increases with depth. Consequently, both temperature and salinity have a stabilizing influence on the water column. This diffusively stable situation is not discussed here further.

Double diffusion occurs when temperature (salinity) tends to stabilize the water column, whereas salinity (temperature) tends to destabilize it, but in such a way that the resulting density profile is stable. If the temperature is stabilizing a finger regime results, whereas if salinity is stabiliz-

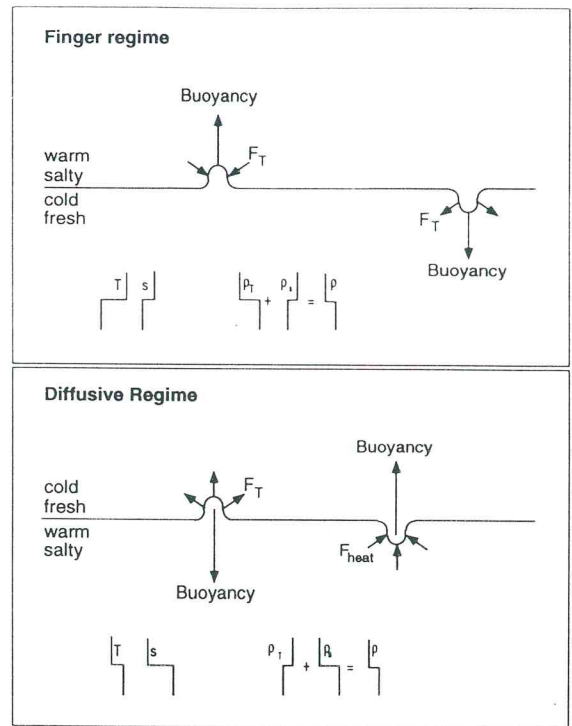


Fig. 15. Double diffusion occurs if the vertical distribution of salt and temperature is such that one component tends to stabilize the water column, while the other tends to destabilize it, leaving an overall stable stratification. In the finger regime (temperature stabilizing), a distorted water parcel exchanges heat approximately $D^T/D^s \sim 70$ times faster than salt, thus creating salt fingers, which move into the adjacent layers. In the diffusive regime (salt-stabilizing), the faster rate of heat exchange causes an enhanced rejection of the distorted water parcel, giving rise to strong mixing within a certain layer. An example of the layering created by the diffusive regime is given in Fig. 16

ing a diffusive regime results (Fig. 15). Because the stabilizing contribution has to be larger than the destabilizing one, the *stability ratio* (often but not accurately called the density ratio) R_p , defined as

$$R_p = \frac{\text{stability due to the stabilizing component}}{\text{instability due to the destabilizing component}} \quad (83)$$

exceeds unity for both regimes. The relative density gradients due to temperature and salinity are given by $\alpha \partial T / \partial z$ and $\beta_s \partial S / \partial z$, respectively (see Eq. 40). Thus,

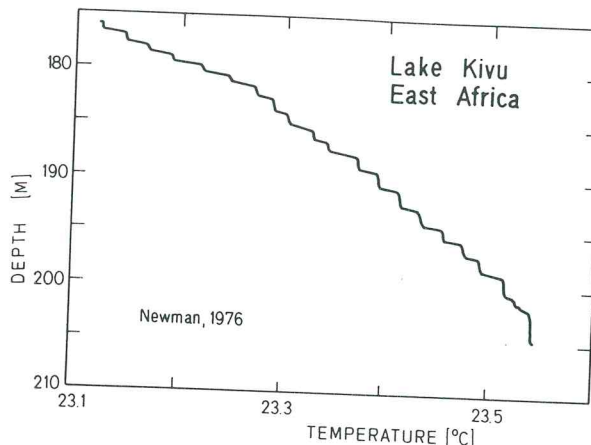


Fig. 16. Step-like temperature structure in Lake Kivu (East Africa) resulting from double diffusion (diffusive regime). In 1976, temperature increased from a minimum of 22.5°C at a depth of 50 m to 26°C near the bottom. The figure shows approximately 20 steps out of a total of approximately 150 (typically, $\Delta z = 0.1$ m, $\Delta T = 0.01$ to 0.03 K, and $\Delta S = 10^{-2}$ g/kg). The regime is sustained by geothermal springs that release warm, salty water into the deep part of the lake. R_p is between 1.3 and 2.1. Using an empirical relationship (Table 11), the vertical heat flux was calculated to lie between 0.7 and 1.6 W m^{-2} . (Redrawn from Newman 1976)

$$R_p = \left(\frac{\alpha \partial T / \partial z}{\beta_s \partial S / \partial z} \right)^{\pm 1}, \quad (84)$$

with +1 (-1) for the finger (diffusive) regime.

The mixing conditions in the water column are determined by two parameters, i.e., by the absolute stability, quantified by N^2 , and by the stability ratio R_p . If $R_p \gg 1$, the destabilizing factor can be ignored, and we would simply expect the vertical mixing intensity to be somehow related to N^2 , but not to R_p . If R_p is only slightly larger than 1, however, the water column can become locally unstable, despite its absolute stability. This is due to the fact that the molecular diffusion of heat occurs approximately two orders of magnitude faster than the molecular diffusion of salt.

6.5.2 Fluxes

The local instability can be understood by considering a cold freshwater layer lying on top of a warm salty layer (diffusive regime; Fig. 15). A water parcel displaced upward slightly from its equilibrium position loses heat to its surroundings, but hardly any salt. As a result, the water parcel is forced back downward beyond its former equilib-

rium position. In turn, if the water parcel is moving downward it gains heat, but nearly no salt. Thus, buoyancy forces it back upward beyond its former position. In other words, unlike the classical stability oscillation (frequency N), double-diffusive regimes are characterized by a situation where the amplitude of a vertical displacement continually increases, leading to enhanced vertical mixing.

In the finger regime (Fig. 15), the downward movement of warm salty water across the density interface is accelerated, because the water loses heat faster than salt, and thus increases in density. As a result fingers of salty water (salt fingers) penetrate from above into the lower layer and enhance vertical mixing. Note that in both cases the accelerated water parcel gets its energy from the potential energy of the water column: Potential energy (buoyancy flux) is released from the stratification by the upward flux of heat in the diffusive regime and the downward flux of salt in the finger regime.

Theoretically, double diffusion comes into play when $1 < R_p < (D_T/D_s) \approx 70$, and is expected to become stronger when R_p approaches unity. Indeed, both laboratory measurements (Turner 1967; McDougall and Taylor 1984) and theory (Stern 1976) show that the flux of salt, heat, and buoyancy due to salt fingers depends only on the stability ratio R_p and the salinity difference ΔS . A similar dependence on R_p and ΔT was found by Turner (1965) for the diffusive regime. It is intuitively clear that for low R_p , the fluxes depend on the difference across the interface of either salinity or temperature, whichever is responsible for the destabilizing tendency. This is simply because the convective plumes (thermals or fingers) have roughly the salinity or temperature (whichever is destabilizing) of the adjacent layer. The drastic increase in the fluxes when R_p approaches unity is also evident as the density profile becomes neutral ($N^2 = 0$). The empirical equations summarized in Table 11 allow the calculation of fluxes in double diffusive regimes based on high-resolution conductivity/temperature/depth (CTD) measurements.

It is interesting to note that in both regimes the buoyancy flux J_b follows a $4/3$ -power law, viz. proportional to $(\Delta S)^{4/3}$ for the finger regime, and to $(\Delta T)^{4/3}$ for the diffusive regime, where ΔS and ΔT are the concentration and temperature differences, respectively, across the interface (Table 11). Surprisingly, J_b seems to be independent of

Table 11. Definitions and flux laws for the two double-diffusive regimes*Definitions*

F_T :	Vertical temperature flux
F_s :	Vertical salt flux
$\alpha F_T, \beta_s F_s$:	Vertical density flux due to temperature and salt flux, respectively
$g\alpha F_T, g\beta_s F_s$:	Buoyancy flux due to temperature and salt flux, respectively

$$\text{Density (or stability) ratio}^a: R_p = \left(\frac{\alpha \partial T / \partial z}{\beta_s \partial S / \partial z} \right)^{\pm 1}$$

$$\text{Density flux ratio}^a: R_f^* = (\alpha F_T / \beta_s F_s)^{\pm 1}$$

Finger regime

$$g\beta_s F_s = -\frac{0.19}{(R_p - 0.5)} g (g D^T)^{1/3} (\beta_s \Delta S)^{4/3}$$

$$\text{for } 1.2 < R_p < 2$$

$$R_f^* = \frac{0.44}{(R_p - 0.6)^{1/2}} \quad (\text{McDougall and Taylor 1984})$$

$$\text{for } R_p > 2:$$

$$R_f^* = 0.56 \quad (\text{Turner 1967})$$

$$R_f^* \approx 0.5 \quad (\text{Schmitt 1979})$$

$$\text{Total buoyancy flux: } J_b = g(\alpha F_T - \beta_s F_s) = g\beta_s F_s (R_f^* - 1)$$

Note: ΔS is the (positive) difference between upper and lower layer

Diffusive regime (Turner 1965, 1968, 1973)

$$\alpha g F_T = \frac{0.32}{R_p^{1/2}} \left(\frac{g}{K_v^T} \right)^{1/3} K^T g (\alpha \Delta T)^{4/3}$$

$$\text{For } 1 < R_p < 2:$$

$$R_f^* = 1.85 - 0.85 R_p$$

$$R_p > 2:$$

$$R_f^* = 0.15$$

$$\text{Total buoyancy flux: } J_b = g(\alpha F_T - \beta_s F_s) = g\alpha F_T (1 - R_f^*)$$

Note: ΔT is the (positive) difference between lower and upper layer

^a Finger regime: exponent +1; diffusive regime: exponent -1

the thickness of the interface. Based on stability theory, however, Kunze (1987) showed that for the finger regime the flux laws listed in Table 11 are only valid for interfaces thinner than approximately 30 cm. At thicker interfaces the fluxes are reduced. In contrast, the diffusive regime, which is more common in lakes, tends to sharpen the interfaces, due to the eroding effect of the convecting thermals. The application of laboratory results to natural conditions is thus less problematic in the diffusive regime than in the finger regime (e.g., see Huppert and Turner 1972).

Double diffusion causes diapycnal mixing that can be compared with shear-induced mixing. In a double-diffusive homogeneous-mixed layer the TKE balance equation (Eq. 54) states that dissipation is equal to buoyancy flux, which is given by the empirical formula in Table 11. We thus obtain

$$\varepsilon = J_b = g\alpha F_T (1 - R_f^*) \quad (85)$$

(for symbols see Table 11). The mean vertical temperature gradient is related to the stability N^2 by the expression

$$\begin{aligned} N^2 &= -\frac{g}{\rho} \frac{\partial \rho}{\partial z} = -g \left(-\alpha \frac{\partial T}{\partial z} + \beta_s \frac{\partial S}{\partial z} \right) \\ &= -g\alpha \frac{\partial T}{\partial z} (R_p - 1). \end{aligned} \quad (86)$$

Thus, by using the heat-flux formula from Table 11 the apparent diapycnal heat diffusivity becomes

$$K_d^T = \frac{-F_T}{\partial T / \partial z} = \frac{(R_p - 1)}{(1 - R_f^*)} \frac{\varepsilon}{N^2} \approx 1.2\varepsilon/N^2 \quad (87)$$

for an arbitrarily chosen $R_p = 2$. (Note that from Table 11 we get $R_f^* = 0.15$.) In contrast, given a

typical mixing efficiency γ_{mix} of 0.1 for shear-induced diapycnal mixing (Eq. 56 and Sect. 6.3), $-J_b = K_d^T N^2 = 0.1\epsilon$. The apparent diffusivity is accordingly given by

$$K_d^T = 0.1\epsilon/N^2. \quad (88)$$

There is thus a difference of one order of magnitude between the diapycnal diffusivity expressions depending on whether dissipation originates from double diffusion or shear. This demonstrates the different character of the two mixing mechanisms as well as the potential importance of double diffusion for diapycnal mixing.

6.5.3 Layering

Laboratory experiments show that in both regimes double diffusion causes layering (finger regime: Stern and Turner 1969; diffusive regime: Turner 1973). According to observations in natural waters layering occurs only if R_p is smaller than 2–4. The layer-generating mechanism is not properly understood. In the diffusive regime, when the water is heated from below, instabilities drive convection, creating a homogeneous bottom layer of increasing thickness. When the heat flux through the top interface and the flux from below become equal, the layer ceases to grow. Then the next layer develops above the first layer at the bottom, and so on (Turner 1973).

For the finger case, the temporal development of the layers is more complicated (Stern and Turner 1969). Observations in the ocean show that in some cases the layers can extend coherently over hundreds of kilometers (Schmitt et al. 1987). In other cases the lateral structure is less than several hundred meters in extent (Padman and Dillon 1987).

6.5.4 Occurrence of Double Diffusion

Double diffusion in lakes occurs in the stratified hypolimnion when sources are available to produce gradients of temperature and dissolved solids that are of equal sign. For the diffusive regime geothermal heat flux, geothermal springs, and the decomposition of organic material (Wüest et al. 1992) provide the necessary heat and salt sources. In Lake Kivu (Fig. 16) it is the geothermal heat flux that keeps the double-diffusive buoyancy flux alive (Newman 1976). Intrusions

produced by river discharge, differential mixing, or the flow over a sill separating two basins (Figs. 7 and 22) can also create double-diffusive conditions. For example, river interflow (Fig. 7) usually favors a diffusive regime at the upper boundary and a salt-finger regime at the lower boundary of the merging river water. Diffusive regimes have also been found in meromictic lakes that have developed from former fjords containing trapped seawater subject to geothermal heating (Sanderson et al. 1986).

6.6 Isopycnal Mixing

6.6.1 Scale Dependence of Isopycnal Mixing

Only little energy is necessary for a water parcel to move adiabatically along a surface of constant density. Thus, isopycnal transport is several orders of magnitude faster than diapycnal transport. As described in Section 3, the distinction between advective and turbulent mass flux is arbitrary in the sense that it depends on the scales that are considered. This is especially true for isopycnal transport, because the eddy size covers the entire range from the length of the lake down to the dissipation scale (mm).

Isopycnal currents have complex spatial and temporal structures, and exhibit fluctuations with various periods. In lakes velocities averaged over long time intervals are usually very small. Over short time scales, however, horizontal velocities can cause significant advection. Thus, a tracer cloud is primarily moved around advectively by eddies that are significantly larger than the size of the tracer patch. In contrast, eddies that are smaller than the tracer distribution generate mixing within the patch, a process that is usually interpreted as turbulent diffusion. Intermediate eddies of a size comparable to that of the tracer cloud cause distortion and stretching of the cloud, due to the shear of the velocity field. In combination with small-scale mixing this leads to an efficient growth of the tracer cloud. Figure 17 shows an example of the horizontal extension of the fluorescent dye uranin 30 h after it was artificially added to Lake Lucerne as a small, roughly circular patch.

In order to separate advective from diffusive transport it is necessary to characterize a tracer cloud by distinguishing the movement of its center of mass (x_s, y_s) from the temporal development of

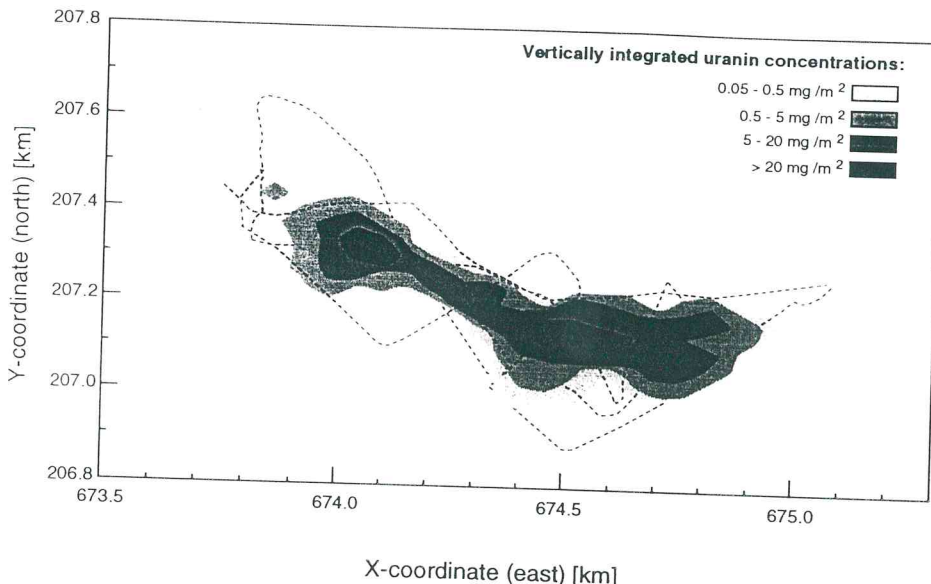


Fig. 17. Radially asymmetrical horizontal concentration distribution of uranin, 30 h after release as a point source into a basin of Lake Lucerne. The shading indicates the vertically integrated concentration of the tracer. The dashed line represents the path of the ship

during the survey of the tracer cloud. This particular tracer distribution represents one point of Fig. 18 (*open circles*), showing the temporal growth of tracer clouds. (Redrawn from Peeters et al. 1993)

its shape relative to the center of mass. The following considerations focus on isopycnal (horizontal) mixing. The influence of vertical mixing is compensated for by using the vertically integrated concentration $C(x,y)$. The center of mass is given by the coordinates

$$\begin{aligned} x_s &= \frac{1}{M} \iint x C(x,y) dx dy; \\ y_s &= \frac{1}{M} \iint y C(x,y) dx dy, \end{aligned} \quad (89)$$

where M is the total mass of the tracer cloud, given by

$$M = \iint C(x,y) dx dy. \quad (90)$$

The shape of the tracer cloud can be described by its statistical characteristics, e.g., by its moments of order n about the center of mass. Often, only the second moments (the variances σ_x^2 and σ_y^2 and the covariance σ_{xy}) are considered. These are defined by

$$\begin{aligned} \sigma_x^2 &= \frac{1}{M} \iint (x - x_s)^2 C(x,y) dx dy; \\ \sigma_y^2 &= \frac{1}{M} \iint (y - y_s)^2 C(x,y) dx dy; \end{aligned}$$

$$\sigma_{xy} = \frac{1}{M} \iint (x - x_s)(y - y_s) C(x,y) dx dy. \quad (91)$$

As demonstrated in Fig. 17, the spreading of a tracer cloud is often highly anisotropic. By rotation of the coordinate system, the x and y axes can be made to coincide with the major and minor principal axes, respectively (Peeters 1994). The corresponding variances are σ_{ma}^2 and σ_{mi}^2 , whereas the covariance is zero. (In fact, the variances along the principal axes are the eigenvalues of the matrix σ_{ij} as calculated from Eq. 91 for an arbitrary coordinate system.) The size of a tracer cloud is somewhat arbitrarily defined (Okubo 1971) as

$$\sigma^2 = 2\sigma_{ma} \sigma_{mi}. \quad (92)$$

This choice is reasonable insofar as in the case of a two-dimensional Gaussian distribution, the area of a circle with radius σ contains 63% of the total tracer mass. (Furthermore, if a radially symmetrical distribution is constructed from a tracer cloud, as is often the case, the corresponding variance σ_r^2 is equal to σ^2 , provided that the cloud can be viewed as an isotropic Gaussian distribution.)

Isopycnal mixing rates are quantified by the growth of the size of tracer clouds. Figure 18 shows a few examples of the temporal increase of σ^2 as a function of the diffusion time t . A common

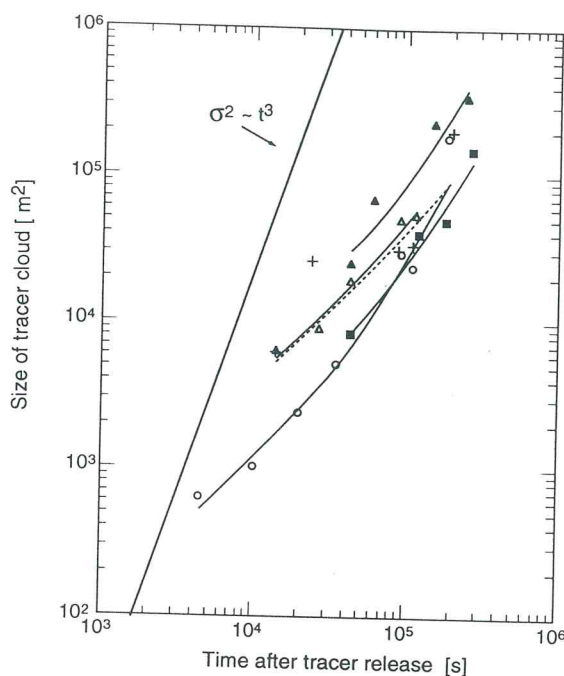


Fig. 18. Size of tracer clouds as a function of time for experiments in Lake Ontario (Murthy 1976; filled symbols), Lake Lucerne (Peeters 1994; open circles) and the ocean (Okubo 1971; crosses). The thin lines represent the fits of the shear-diffusion model (Eq. 98) to data from experimental tracer clouds such as those shown in Fig. 17. The thick solid line represents the fit to the inertial-subrange model (Eq. 96) of data from several dye experiments in ocean surface waters summarized by Okubo (1971). This comparison supports the superiority of the shear-diffusion model to describe the long-term spreading of a tracer. (Redrawn from Peeters et al. 1993)

approach to characterizing the growth rate is by approximating the size σ^2 using the simple power-law relation

$$\sigma^2(t) = at^m. \quad (93)$$

As a first step we can try to interpret observations of isopycnal spreading in terms of an isotropic first-order local closure scheme (Fickian diffusion; Eq. 17). The apparent diffusivity K_i would then be related to $\sigma^2(t)$ by

$$K_i = \frac{1}{4} \frac{d\sigma^2(t)}{dt}. \quad (94)$$

In order for K_i to be constant with time, $m = 1$ would be needed. In fact, measurements in lakes (Murthy 1976; Peeters et al. 1993), fjords and coastal waters (Kullenberg 1972), and oceanic surface waters (Okubo 1971) show that irrespec-

tive of macroscopic conditions the growth of tracer clouds is neither isotropic (Fig. 17) nor linear with time (Fig. 18), because nearly all observations yield values of m larger than 1. This implies that isopycnal diffusion is dependent on length scale and is non-Fickian. Combining Eqs. (93) and (94) yields an expression relating the apparent diffusivity K_i to the length scale σ of the tracer distribution:

$$K_i = A \sigma^{[2(m-1)/m]} \quad (A = \frac{m}{4} a^{1/m}). \quad (95)$$

The anisotropic character of isopycnal mixing is addressed in the following brief discussion on diffusion models.

6.6.2 Diffusion Models

There is no well-founded theory on isopycnal diffusion in lakes. In fact, almost all of the models listed in Table 12 are of empirical origin, rather than being based on a deeper understanding of the physics behind the mixing processes.

The simplest model, corresponding to Fickian diffusion, is parameterized by a constant diffusivity K_i . As discussed previously (Eq. 94), cloud size, according to this model, should grow linearly with elapsed diffusion time t . In contrast to small-scale diapycnal diffusion, isopycnal transport also occurs over large scales. We therefore expect to find Fickian-type isopycnal mixing only for very small patches. In fact, isopycnal Fickian diffusion has never been observed in field studies.

A particularly popular diffusion model is based on the assumption that the turbulent regime falls into the inertial subrange. As can be recalled from Section 5.5, this means that energy enters at scales larger than the spatial scale under consideration and dissipates at smaller scales, and also that turbulence is steady, homogeneous, and isotropic. For such a situation the similarity theory (Kolmogorov 1941) predicts that the cloud size σ^2 will grow proportional to t^3 if the initial patch is small (Richardson 1926; Batchelor 1950). Furthermore, the spreading of the cloud should depend on the intensity of the turbulence as measured by the rate of dissipation ε of TKE. Dimensional analysis leads to the expression

$$\sigma^2 = \text{const } \varepsilon t^3. \quad (96)$$

Table 12. Isopycnal diffusion models

Diffusion model	Physical basis and parameter	Power law for $\sigma^2(t)$ (Eq. 93)	Diffusion law for K_i (Eq. 95)	References
Fickian	Constant diffusivity in analogy to molecular diffusion	$m = 1$	$K_i = \text{constant}$	
Diffusion velocity (or Joseph-Sendner)	Diffusion due to relative velocity v ; velocity v and length scale L	$m = 2$	$K_i = v L$	Joseph and Sendner (1958)
Inertial subrange	Similarity in the inertial subrange; energy dissipation ε and length scale L	$m = 3$	$K_i = c \varepsilon^{1/3} L^{4/3}$	Okubo and Ozmoidov (1970)
Shear diffusion	Interaction of horizontal and vertical shear ($\partial u / \partial y$ and $\partial u / \partial z$, respectively) with small-scale horizontal and vertical diffusion (K_h and K_d , respectively)	$m = 1-2$	$K_i = f\left(\frac{\partial u}{\partial y}, \frac{\partial u}{\partial z}, K_h, K_d\right)$ See Eq. (98)	Young et al. (1982) Taylor (1953) Kullenberg (1972) Carter and Okubo (1965) Peeters (1994)
"Half-past-one-in-the-morning"	No physical basis	$m = 1.5$	$K_i = \text{const } L^{2/3}$	Ewart and Bendiner (1981)

The apparent isopycnal diffusivity is calculated from Eq. (94):

$$K_i = \text{const } \varepsilon^{1/3} \sigma^{4/3}. \quad (97)$$

This specific scale dependence of K_i is well known from the work of Okubo (1971), who compiled the most reliable data from many different dye experiments in ocean surface waters and demonstrated a surprisingly good agreement with the 4/3-power law over distances from 100 m to 1000 km. However, this agreement has often led to serious misinterpretations. Because the diagram represents an ensemble of experiments with different initial sizes and different environmental conditions, it does not necessarily describe the temporal development of an individual tracer distribution. In fact, as shown by Peeters (1994), individual clouds, even the original clouds of Okubo (1971; Fig. 18), grow more slowly with time (or with size) than predicted by Eq. (96).

There is an even more severe reservation with regard to the inertial subrange mixing model, viz. the obvious anisotropic spreading of tracer clouds. Because natural waters are always stratified to some extent, it does not come as a surprise that turbulence in the vertical is suppressed. It is more difficult to understand why isotropy does not

hold, at least in the horizontal direction. A relevant argument is introduced by the *shear-diffusion model* (Okubo 1967; Kullenberg 1972; Young et al. 1982; Peeters 1994) in which a nonturbulent shearing-velocity field is combined with small-scale (Fickian) turbulence, expressed by the small-scale horizontal and diapycnal diffusivity, K_h and K_d , respectively. In this model it is assumed that the small-scale horizontal turbulent diffusivities are spatially homogeneous ($K_x = K_y = K_h$), and that the nonturbulent velocity field is along the x axis and has the simple form $u = a \cdot y + b \cdot z$. Then the variances in the lengths of the major and minor principal axes of an evolving tracer cloud are given by the following expressions (Peeters 1994):

$$\begin{aligned} \sigma_{ma}^2 &= 2K_h t + \frac{1}{3}(a^2 K_h + b^2 K_d)t^3 + \\ &\quad \sqrt{K_h^2 a^2 t^4 + [\frac{1}{3}(a^2 K_h + b^2 K_d)t^3]^2}; \\ \sigma_{mi}^2 &= 2K_h t + \frac{1}{3}(a^2 K_h + b^2 K_d)t^3 - \\ &\quad \sqrt{K_h^2 a^2 t^4 + [\frac{1}{3}(a^2 K_h + b^2 K_d)t^3]^2}; \quad (98) \\ \sigma^2 &= 2\sigma_{ma} \sigma_{mi} \\ &= 2\sqrt{4K_h^2 t^2 + \frac{1}{3}K_h(a^2 K_h + 4b^2 K_d)t^4}. \end{aligned}$$

In rivers and streams the combined action of lateral and vertical shear ($a = \partial u / \partial y$ and $b = \partial u / \partial z$, respectively), as well as horizontal and

vertical small-scale diffusion (K_h and K_d , respectively), produces stretching and thus growth of the patch along the major principal axis, because the tracer is distributed by diffusion among layers of different horizontal velocities. As long as the vertical and horizontal extension, and thus the velocity shear, can be assumed to be unbounded relative to the actual size of the tracer cloud, the growth in the variance of the tracer distribution with time (second term in Eq. 98) increases progressively with larger shear (a and b) and larger diffusivity (K_h , K_d).

Note that for short times t the growth in cloud size σ^2 is proportional to the elapsed diffusion time t ($m = 1$, as for the Fickian model), whereas for long time intervals the growth of σ^2 is proportional to the square of elapsed time ($m = 2$), and the variance along the major principal axis σ_{ma}^2 can even increase proportionally to t^3 (see second and last terms in Eq. 98) as follows:

$$\sigma_{ma}^2 \sim \frac{2}{3}(a^2 K_h + b^2 K_d) t^3 \quad (99)$$

if t is very large. Hence, the inertial subrange model is not the only one that implies a 4/3-power law for the apparent isopycnal diffusivity K_i , at least along the major axis.

6.6.3 Experimental Observations

Among the models presented previously, only the shear-diffusion model is able to explain the two most important experimental findings on isopycnal diffusion in lakes, which are: (1) the tracer distributions are not radially symmetrical, but are stretched out along the direction of the main current (Fig. 17), and (2) the growth rate of the cloud sizes is less than predicted by the inertial subrange model, but increases with increasing elapsed diffusion time t (Fig. 18). The anisotropic spreading of individual dye clouds has been observed by Murthy (1976) in Lake Ontario. The variance along the length of the cloud exceeded that along its breadth by a factor of 5–10. Comparable anisotropy has been found in experiments carried out in several medium-sized Swiss lakes (Peeters et al. 1993; Fig. 17).

If the inertial subrange model provides the right qualitative dependence on ϵ (Eq. 97), the apparent isopycnal diffusion below the pycnocline of a stratified lake should be much smaller than in surface waters. Values of K_i observed by Murthy

(1976) in the hypolimnion of Lake Ontario were indeed one to two orders of magnitude smaller than those found in the epilimnion. A well-sampled dye experiment in the stratified water column of the Pacific (Ewart and Bendiner 1981) demonstrated that diffusivity decreased with depth at depths less than 500 m. Both experiments support the explanation that a decrease in TKE is responsible for the decrease in the apparent isopycnal diffusivity K_i .

It is less clear how shear-induced horizontal diffusion varies within the hypolimnion. As shown in Fig. 13, the diapycnal diffusivity is inversely related to the density stratification N , and thus commonly increases with depth below the pycnocline. In contrast, vertical shear usually has its maximum in the upper thermocline, where stratification is largest (see Sect. 6.1). In the density-stratified hypolimnion the vertical shear usually oscillates with time (see Sect. 6.1), e.g., $\partial u / \partial z \approx \sin(\omega t)$. The corresponding variance then increases only linearly with time (Kullenberg 1972):

$$\sigma^2 = \text{const } K_d \left(\frac{\partial u}{\partial z} \right)^2 t. \quad (100)$$

Isopycnal diffusion in lakes is generally smaller than in oceans (Fig. 18) and in fjords (Kullenberg 1972), and depends strongly on external forcing, i.e., on storm events (see Sect. 7.1). Diffusivities measured by Murthy (1976) and Peeters (1994) in the hypolimnion of various lakes range from $0.02 \text{ m}^2 \text{s}^{-1}$ to less than $0.3 \text{ m}^2 \text{s}^{-1}$, i.e., about five times smaller than in oceans. Under special conditions, e.g., below ice (Colman and Armstrong 1987), they may reach extremely low values. Because the two shear components ($\partial u / \partial z$ and $\partial u / \partial y$) are difficult to predict, since they depend on the local forcing, the parameterization of scale-dependent isopycnal mixing is generally difficult as well.

6.6.4 Intrusions

At lake surfaces wind is the main driving force for the currents that are responsible for velocity shear, and thus for isopycnal diffusion. In contrast, in the density-stratified hypolimnion, currents are also driven by intrusion, i.e., by isopycnal pressure forces resulting from horizontal-density gradients between adjacent water columns and from lateral water input. Intrusions

can have several origins (Fig. 7) including plunging rivers, subsurface springs, the subsurface withdrawal of water, differential mixing at the sediment surface and at topographical features such as sills and narrows, differential deepening of the pycnocline due to spatial heterogeneity of the surface wind stress, and large-scale exchange between basins with different mixing characteristics (Fig. 22). In the epilimnion, intrusions also result from differential cooling and heating, especially in the shallow parts of a lake. Because of the limited depth, the daily variation of the surface temperature is larger in shallow side arms than, for instance, in the open lake. Consequently, during the heating period the surface water from the side arms floods the open lake (Patterson 1987). In contrast, during cooling, surface water sinks to the bottom of the side arms, creeps down the slope, and merges into the lake interior (Horsch and Stefan 1988). There is no general theory for describing the vertical mixing due to horizontal density currents and intrusions, although their significance has become more apparent during the past few years. Because intrusions are directed, a diffusion scheme is hardly adequate for their description.

6.6.5 Diapycnal Effects of Isopycnal Mixing

Surfaces along which water moves without experiencing a restoring buoyancy force are termed *neutral surfaces* (McDougall 1987b). Neutral surfaces are nearly identical to isopycnal surfaces. Temperature and salinity changes along neutral surfaces are related by $\text{ad}\theta = \beta_s dS$, where θ is potential temperature (Eq. 39). If water moving along a neutral surface mixes laterally with surrounding water, water with a new temperature and salinity is created. Because the equation of state of water is nonlinear (Eq. 29), the modified water has a density that is larger than the density corresponding to the particular neutral surface. The parcel thus experiences a force perpendicular to the neutral (or isopycnal) surface. As mentioned in Section 4.1, the two largest contributions to the nonlinear effect are *thermobaricity* (caused by the pressure dependence of α) and *cabbeling* (caused by the temperature dependence of α) (McDougall 1987a).

Cabbeling is well known in lakes. For example, when equal volumes of water of 3 °C from the open lake and 5 °C from near the shore merge,

the mixed water of 4 °C is heavier and sinks. This effect leads to the well-known thermal bar phenomenon. Figure 19 shows a thermal bar observed in Lake Baikal in early summer. The lines of constant salinity indicate the strong vertical exchange near the thermal bar, approximately 1.5 km offshore. Because the shape of the $\rho(T)$ function is such that mixed water is always heavier than the original waters, cabbeling not only occurs at temperatures near 4 °C; yet, it always causes downwelling of fluid through

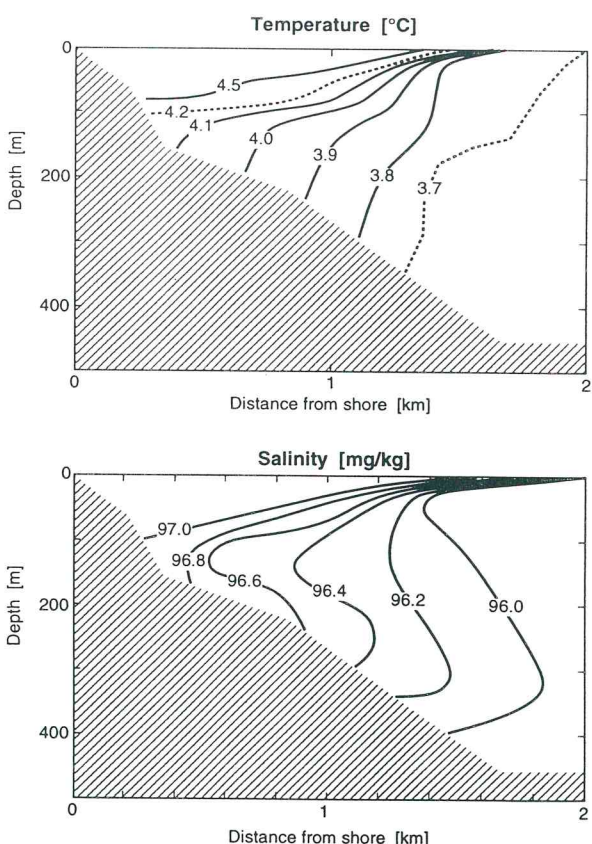


Fig. 19. Formation of the thermal bar in Lake Baikal as observed on 7 June 1993 at the eastern shore of the middle basin near Boldakova. In spring, the nearshore waters warm up faster than the waters of the central part of the lake. The mechanisms for this differential heating are not yet fully understood, but it seems that at least part of the warming is due to relatively warm water from the Selenga River, the major inflow to Lake Baikal, flowing north along the eastern shore. The upper figure shows the isotherms (temperatures in °C) in an east/west section perpendicular to the shore. At the surface, the thermal bar, determined by the temperature of maximum density (4 °C), lies approximately 1.5 km offshore. As shown in the lower figure, the lines of constant salinity indicate fast vertical mixing in this zone

neutral surfaces. In contrast, thermobaricity, depending on the slope of the neutral surface, can lead to either upwelling or downwelling.

11b) are small they do not survive long, unless they are continually fed with energy from the large-scale processes.

7 Mixing and Its Ecological Relevance

7.1 Time Scales of Mixing

Mixing phenomena in lakes cover a wide range of time scales, from hundreds to thousands of years in the case of permanent stratification to seconds for surface waves and turbulent eddies (Table 13). On one hand, this enormous range reflects the spectrum of external forces extending from individual wind gusts up to climate changes; on the other hand, the time scales are also determined by the characteristics of the various physical phenomena that occur internally in lakes, which are discussed in the following sections.

7.1.1 Seconds and Minutes

The processes at one end of the mixing hierarchy, the short- and small-scale events, bridge the gap from stirring to mixing and are thus the essential elements for mixing. Here, we find the surface waves and the turbulent overturns depicted in Fig. 11a. However, because these features (Fig.

7.1.2 Hours

This is the most typical time scale for epilimnetic processes, although the development of some hypolimnetic processes, e.g., storm-induced turbidity currents and standing internal waves, also occur on the same time scale. In contrast to the internal-wave field, which is important for hypolimnetic mixing, the energy that drives mixing in the epilimnion cannot easily be stored in a non-turbulent way. The response of the epilimnion to wind stress and surface buoyancy flux is therefore immediate and fast. The typical response time of a nonstratified epilimnion is given by a characteristic turbulent velocity u_{turb} and the depth of the mixed layer h_{mix} :

$$t_{\text{resp}} = \frac{h_{\text{mix}}}{u_{\text{turb}}} \quad (101)$$

The characteristic turbulent velocity u_{turb} is defined as the friction velocity, $u_* = (\tau_o/\rho)^{1/2}$, if wind-driven turbulence dominates, and as $u_b = (h_{\text{mix}} J_b^0)^{1/3}$ for convectively driven mixing (Dear-dorff 1970). This scale represents the time lag between the onset of the forcing and the time

Table 13. Characteristic time scales of mixing processes in lakes

Time scale	Process	Examples
Seconds and minutes	Surface waves	
	Turbulent overturns	Thorpe (1977) and Dillon (1982)
	Stability oscillation in stratified water	
	Langmuir circulation	Leibovich (1983)
Hours	Wind setup	Spigel and Imberger (1980)
	Internal waves	
	Diurnal mixed layer	Imberger (1985)
	Lateral convection due to differential heating/cooling	Horsch and Stefan (1988)
	Convective turbulence	Lombardo and Gregg (1989)
	Turbidity currents	Lambert (1988)
Days	Inertial modes	
	Mixing due to storms	Imboden et al. (1988)
	Basin modes (topographical waves)	Saylor et al. (1980)
Weeks and months	Annual stratification cycles	
	Basin-wide exchange due to horizontal density gradients	Wüest et al. (1988)
	Internal-wave damping in regularly shaped basins	Mortimer (1974), Csanady (1974)
	Thermal bar	
Years	Meromixis	Sanderson et al. (1986), Steinhorn (1985)

when turbulence in the mixed layer becomes stationary and pycnocline erosion starts. The following example yields typical values for t_{resp} : For a wind speed $W_{10} = 5 \text{ m s}^{-1}$, the friction velocity u_* , and thus u_{turb} , is roughly $5 \times 10^{-3} \text{ m s}^{-1}$, yielding $t_{\text{resp}} \sim 0.5 \text{ h}$ for $h_{\text{mix}} = 10 \text{ m}$. In the case of a positive surface buoyancy flux J_b^o , caused for instance by surface cooling, we obtain a value u_b of the same magnitude as u_* if $J_b^o = 10^{-8} \text{ W kg}^{-1}$. This buoyancy flux would result, for example, from a net heat loss $H_{\text{net}} = -60 \text{ W m}^{-2}$ from a water body at 10°C .

Buoyancy flux and wind shear are hardly ever in balance in the epilimnion. Thus, during the day a weak stratification, the *diurnal pycnocline*, is usually formed. An increase in the production of TKE causes the turbulence front to move downward from the surface, resulting in erosion of the diurnal pycnocline. Associated with the mixing of a layer of depth h_{mix} with stratification N is a change in potential energy of $\frac{1}{12}\rho N^2 h_{\text{mix}}^3 [\text{J m}^{-2}]$, provided that the density of the mixed water can be approximated by a linear function of the properties of the water that determine its density (usually temperature and salinity). The change in potential energy is fueled by the buoyancy flux J_b , which, as discussed in Section 5.4, is roughly 10% of the total dissipation (Eq. 56). Given this mixing efficiency and the vertical profiles of dissipation for wind and convectively driven surface turbulence (Fig. 10), i.e., $\varepsilon_w(z) = \frac{u_*^3}{kz}$ and $\varepsilon_c(z) = J_b^o$, we can estimate

the mixing time scales simply by integration. The resulting time scale is

$$t \approx \frac{5}{3} N^2 h_{\text{mix}}^3 k / u_*^3 \quad (102)$$

for wind-driven turbulence and

$$t \approx \frac{5}{2} N^2 h_{\text{mix}}^2 / J_b^o \quad (103)$$

for convectively driven mixing. The difference in the form of the dependence of t on layer depth h_{mix} again reflects the high deepening efficiency of the wind in shallow water and the dominance of convection at greater depth. An example for the diurnal energetics of the epilimnion under different forcing was given by Imberger (1985).

Mixing events in the hypolimnion generally have time scales on the order of days. In Fig. 20, however, a fascinating example is shown where photo-autotrophic bacteria are able to produce convective mixing in the hypolimnion on time scales of hours to days.

7.1.3 Days

Internal waves in lakes have time periods of hours to days. Forcing is applied at the same time scales, because wind-speed spectra have a synoptic scale maximum (i.e., 1 to several days). If a wind event lasts longer than roughly a quarter of the seiche period of the first internal horizontal mode, first-mode seiching is the dominant response to the

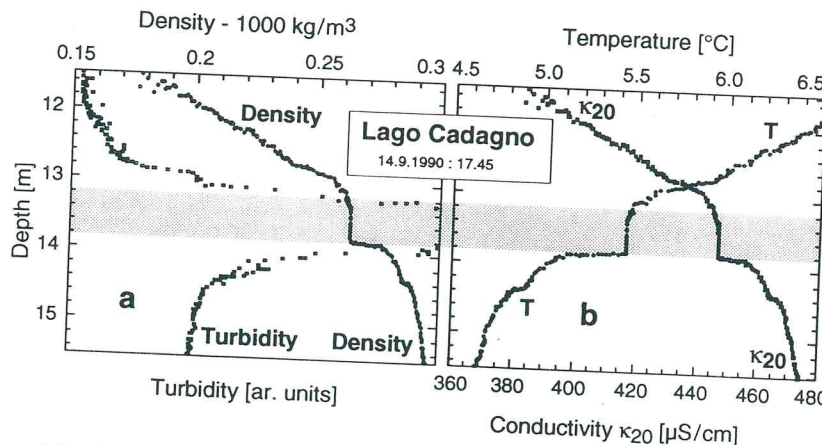


Fig. 20. Turbidity and density (a) as well as temperature and the ionic concentration (b) in Lago Cadagno reveal a homogeneous layer (indicated by the gray shading) of 0.8 m thickness in a depth of approximately 13.5 m. The well-mixed layer coincides with a dense population of photo-autotrophic sulfur bacteria growing in the oxic-

anoxic transition zone. Based on turbulent kinetic energy arguments, it can be shown that the microorganisms are able to mix this layer convectively within a few hours by means of swimming. (Redrawn from Wüest 1994)

wind. An exceptional situation occurs if a lake that is predominantly driven by diurnal winds has an internal mode of higher order with a period close to 24 h. This is the case in Alpnachersee, a small basin of Lake Lucerne (Switzerland). Münnich et al. (1992) found the *first horizontal/second vertical* mode to be the dominant internal mode during most of the time (see Sect. 6.1 and Fig. 14a).

Further development of the internal-wave motion is complex. The first mode generally decays into modes of higher horizontal and vertical order (Wiegand and Chamberlain 1987). The time scale for the decay of the internal-wave field is strongly dependent on mixing. If nonlinearities occur, damping is strong and intense mixing occurs even within one seiche period. An example from Zugersee (Switzerland) is given in Fig. 21. In contrast, small internal amplitudes in regularly shaped basins are only moderately damped and can last for weeks (Lemmin 1987).

7.1.4 Weeks and Months

The annual stratification of a lake is the most prominent feature occurring on a time scale of weeks and months. The seasonal pycnocline represents an integral response to heating, wind stress, convectively driven turbulence, and river inflows. However, the temporal evolution of the vertical density stratification may vary slightly over the lake surface. This is especially the case during the initial phase of the seasonal temperature stratification when the density gradients are still small, and slight differences in the wind-shear stress, for example, may result in significant variations in pycnocline depth. Such horizontal density gradients, coupled to the stratification cycle, may cause long-lasting basinwide currents.

Another source of horizontal density gradients is given by river inflows of different thermal or chemical characteristics. The induced basinwide exchanges may be long-lasting or even permanent, especially if the density difference among the inflows is due to different geochemical composition. An example from Lake Lucerne (Switzerland), where both thermal and geochemical effects are important, is given in Fig. 22.

In large lakes in which the surface temperature has dropped below 4°C during the winter, a thermally driven circulation pattern may occur in spring, when the water in the zones near the shore

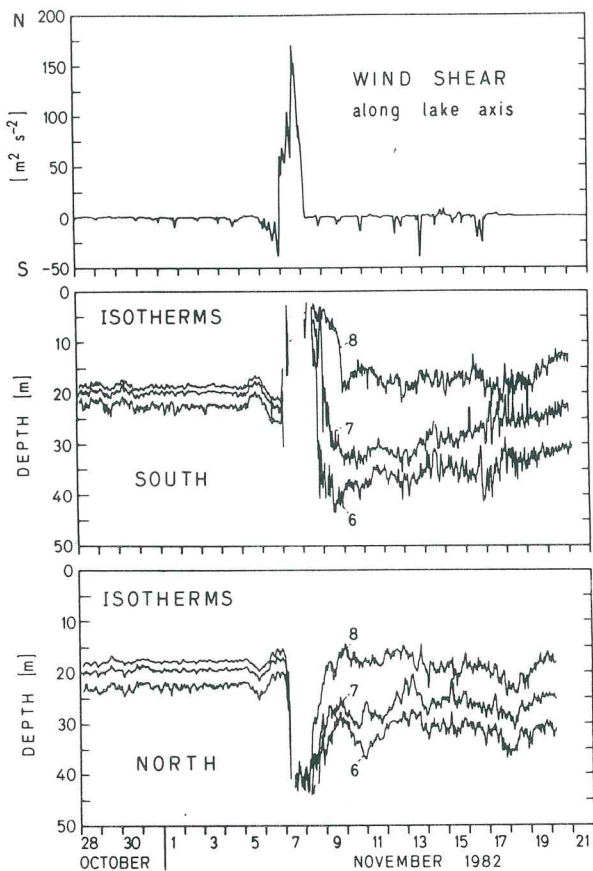


Fig. 21. Wind stress (upper panel) along the main axis of Zugersee (Switzerland) and corresponding isotherm depths during a vigorous föhn storm with wind speeds measured at a nearby weather station exceeding 45 m s^{-1} . The storm blowing from the south began on 7 November 1982, after a short period during which the wind blew from the north. At the southern end of the lake cold water was brought to the surface (middle panel), while at the northern end (lower panel) the warm surface water was pushed down below 45 m, the lower end of the thermistor string. After the storm large-amplitude internal waves, generated by nonlinear interactions, remained in the lake for more than 10 days. The first mode of the internal seiche, however, was strongly damped, due to shear instabilities (Fig. 11) leading to an increase in short-term diapycnal eddy diffusion of nearly three orders of magnitude compared with the preceding 6 months (see also Fig. 13). (Redrawn from Imboden et al. 1988)

warms up faster than in the middle of the lake. This difference may be caused by warm river water, by reduced vertical wind mixing, or by a combination of both. Thus, during the onset of stratification a situation occurs in which part of the lake surface is occupied by water that is warmer than 4°C, while the rest of the surface

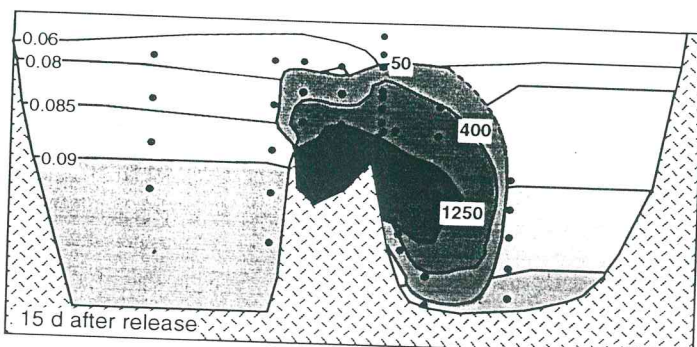


Fig. 22. Urnersee (right) and Gersauersee (left), separated by two sills, are adjacent deep basins of Lake Lucerne (Switzerland), with similar topography but remarkably different wind exposure. Urnersee experiences diurnal winds and occasional strong storms from the south (right), whereas the wind over the sheltered Gersauersee is usually weak. In spring, large-scale wind mixing results in the subsurface water of the wind-exposed Urnersee becoming warmer and lighter. This differential mixing generates a weak horizontal density gradient between the two basins, demonstrated by the change of depths of the isopycnals between the basins.

As a consequence, nearly the whole of the deep water of Urnersee is replaced by a slow but long-lasting exchange flow of approximately $10^7 \text{ m}^3 \text{ d}^{-1}$ of water (Wüest et al. 1988). The figure shows the effect of this exchange via the distribution of SF_6 , 15 days after its release into the intermediate basin (redrawn from Schlatter 1991). Once the horizontal-density gradient has vanished, water from below the sill can still undergo exchange by a process termed seiche pumping, in which heavier water can flow over the sill during the maximum rise of the isotherms and merge into the deep part of Urnersee. (Van Senden and Imboden 1989)

water is still colder than 4°C . The two water masses are separated by a transition zone (thermal bar) where water sinks to the deeper part of the lake, due to cabbeling. As the heating continues the thermal bar moves offshore until the temperature of the entire surface exceeds 4°C . Because of the Coriolis effect, specific thermally driven coastal currents are induced by the thermal bar (Csanady 1974; Mortimer 1974). Figure 19 shows a thermal bar in Lake Baikal, Siberia.

7.1.5 Years

During periods of lowest stability, if convective mixing due to heat loss and wind shear is too weak to destroy the density stratification, part of the lake may remain permanently stratified. This is called *meromixis*. Mixing rates in the deep layers of meromictic lakes are extremely slow, approaching rates of molecular diffusion. In such a situation differences in the molecular-diffusion coefficients of ions may become relevant. An instructive example of *differential diffusion* occurring over a time scale of 10 000 years is given by Sanderson et al. (1986) for the case of seawater trapped in a deep fjord lake.

Another interesting example of meromixis was found in the Dead Sea, a deep ($\approx 320 \text{ m}$), warm (minimum temperature $\approx 18^\circ\text{C}$), and hypersaline

($S = 280 \text{ g/kg}^{-1}$) lake (Steinhorn 1985). The meromixis originates from the freshwater input to the lake from the rivers, which creates a strong pycnocline. During the past 300 years winter cooling was not able to overcome this strong stratification. In the past few decades, however, and especially since 1964, an increasing fraction of the water from the Jordan and Yarmuk rivers has been diverted for irrigation purposes, resulting in a decrease in the amount of fresh water flowing into the Dead Sea. Consequently, because of evaporation, the thickness of the less-saline surface layer decreased and the water level of the lake dropped. Furthermore, the salinity differences between surface and deep waters were reduced from 50% in 1864 to $<0.1\%$ in 1978. The final consequence of this was that the long period of strong meromixis ended in early 1979. Since then the meromictic structure has been variable. The Dead Sea can now turn over during winter depending on the strength, timing, and duration of river inflow, evaporation, and cooling (Anati et al. 1987).

7.2 Reactive Species and Patchiness

The distribution of a chemical or biological species in a lake is determined by the ratio of two kinds of time scales, the reaction and input time scales on

one hand, and the mixing time scales on the other. The latter have already been discussed extensively in the preceding sections and are summarized in Table 13. We now add a few remarks on reaction rates.

The time scales of reactions range from milliseconds (or less) to millions of years. Examples for the former are fast equilibrium reactions (e.g., hydrolysis), and for the latter the slow diagenetic transformations occurring in ocean and lake sediments or the radioactive decay of long-living isotopes such as ^{238}U . Although reactions exhibit a great variety of kinetics (zero, first, and higher orders), the instantaneous rate of change can be characterized by the relative rate λ_r (or the reaction time τ_r)

$$\lambda_r = \tau_r^{-1} = \frac{1}{C} \left| \frac{dC}{dt} \right|_{\text{reaction}} . \quad [\text{s}^{-1}] \quad (104)$$

For a first-order reaction, such as radioactive decay, λ_r is constant; otherwise, λ_r represents an instantaneous pseudo-first-order rate that changes its size with changing concentrations of the reaction partners.

A simple way to deal with the simultaneous action of mixing and reaction is to compare the relative size of mixing and reaction times, τ_{mix} and τ_r (Imboden and Lerman 1978). As demonstrated previously, because mixing in aquatic systems usually consists of a whole set of simultaneous processes occurring on different time scales, it is appropriate to consider the effect of a reaction (characterized by τ_r) on a whole spectrum of mixing processes such as the turbulent velocity spectrum in the inertial subrange, $E(k)$, defined in Eq. (57).

Corrsin (1961) calculated the spatial spectrum of a reactive species, $E_c(k)$, undergoing a first-order reaction in an isotropic, stationary turbulent field. He found that there exists a critical wave number k_r , given by

$$k_r = |\lambda_r|^{3/2} \varepsilon^{-1/2}, \quad [\text{m}^{-1}] \quad (105)$$

below which the velocity and concentration spectra diverge. If k_r lies in the inertial-convective subrange (see Sect. 5.5), we expect to find a k range of large (and thus slow) modes where $E(k)$ and $E_c(k)$ are different and therefore reveal the non-conservative nature of the reactive species. In contrast, for short wavelengths (large k), the two spectra would be identical. The critical-length scale k_r^{-1} , above which tracer-specific patterns are to be expected, lies between approximately 10^3 m

at large turbulence intensity for species reacting within hours and 10^5 m at high intensity for species reacting within months. (Species with much shorter or longer reaction times are not relevant to the above!) Strictly speaking, these length scales are much larger than the Kolmogorov Scale (Table 6). Therefore, it is not clear how Corrsin's theory can be applied to the conditions existing in lakes.

Denman et al. (1977) showed that for a tracer with positive reaction (e.g., phytoplankton growth), the spectrum $E_c(k)$ should reach a maximum at $1.3 k_r$. Powell et al. (1975) measured the velocity and chlorophyll spectra in Lake Tahoe (California/Nevada). In the chlorophyll spectrum they found a peak at $k = 10^{-2} \text{ m}^{-1}$, which was not present in the velocity spectrum, and which they attributed to Langmuir circulation. In light of the theory of Denman et al. (1977), the peak could also be the result of phytoplankton growth (see Imboden 1990, for details).

The interplay of turbulence and reactivity produces a pattern in the spatial concentration distribution, which, for certain wave numbers, bears the imprint of the reaction. This is equivalent to saying that reaction creates patchiness. In fact, patchiness is a special property of biological species. Yet, turbulence is not the only explanation for the occurrence of patchiness; another source of patchiness is related to the nonlinear nature of biological processes such as the predator-prey interaction described, for example, by the Lotka-Volterra model. Steele (1974) was the first to draw attention to the special phenomena that appear if the nonlinear Lotka-Volterra interaction is combined with a spatial diffusion term. We first discuss the equation for a prey (e.g., a phytoplankton species, described by its concentration P) during exponential growth (growth rate α) under the influence of Fickian (turbulent) diffusion (diffusivity K):

$$\frac{\partial P}{\partial t} = \alpha P + K \frac{\partial^2 P}{\partial x^2}. \quad (106)$$

(For simplicity, only one dimension is considered here!) Assume that at some initial time t , $P(x)$ has an arbitrary spatial variance expressed by the Fourier-transform function $\hat{P}(k)$. Its time rate of change is

$$\frac{\partial \hat{P}}{\partial t} = (\alpha - k^2 K) \hat{P}. \quad (107)$$

Thus, the mode $\hat{P}(k)$ can only grow provided that

$$k < \left(\frac{\alpha}{K}\right)^{1/2}. \quad (108)$$

This is equivalent to saying that a species patch can only grow in size provided that its length scale L is larger than a critical size L_{crit} :

$$L > L_{\text{crit}} = 2\pi \left(\frac{K}{\alpha}\right)^{1/2}. \quad (109)$$

L_{crit} is the well-known critical-length scale first introduced by Kierstead and Slobodkin (1953). Because the growth rate α decreases at higher trophic levels (zooplankton, fish, etc.), the minimum stable patch size L_{crit} becomes larger with higher trophic level. Steele (1978) developed this model further to explain the patchiness of biomass in the ocean (Fig. 23).

The terms involving interactions between different species, such as the predator-prey interaction appearing in the Lotka-Volterra model,

mix the different k modes, modify the stability criterion, and create new spatial structure in the ecosystem such as "prey-predator waves" (Dubois 1975).

Further discussion of the problem of spatial variability in ecological systems is beyond the scope of this chapter. The interested reader is referred to Platt and Denman (1975) as well as Wroblewski and O'Brien (1976), in which the role of mixing in the evolution and stability of ecosystems is treated.

7.3 Mixing and Growth: The Search for an Ecological Steering Factor

The problem of influence of turbulence on phytoplanktonic species selection and photosynthesis is as yet unsolved. The literature on the subject is contradictory. For instance, Lewis et al. (1984a) concluded for the upper mixed layer in Bedford Basin (Nova Scotia) that "dissipation of turbulent kinetic energy was a strong determinant of algal photosynthetic rate." In contrast, Gallegos and Platt (1982) found in the eastern Canadian Arctic that mixing had only little effect on primary production in the water column.

In the meantime, new insight has been gained by combining measurements of physical and biological parameters with computer models of photosynthesis. Lewis et al. (1984b) developed a theory that characterizes the mixing/production relationship by two nondimensional numbers. The first of these is the mixing-photoadaptation ratio, which is large if the time taken by the plankton to move through different light zones is short compared with the typical photoadaptation time. The second number measures the degree of homogeneity of light intensities within the mixed layer. To summarize the ideas of Lewis et al. (1984b), fast mixing and small light gradients in the mixing layer favor the appearance of a homogeneous planktonic community, whereas low turbulence and large light gradients lead to the establishment of distinct communities that differ with regard to their light-adaptation characteristics.

There are as yet no comparable studies on lakes. In fact, the many factors that influence the dynamics of a lake (Table 1 and Fig. 7) make it more difficult to separate the effect of mixing from other effects. Based on a dynamic model for photosynthesis, however, Pahl-Wostl and

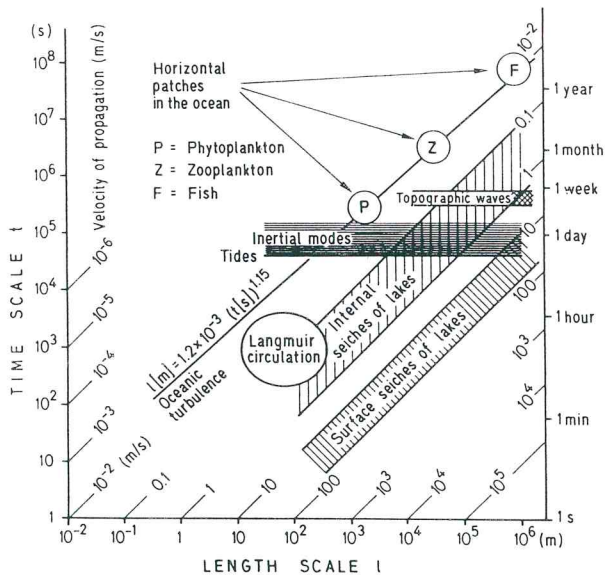


Fig. 23. Typical length and time scales of mixing modes in lakes: The diagonals of gradient 1 represent lines of constant velocity of propagation (e.g., surface seiches move with velocities between approximately 10 and 100 m s⁻¹). Included is Okubo's (1971) fit between length and time scales for oceanic turbulence. Typical scales of biological patchiness (phytoplankton, zooplankton, and fish) taken from Steele (1978) can be interpreted as the direct consequence of the influence of the isopycnal turbulent scales on species with different growth rates. (Imboden 1990)

Imboden (1990) gave some theoretical arguments supporting the idea that the mixing regime of a lake could play a role not only in the spatial distribution of abiotic components, but also in the competition between biological species. Building and strengthening a bridge to link the various limnological disciplines will certainly be among the most urgent and exciting tasks to be tackled in lake research in the future.

References

- Amorocho J, deVries JJ (1980) A new evaluation of the wind stress coefficient over water surfaces. *J Geophys Res* 85:433–442
- Anati DA, Stiller M, Shasha S, Gat JR (1987) Changes in the thermohaline structure of the Dead Sea: 1979–1984. *Earth Planet Sci Lett* 84:109–121
- Armi L (1978) Some evidence for boundary mixing in the deep ocean. *J Geophys Res* 83:1971–1979
- Armi L (1979) Effects of variation in eddy diffusivity on property distributions in the ocean. *J Mar Res* 37:515–530
- Barry RG, Chorley RJ (1976) Atmosphere, weather and climate. Methuen, London
- Batchelor GK (1950) The application of the similarity theory of turbulence to atmospheric diffusion. *Q J R Meteorol Soc* 76:133–146
- Batchelor GK (1959) Small-scale variation of convected quantities like temperature in turbulent fluid. *J Fluid Mech* 5:113–139
- Boudreau BP, Imboden DM (1987) Mathematics of tracer mixing in sediments: III. The theory of non-local mixing within sediments. *Am J Sci* 287: 693–719
- Brutsaert W (1975) On a derivable formula for long-wave radiation from clear skies. *Water Resour Res* 11:742–744
- Bührer H, Ambühl H (1975) Die Einleitung von gereinigtem Abwasser in Seen. *Schweiz Z Hydrol* 37:347–369
- Bünti JL (1914) Chronicle. *Neujahrsbl Uri*, Altdorf 20:8–9
- Caldwell DR, Chriss TM (1979) The viscous sublayer at the sea floor. *Science* 205:1131–1132
- Carter HH, Okubo A (1965) A study of the physical processes of the movement and dispersion in the Cape Kennedy area. Final Rep under US Atomic Energy Comm, Chesapeake Bay Inst, John Hopkins Univ, Rep No NYO-2973-1, 164 pp
- Chen CTA, Millero FJ (1986) Precise thermodynamic properties for natural waters covering only the limnological range. *Limnol Oceanogr* 31:657–662
- Chriss TM, Caldwell DR (1982) Evidence for the influence of form drag on bottom boundary layer flow. *J Geophys Res* 87:4148–4154
- Chriss TM, Caldwell DR (1984) Universal similarity and the thickness of the viscous sublayer at the ocean floor. *J Geophys Res* 89:6403–6414
- Chung Y, Kim K (1980) Excess ^{222}Rn and the benthic layer in the western and southern Indian ocean. *Earth Planet Sci Lett* 49:351–359
- Colman JA, Armstrong DE (1987) Vertical eddy diffusivity determined with Radon-222 in the benthic boundary layer of ice covered lakes. *Limnol Oceanogr* 32:577–590
- Corrsin S (1961) The reactant concentration spectrum in turbulent mixing with a first-order reaction. *J Fluid Mech* 11:407–416
- Csanady GT (1974) Spring thermocline behavior in Lake Ontario during IFYGL. *J Phys Oceanogr* 4:425–445
- Deardorff JW (1970) Convective velocity and temperature scales for unstable planetary boundary layer and for Rayleigh convection. *J Atmos Sci* 27:1211–1213
- Deardorff JW, Willis CE, Lilly DK (1969) Laboratory investigation of non-steady penetrative convection. *J Fluid Mech* 28:675–704
- Denman KL, Miyake M (1973) Upper layer modification at Ocean Station Papa: observations and simulations. *J Phys Oceanogr* 3:185–196
- Denman KL, Okubo A, Platt T (1977) The chlorophyll fluctuation spectrum in the sea. *Limnol Oceanogr* 22:1033–1038
- Dewey RK, Crawford WR (1988) Bottom stress estimates from vertical dissipation rate profiles on the continental shelf. *J Phys Oceanogr* 87:1167–1177
- Dewey RK, Crawford WR, Gargett AE, Oakey NS (1987) A microstructure instrument for profiling oceanic turbulence in coastal bottom boundary layers. *J Atmos Oceanic Technol* 4:288–297
- Dillon TM (1982) Vertical overturns: a comparison of Thorpe and Ozmidov length scales. *J Geophys Res* 87:9601–9613
- Dillon TM, Caldwell DR (1980) The Batchelor spectrum and dissipation in the upper ocean. *J Geophys Res* 85:1910–1916
- Dillon TM, Powell TM (1979) Observations of a surface mixed layer. *Deep-Sea Res* 26(A):915–932
- Dillon TM, Richman JG, Hansen CG, Pearson MD (1981) Near-surface turbulence measurements in a lake. *Nature* 290:390–392
- Dimai A, Gloor M, Wüst A (1994) Bestimmung der Intensität von Turbulenz in der Bodengrenzschicht von Seen. *Limnologica* 24:339–350
- Dubois DM (1975) A model of patchiness for prey-predator plankton populations. *Ecol Modelling* 1:67–80
- Eckart C (1948) An analysis of the stirring and mixing processes in incompressible fluids. *J Mar Res* 7: 265–275
- Elliott AJ (1984) Measurements of the turbulence in an abyssal boundary layer. *J Phys Oceanogr* 14:1778–1786
- Ewart TE, Bendiner WP (1981) An observation of the horizontal and vertical diffusion of a passive tracer in the deep ocean. *J Geophys Res* 86:10974–10982
- Forel FA (1876) La formule des seiches. *C R Acad Sci Paris* 83:712–714
- Fozdar FM, Parker GJ, Imberger J (1985) Matching temperature and conductivity sensor response

- characteristics. *J Phys Oceanogr* 15:1557–1569
- Gallegos CL, Platt T (1982) Phytoplankton production and water motion in surface mixed layers. *Deep-Sea Res* 29:65–76
- Gargett AE, Sanford TS, Osborn TR (1979) Surface mixing layers in the Sargasso Sea. *J Phys Oceanogr* 9:1090–1111
- Gargett AE, Osborn TR, Nasmyth PW (1984) Local isotropy and the decay of turbulence in a stratified fluid. *J Fluid Mech* 144:231–280
- Garrett C (1990) The role of secondary circulation in boundary mixing. *J Geophys Res* 95:3181–3188
- Garrett C (1991) Marginal mixing theories. *Atmos Ocean* 29:313–331
- Gill AE (1982) Ocean atmosphere dynamics. Academic Press, New York
- Gloos M, Wüest A, Münnich M (1994) Benthic boundary mixing and resuspension induced by internal seiches. *Hydrobiologia* 284:59–68
- Grant WD, Williams III AJ, Glenn SM (1984) Bottom stress estimates and their prediction on the northern California continental shelf during CODE-1: the importance of wave-current interaction. *J Phys Oceanogr* 14:506–527
- Gregg MC (1987) Diapycnal mixing in the thermocline: a review. *J Geophys Res* 92:5249–5286
- Gregg MC, Sanford TB (1988) The dependence of turbulent dissipation on stratification in a diffusively stable thermocline. *J Geophys Res* 93:12381–12392
- Gust G (1982) Tools for oceanic small-scale, high-frequency flows: metal-clad hot wires. *J Geophys Res* 87:447–455
- Gust G, Weatherly GL (1985) Velocities, turbulence and skin friction in a deep-sea logarithmic layer. *J Geophys Res* 90:4779–4792
- Herdendorf CE (1990) Distribution of the world's large lakes. In: Tilzer M, Serruya C (eds) Large lakes: ecological structure and function. Springer, Berlin, Heidelberg, New York, pp 3–38
- Hinze JO (1975) Turbulence, 2nd edn. McGraw-Hill, New York, 618 pp
- Horn W, Mortimer CH, Schwab DJ (1986) Wind-induced internal seiches in Lake Zurich observed and modeled. *Limnol Oceanogr* 31:1232–1254
- Horsch GM, Stefan HG (1988) Convective circulation in littoral water due to surface cooling. *Limnol Oceanogr* 33:1068–1083
- Huppert HE, Turner JS (1972) Double-diffusive convection and its implications for the temperature and salinity structure of the ocean and Lake Vanda. *J Phys Oceanogr* 2:456–461
- Hutchinson GE (1957) A treatise on limnology. Wiley, New York
- Hutter K (1983) Hydrodynamics of lakes. Springer, Berlin, Heidelberg, New York
- Imberger J (1985) The diurnal mixed layer. *Limnol Oceanogr* 30:737–770
- Imberger J, Patterson JC (1990) Physical Limnology. Advances in applied mechanics. Academic Press, Cambridge, pp 303–475
- Imboden DM (1981) Tracer and mixing in the aquatic environment. Swiss Federal Institute of Technology, Zürich
- Imboden DM (1990) Mixing and transport in lakes: mechanisms and ecological relevance. In: Tilzer M, Serruya C (eds) Large lakes: ecological structure and function. Springer, Berlin, Heidelberg, New York, pp 47–80
- Imboden DM, Lerman A (1978) Chemical models of lakes. In: Lerman A (ed) Lakes – chemistry, geology, physics. Springer, Berlin, Heidelberg, New York, pp 341–356
- Imboden DM, Joller T (1984) Turbulent mixing in the hypolimnion of Baldeggsee (Switzerland) traced by natural radon-222. *Limnol Oceanogr* 29:831–844
- Imboden DM, Stotz B, Wüest A (1988) Hypolimnic mixing in a deep alpine lake and the role of a storm event. *Verh Int Verein Limnol* 23:67–73
- Ivey CN, Imberger J (1991) On the nature of turbulence in a stratified fluid. Part I. The energetics of mixing. *J Phys Oceanogr* 21:650–659
- Joseph J, Sendner H (1958) Über die horizontale Diffusion im Meer. *Dtsch Hydrogr Z* 11:49–77
- Kelvin L, Thomson SW (1875) On an alleged error in Laplace's theory of the tides. *Philos Mag* 4:227–242
- Kierstead H, Slobodkin LB (1953) The size of water masses containing plankton blooms. *J Mar Res* 12:141–147
- Kolmogorov AN (1941) The local structure of turbulence in an incompressible viscous fluid for very large Reynolds numbers. *Dokl Akad Nauk USSR* 30:299–303
- Kuhn W (1979) Aus Wärmehaushalt und Klimadaten berechnete Verdunstung des Zürichsees. *Vierteljahrsschr Naturforsch Ges Zür* 123:261–283
- Kullenberg G (1972) Apparent horizontal diffusion in stratified vertical shear flow. *Tellus* 24:17–28
- Kullenberg G, Murthy CR, Westerberg H (1973) An experimental study of diffusion characteristics in the thermocline and hypolimnion regions of Lake Ontario. *Proc 16th Conf Great Lakes Res*, pp 774–790
- Kunze E (1987) Limits on growing, finite length salt fingers: a Richardson number constraint. *J Mar Res* 45:533–556
- Lambert A (1988) Records of riverborne turbidity currents and indications of slope failure in the Rhone delta of Lake Geneva. *Limnol Oceanogr* 33: 458–468
- Langmuir I (1938) Surface motion of water induced by wind. *Science* 87:119–123
- LeBlond PH, Mysak LA (1978) Waves in the ocean. Elsevier, Amsterdam
- Ledwell JR, Watson AJ, Law CS (1993) Evidence for slow mixing across the pycnocline from an open-ocean tracer-release experiment. *Nature* 364: 701–703
- Leeder MR (1983) On the dynamics of sediment suspension by residual Reynolds stresses – confirmation of Bagnold's theory. *Sedimentology* 30:485–491
- Leibovich S (1983) The form and dynamics of Langmuir circulations. *Annu Rev Fluid Mech* 15:391–427
- Leimin U (1987) The structure and dynamics of internal waves in Baldeggsee. *Limnol Oceanogr* 32:43–61
- Leimin U, Mortimer CH (1986) Tests of an extension to internal seiches of Defant's procedure for determination of seiche characteristics in real lakes.

- Limnol Oceanogr 31:1207–1231
- Lewis MR, Horue EPW, Cullen JJ, Oakey NS, Platt T (1984a) Turbulent motions may control phytoplankton photosynthesis in the upper ocean. *Nature* 311:49–50
- Lewis MR, Cullen JJ, Platt T (1984b) Relationship between vertical mixing and photoadaptation of phytoplankton: similarity criteria. *Mar Ecol Prog Ser* 15:141–149
- Lighthill J (1978) Waves in fluids. Cambridge Univ Press, Cambridge
- Lombardo CP, Gregg MC (1989) Similarity scaling of ε and χ in a convecting surface boundary layer. *J Geophys Res* 94:6273–6284
- Marti DE, Imboden DM (1986) Thermische Energieflüsse an der Wasseroberfläche: Beispiel Sempachersee. *Schweiz Z Hydrol* 48:196–229
- McDougall TJ (1987a) Thermobaricity, cabbeling and water mass conversion. *J Geophys Res* 92: 5448–5464
- McDougall TJ (1987b) Neutral surfaces. *J Phys Oceanogr* 17:1950–1964
- McDougall TJ, Taylor JR (1984) Flux measurements across a finger interface at low values of the stability ratio. *J Mar Res* 42:1–14
- Miller MC, McCave IN, Komar PD (1977) Threshold of sediment motion under unidirectional currents. *Sedimentology* 24:507–527
- Mortimer CH (1974) Lake hydrodynamics. *Verh Int Verein Limnol* 20:124–197
- Mortimer CH (1975) Substantive corrections to SIL communications (IVL Mitteilungen) Numbers 6 and 20. *Verh Int Verein Limnol* 19:60–72
- Mortimer CH (1979) Strategies for coupling data collection and analysis with dynamic modelling of lake motion. In: Graf WH, Mortimer CH (eds) Hydrodynamics of lakes. Elsevier, Amsterdam, pp 183–222
- Münnich M (1993) On the influence of bottom topography on the vertical structure of internal seiches. Diss No 10434, ETH Zürich
- Münnich M, Wüest A, Imboden DM (1992) Observations of the second vertical mode of the internal seiche in an alpine lake. *Limnol Oceanogr* 37: 1705–1719
- Murthy CR (1976) Horizontal diffusion characteristics in Lake Ontario. *J Phys Oceanogr* 6:76–84
- Mysak LA, Salvadè G, Hutter K, Scheiwiler T (1983) Lake of Lugano and topographic waves. *Nature* 306:46–48
- Newman FC (1976) Temperature steps in Lake Kivu: a bottom heated saline lake. *J Phys Oceanogr* 6: 157–163
- Oakey NS (1982) Determination of the rate of dissipation of turbulent energy from simultaneous temperature and velocity shear microstructure measurements. *J Phys Oceanogr* 12:256–271
- Oakey NS, Elliott JA (1982) Dissipation within the surface mixed layer. *J Phys Oceanogr* 12:171–185
- Okubo A (1967) The effect of shear in an oscillatory current on horizontal diffusion from an instantaneous source. *Limnol Oceanogr* 1:194–204
- Okubo A (1971) Oceanic diffusion diagrams. *Deep-Sea Res* 18:789–802
- Okubo A, Ozmidov RV (1970) Empirical dependence of the coefficient of horizontal turbulent diffusion in the ocean on the scale of the phenomenon in question. *Izv Atm Oc Phys* 6:534–536
- Osborn TR (1974) Vertical profiling of velocity microstructure. *J Phys Oceanogr* 4:109–115
- Osborn TR (1980) Estimates of the local rate of vertical diffusion from dissipation measurements. *J Phys Oceanogr* 10:83–89
- Osborn TR, Cox CS (1972) Oceanic fine structure. *Geophys Fluid Dyn* 3:321–345
- Padman L, Dillon TM (1987) Vertical heat fluxes through the Beaufort Sea thermohaline staircase. *J Geophys Res* 92:10799–10806
- Pahl-Wostl C, Imboden D (1990) DYPHORA – A dynamic model for the rate of photosynthesis of algae. *J Plankton Res* 12:1207–1221
- Patterson JC (1987) A model for convective motions in reservoir side arm. *Proc XXII, IAHR Congr Lausanne* 1987, pp 68–73
- Peeters F (1994) Horizontale Mischung in Seen. Diss No 10476 ETH Zürich, p 147
- Peeters F, Wüest A, Imboden DM (1993) Comparison of the results of tracer experiments in lakes with predictions based on horizontal mixing models. *Verh Int Verein Limnol* 25:67–74
- Peters H, Gregg MC (1987) Some dynamical and statistical properties of equatorial turbulence. In: Nihoul J (ed) Small-scale turbulence and mixing in the ocean, Proc of the 19th Int Liège Colloq on Ocean hydrodynamics. Elsevier, Amsterdam
- Peters H, Gregg MC, Toole JM (1988) On the parametrization of equatorial turbulence. *J Geophys Res* 93:1199–1218
- Platt T, Denman KL (1975) Spectral analysis in ecology. *Annu Rev Ecol Syst* 6:189–210
- Powell T, Jassby A (1974) The estimation of vertical eddy diffusivities below the thermocline in lakes. *Water Resour Res* 10:191–198
- Powell TM, Richerson PJ, Dillon TM, Agee BA, Dozier BJ, Godden DA, Myrup LO (1975) Spatial scales of current speed and phytoplankton biomass fluctuations in Lake Tahoe. *Science* 189:1088–1090
- Quay PD, Broecker WS, Hesslein RH, Schindler DW (1980) Vertical diffusion rates determined by tritium tracer experiments in the thermocline and hypolimnion of two lakes. *Limnol Oceanogr* 25:201–218
- Richardson LF (1926) Atmospheric diffusion on a distance-neighbour graph. *Proc R Soc A* 110: 709–737
- Sanderson B, Perry K, Pederson T (1986) Vertical diffusion in meromictic Powell Lake, British Columbia. *J Geophys Res* 91:7647–7655
- Saylor JH, Huang JCK, Reid RO (1980) Vortex modes in southern Lake Michigan. *J Phys Oceanogr* 10: 1814–1823
- Schlatter JW (1991) Schwefelhexafluorid als Tracer zum Studium von Mischungsprozessen in Seen. Diss No 9596, ETH Zürich
- Schmitt RW (1979) Flux measurements on salt fingers at an interface. *J Mar Res* 37:419–436
- Schmitt RW, Perkins H, Boyd JD, Stalcup MC (1987) C-salt: an investigation of the thermohaline staircase in the western tropical North Atlantic. *Deep-Sea*

- Res 34:1655–1665
- Shay TJ, Gregg MC (1986) Convectively driven turbulent mixing in the upper ocean. *J Phys Oceanogr* 16:1777–1798
- Shields A (1936) Anwendung der Ähnlichkeitsmechanik und der Turbulenzforschung auf die Geschiebebewegung. Mitt Preuss Versuchsanst Wasserbau Schiffbau 26, Berlin, pp 1–26
- Siegenthaler C, Sturm M (1991) Slump induced surges and sediment transport in Lake Uri, Switzerland. *Verh Int Verein Limnol* 24:955–958
- Soloviev AV (1990) Coherent structures at the ocean surface in convectively unstable conditions. *Nature* 346:157–160
- Soulsby RL (1983) The bottom boundary layer of shelf seas. In: Johns B (ed) *Physical oceanography of coastal and shelf seas*. Elsevier, Amsterdam, pp 189–266
- Spigel RH, Imberger J (1980) The classification of mixed-layer dynamics in lakes of small to medium size. *J Phys Oceanogr* 10:1104–1121
- Steele JH (1974) Spatial heterogeneity and population stability. *Nature* 248:83
- Steele JH (1978) Some comments on plankton patches. In: Steele JH (ed) *Spatial pattern in plankton communities*. Nato Conf Ser IV. Plenum, New York, pp 1–20
- Steinhorn I (1985) The disappearance of the long term meromictic stratification of the Dead Sea. *Limnol Oceanogr* 30:451–462
- Stern ME (1976) Maximum buoyancy flux across a salt finger interface. *J Mar Res* 34:95–110
- Stern ME, Turner JS (1969) Salt fingers and convecting layers. *Deep-Sea Res* 16:497–511
- Stocker T, Hutter K (1987) Topographic waves in channels and lakes on the f-plane. Springer, Berlin, Heidelberg, New York
- Stull RB (1984) Transient turbulence theory. Part 1. The concept of eddy mixing across finite distances. *J Atmos Sci* 41:3351–3367
- Stull RB (1986) Transient turbulence theory. Part 3. Bulk dispersion rate and numerical stability. *J Atmos Sci* 43:50–57
- Stull RB (1988) An introduction to boundary layer meteorology. Kluwer, Dordrecht
- Swinbank WC (1963) Long-wave radiation from clear skies. *Q J R Meteorol Soc* 89:339–348
- Taylor GI (1953) Dispersion of soluble matter in solvent flowing slowly through a tube. *Proc R Soc Lond A* 219:186–203
- Thorpe SA (1969) Experiments on the stability of stratified shear flows. *Radio Sci* 4:1327–1332
- Thorpe SA (1977) Turbulence and mixing in a Scottish loch. *Philos Trans R Soc Lond Ser A* 286:125–181
- Thorpe SA (1988) The dynamics of the boundary layers of the deep ocean. *Sci Prog* 72:189–206
- Toole JM, Polzin KL, Schmitt RW (1994) Estimates of diapycnal mixing in the abyssal ocean. *Science* 264:1120–1123
- Turner JS (1965) The coupled turbulent transports of salt and heat across a sharp density interface. *Int J Heat Mass Transfer* 8:759–767
- Turner JS (1967) Salt fingers across a density interface. *Deep-Sea Res* 14:599–611
- Turner JS (1968) The behavior of a stable salinity gradient heated from below. *J Fluid Mech* 33: 183–200
- Turner JS (1973) Buoyancy effects in fluids. Cambridge Univ Press, Cambridge
- Van der Hoven I (1957) Power spectrum of horizontal wind speed in the frequency range from 0.0007 to 900 cycles per hour. *J Meteorol* 14:160
- Van Senden DC, Imboden DM (1989) Internal seiche pumping between sill-separated basins. *Geophys Astrophys Fluid Dyn* 48:135–150
- Weatherly GL (1972) A study of the bottom boundary layer of the Florida current. *J Phys Oceanogr* 2: 54–72
- Wehrli B (1993) Chemie am Seegrund. *Vierteljahrsschr Naturforsch Ges Zürich* 138:1–11
- Welander P (1968) Theoretical forms for the vertical exchange coefficients in a stratified fluid with application to lakes and seas. *Geophys Gothenburg* 1:1–27
- Wiegand RC, Chamberlain V (1987) Internal waves of the second vertical mode in a stratified lake. *Limnol Oceanogr* 32:29–42
- Wimbush M, Munk W (1970) The benthic boundary layer. In: Maxwell AE (ed) *The sea*, vol 4. Interscience, New York, pp 731–758
- Woods JD (1968) Wave-induced shear instability in the summer thermocline. *J Fluid Mech* 32:791–800
- Woods AW (1991) Boundary-driven mixing. *J Fluid Mech* 226:625–654
- Wroblewski JS, O'Brien JJ (1976) A spatial model of phytoplankton patchiness. *Mar Biol* 35:161–175
- Wüest A (1987) Ursprung und Grösse von Mischungssprozessen im Hypolimnion natürlicher Seen. Diss No 8350, ETH Zürich
- Wüest A (1994) Interaktionen in Seen: Die Biologie als Quelle dominanter physikalischer Kräfte. *Limnologica* 24:93–104
- Wüest A, Imboden DM, Schurter M (1988) Origin and size of hypolimnic mixing in Urnersee, the southern basin of Vierwaldstättersee (Lake Lucerne). *Schweiz Z Hydrol* 50:40–70
- Wüest A, Aeschbach-Hertig W, Baur H, Hofer M, Kipfer R, Schurter M (1992) Density structure and tritium-helium age of deep hypolimnetic water in the northern basin of Lake Lugano. *Aquat Sci* 54:205–218
- Wüest A, van Senden DC, Imberger J, Piepke G, Gloor M (1994) Diapycnal diffusivity measured by microstructure and tracer techniques: a comparison. Symp on Turbulent flow, Grenoble, 8 pp
- Wunsch C (1972) The spectrum from two years to two minutes of temperature fluctuations in the main thermocline at Bermuda. *Deep-Sea Res* 19:577–593
- Wyngaard JC, Cote OR (1971) The budget of turbulent kinetic energy and temperature variance in the atmosphere surface layer. *J Atmos Sci* 28:190–201
- Young WR, Rhines PB, Garrett CJR (1982) Shear-flow dispersion, internal waves and horizontal mixing in the ocean. *J Phys Oceanogr* 12:515–527